DEVELOPMENT OF A DYNAMIC FLIGHT MODEL FOR A JET TRAINER AIRCRAFT

A THESIS SUBMITTED TO
THE GRADUATE SCHOOL OF NATURAL AND APPLIED SCIENCES
OF
MIDDLE EAST TECHNICAL UNIVERSITY

BY

MUHANED GILANI

IN PARTIAL FULFILLMENT OF THE REQUIREMENTS FOR
THE DEGREE OF MASTER OF SCIENCE

IN

AEROSPACE ENGINEERING

APRIL, 2007

Approval of the Graduate School of Natural and Applied Sciences.

_____
Prof. Dr. Canan Özgen
Director

I certify that this thesis satisfies all the requirements as a thesis for the degree of Master of Science.

_____
Prof. Dr. İsmail H. Tuncer
Head of Department

This is to certify that we have read this thesis and that in our opinion it is fully adequate, in scope and quality, as a thesis for the degree of Master of Science.

_____
Assoc. Prof. Dr. Serkan Özgen
Supervisor

Examining Committee Members

Prof. Dr.Nafız Alemdaroğlu	(METU,AEE)	_____
Assoc. Prof. Dr. Serkan Özgen	(METU,AEE)	_____
Prof.Dr. Zafer Dursunkaya	(METU,MEE)	_____
Prof. Dr. Yavuz Yaman	(METU,AEE)	_____
Asst. Prof. Dr. Melin Şahin	(METU,AEE)	_____

I hereby declared that all information in this document has been obtained and presented in accordance of academic rules and ethical conduct. I also declared that, as required by these rules and conduct, I have fully cited and referenced all material and results that are not original to this work.

Name, Last name: Muhaned Gilani

Signature:

ABSTRACT

DEVELOPMENT OF A DYNAMIC FLIGHT MODEL OF A JET TRAINER AIRCRAFT

GILANI, MUHANED

M.S., Department of Aerospace Engineering

Supervisor: Assoc. Prof. Dr. SERKAN ÖZGEN

April 2007, pages 107

A dynamic flight model of a jet trainer aircraft is developed in MATLAB-SIMULINK. Using a six degree of freedom mathematical model, non-linear simulation is used to observe the longitudinal and lateral-directional motions of the aircraft following a pilot input. The mathematical model is in state-space form and uses aircraft stability and control derivatives calculated from the aircraft geometric and aerodynamic characteristics. The simulation takes the changes in speed and altitude into consideration due to pilot input and demonstrates the non-linearity of the aircraft motion. The results from the simulation are compared with the results from flight characteristics manual of the actual aircraft to validate the mathematical model used. The simulation is carried out for a number of airspeed and altitude combinations to examine the effect of changing speed and altitude on the aircraft dynamic response.

Keywords: Flight Dynamics, Longitudinal Motion, Lateral Motion, 6DOF, Mathematical Model, Simulation, MATLAB, SIMULINK.

ÖZ

JET MOTORLU BİR EĞİTİM UÇAĞININ DİNAMİK UÇUŞ MODELİNİN GELİŞTİRİLMESİ

GILANI, MUHANED

Yüksek Lisans, Havacılık ve Uzay Mühendisliği Bölümü
Tez Danışmanı: Doç. Dr. Serkan ÖZGEN
Nisan 2007, 107 sayfa

Jet motorlu bir eğitim uçağının dinamik uçuş modeli MATLAB-SIMULINK yazılımı kullanılarak geliştirilmiştir. Uçağın pilot kumandasına boylamsal ve yanal harekette verdiği tepkileri gözlemlemek için, altı yönde hareket serbestliği olan matematiksel model kullanılarak, doğrusal olmayan bir benzetişim geliştirilmiştir. Matematik model durum-uzay halinde olup, uçağın geometrik ve aerodinamik özellikleri kullanılarak hesaplanan kararlılık ve kumanda türevlerini içermektedir. Benzetişim, pilot kumandasına bağlı sürat ve irtifa değişimlerini göz önüne almakta ve uçağın doğrusal olmayan hareketini sergilemektedir. Matematiksel modelin doğrulanması amacıyla, benzetişimden elde edilen sonuçlar, gerçek uçağın uçuş karakteristikleri el kitabında bulunan verilerle karşılaştırılmıştır. Değişen sürat ve irtifanın uçağın dinamik tepkisine olan etkisini irdelemek amacıyla, benzetişim değişik sürat ve irtifa kombinasyonları için çalıştırılmıştır.

Anahtar Kelimeler: Uçuş Dinamiği, Boylamsal Hareket, Yanal Hareket, 6 Serbestlik Derecesi, Matematiksel Model, Benzetişim, MATLAB, SIMULINK.

To all who raised me up to more than I can be..

ACKNOWLEDGMENTS

It is my great pleasure to thank the many people who enabled me to perform this work.

I am extremely grateful to my supervisor, Dr. Serkan Özgen for his outstanding guidance, support, patience and dedication have been an invaluable source of inspiration and motivation for me throughout the course of this research.

A very special expression of appreciation is also to Sabudh Bahandari, Mustafa Kaya, Muner Alfarra, EzAldeen Kenshel and Saleh Basha for their dedication and selfless assistance.

I would like to extend a sincere expression of appreciation to my family for the support and inspiration throughout my career. I am also grateful to all of my friends whose role in completing this work is of great value.

The department of Aerospace Engineering deserves special thanks for providing educational assistance and other support to me for the completion of master's degree.

I cannot end without thanking the lovely L-39 enthusiasts all around the world. Their ideas, experience and knowledge inspire me and guide me to keep on track till the end of this work.

TABLE OF CONTENTS

LIST OF TABLES

LIST OF FIGURES

FIGURES

LIST OF SYMBOLS

SYMBOL	DESCRIPTION	UNITS
A	System Matrix	
B	Input Matrix	
b	Wing Span	m
C	Output Matrix	
c	Wing Chord	m
$\bar{c}$	Mean Aerodynamic Chord	m
C_r	Wing Root Chord	m
C_D	Airplane Drag Coefficient	
C_{D0}	Airplane Drag Coefficient at Zero Angle of Attack	
C_{D_α}	Variation of Drag Coefficient with Angle of Attack	1/rad
C_{D_u}	Variation of Drag Coefficient with Dimensionless Speed	
C_L	Airplane Lift Coefficient	
C_{L_0}	Lift Coefficient at Zero Angle of Attack	
C_{l_β}	Variation of Airplane Rolling Moment Coefficient with Sideslip Angle.	1/rad
$C_{l_{\delta_a}}$	Variation of Airplane Rolling Moment Coefficient with Aileron Deflection Angle	1/rad
$C_{l_{\delta_r}}$	Variation of Airplane Rolling Moment Coefficient with Rudder Deflection Angle	1/rad
C_{l_p}	Variation of Airplane Rolling Moment Coefficient with Dimensionless Roll Rate	1/rad

SYMBOL	DESCRIPTION	UNITS
	Dimensionless Yaw Rate	
C_{L_α}	Variation of Lift Coefficient with Angle of Attack	1/rad
$C_{l_{\delta_e}}$	Variation of Airplane Lift Coefficient with Elevator Deflection Angle.	1/rad
C_{L_u}	Variation of Lift Coefficient with Speed.	
C_{m_α}	Variation of Airplane Pitching Moment Coefficient with Angle of Attack.	1/rad
$C_{m_{\dot{\alpha}}}$	Variation of Airplane Pitching Moment Coefficient with Rate of Change of Angle of Attack	1/rad
$C_{m_{\delta_e}}$	Variation of Airplane Pitching Moment Coefficient with Elevator Deflection Angle	1/rad
C_{m_q}	Variation of Airplane Pitching Moment Coefficient with Pitch Rate	1/rad
C_{m_u}	Variation of Pitching Moment Coefficient with Dimensionless Speed	
C_{n_β}	Variation of Airplane Yawing Moment Coefficient with Angle of Sideslip.	1/rad
$C_{n_{\delta_a}}$	Variation of Airplane Yawing Moment Coefficient with Aileron Deflection Angle.	1/rad
$C_{n_{\delta_r}}$	Variation of Airplane Yawing Moment Coefficient with Rudder Deflection Angle.	1/rad
C_{n_p}	Variation of Airplane Yawing Moment Coefficient with Dimensionless Roll Rate	1/rad
C_{n_r}	Variation of Airplane Yawing Moment Coefficient with Dimensionless Yaw Rate	1/rad

SYMBOL	DESCRIPTION	UNITS
C_{T_u}	Variation of Airplane Thrust Coefficient with Dimensionless Speed	
C_{x_α}	Variation of Airplane X-Force Coefficient with Angle of Attack	1/rad
C_{x_u}	Variation of Airplane X-Force Coefficient with Dimensionless Speed	
C_{y_p}	Variation of Airplane Side Force Coefficient with Sideslip Angle	1/rad
C_{y_r}	Variation of Airplane Side Force Coefficient with Aileron Angle	1/rad
$C_{\delta_{yr}}$	Variation of Airplane Side Force Coefficient with Rudder Angle	1/rad
C_{y_p}	Variation of Airplane Side Force Coefficient with Dimensionless Rate of Change of Roll Rate.	1/rad
C_{y_r}	Variation of Airplane Side Force Coefficient with Dimensionless Rate of Change of Yaw Rate	1/rad
C_{z_α}	Variation of Airplane Z-Force Coefficient with Angle of Attack	1/rad
$C_{z_{\dot{\alpha}}}$	Variation of Airplane Z-Force Coefficient with Rate of Change of Angle of Attack	1/rad
C_{z_q}	Variation of Airplane Z-Force Coefficient with Dimensionless Pitch Rate	1/rad
C_{z_u}	Variation of Airplane Z-Force Coefficient with Dimensionless Speed	
D	Matrix to Represent Direct Coupling between Input and Output	
e	Oswald's Efficiency Factor	

SYMBOL	DESCRIPTION	UNITS
I_x	Airplane Moments of Inertia about X-Axis	$kg.m^2$
I_y	Airplane Moments Of Inertia about Y-Axis	$kg.m^2$
I_z	Airplane Moments Of Inertia about Z-Axis	$kg.m^2$
L_β	Roll Angular Acceleration per Unit Sideslip Angle	$rad/sec^2/rad$
L_p	Roll Angular Acceleration per Unit Roll Rate	1/sec
L_r	Roll Angular Acceleration per Unit Yaw Rate	1/sec
L_{δ_a}	Roll Angular Acceleration per Unit Aileron Angle	$rad/sec^2/rad$
L_{δ_r}	Roll Angular Acceleration per Unit Yaw Angle	$rad/sec^2/rad$
M_α	Pitch Angular Acceleration per Unit Angle of Attack	$1/sec^2$
M_u	Pitch Angular Acceleration per Unit Change in Speed	rad/sec/m
$M_{\dot{\alpha}}$	Pitch Angular Acceleration per Unit Rate of Change of Angle of Attack.	1/sec
N_β	Yaw Angular Acceleration per Unit Sideslip Angle	$rad/sec^2/rad$
N_p	Yaw Angular Acceleration per Unit Roll Rate	1/sec
N_r	Yaw Angular Acceleration per Unit Yaw Angle	1/sec
N_{δ_a}	Yaw Angular Acceleration per Unit Aileron Angle	$rad/sec^2/rad$
N_{δ_r}	Yaw Angular Acceleration per Unit Rudder Angle	$rad/sec^2/rad$
p	Airplane Roll Rate	rad/sec
Δp	Change in Airplane Roll Rate	rad/sec
q	Airplane Pitch Rate	rad/sec
Δq	Change in Airplane Pitch Rate	rad/sec
r	Airplane Yaw Rate	rad/sec
Δr	Change in Airplane Yaw Rate	rad/sec

SYMBOL	DESCRIPTION	UNITS
U	Horizontal Component of Airplane Speed	m/sec
η1	Input Vector	
Δu	Change in Speed of the Airplane	m/sec
U	Speed of the Airplane	m/sec
U_0	Reference Speed of the Airplane	m/sec
v	Airplane Side Velocity	m/sec
w	Airplane Vertical Velocity	m/sec
X_α	Airplane Forward Acceleration per Unit Angle of Attack	$m/sec^2/rad$
X_u	Airplane Forward Acceleration per Unit Change in Speed	1/sec
X_{δ_e}	Airplane Forward Acceleration per Unit Elevator Angle	1/sec
y_1	Distance of Inboard Edge of Aileron From X-Axis	m
y_2	Distance of Outboard Edge of Aileron From X-Axis	m
Y_β	Airplane Lateral Acceleration per Unit Sideslip Angle	$m/sec^2/rad$
Y_p	Lateral Acceleration per Unit Roll Rate	m/sec/rad
Y_r	Lateral Acceleration per Unit Yaw Rate	m/sec/rad
Y_{δ_a}	Lateral Acceleration per Unit Aileron Angle	$m/sec^2/rad$
Y_{δ_r}	Lateral Acceleration per Unit Rudder Angle	$m/sec^2/rad$
Z_α	Vertical Acceleration per Unit Angle of Attack	$m/sec^2/rad$
$Z_{\dot{\alpha}}$	Vertical Acceleration per Unit Rate of Change of Angle of Attack	m/sec/rad
Z_{δ_e}	Vertical Acceleration per Unit Elevator Angle	$m/sec^2/rad$
Z_q	Vertical Acceleration per Unit Pitch Rate	m/sec/rad
Z_u	Vertical Acceleration per Unit Change in Speed	1/sec
α	Angle of Attack	deg
α_0	Angle of Attack at Zero Lift	deg

SYMBOL	DESCRIPTION	UNITS
$\Delta\alpha$	Change in Angle of Attack	deg
β	Angle of Sideslip	deg
$\Delta\beta$	Change in Sideslip Angle	deg
Γ	Geometric Dihedral Angle	deg
ε	Downwash Angle at Horizontal Stabilizer	deg
ε_0	Downwash Angle at Horizontal Stabilizer at Zero Angle of Attack	deg
η_h	Dynamic Pressure Ratio at the Horizontal Tail	
η_v	Dynamic Pressure Ratio at the Vertical Tail	
θ	Airplane Pitch Attitude Angle	deg
$\Delta\theta$	Change in Airplane Pitch Attitude Angle	deg
λ	Taper Ratio	
Λ	Wing Sweep Angle	deg
σ	Side Wash Angle	deg
Φ	Airplane Roll Angle	deg
$\Delta\Phi$	Change in Airplane Roll Angle	deg
Ψ	Airplane Yaw Angle	deg
δ_a	Aileron Deflection Angle	deg
$\Delta\delta_a$	Change in Aileron Deflection Angle	deg
δ_e	Elevator Deflection Angle	deg
$\Delta\delta_e$	Change in Elevator Deflection Angle	deg
δ_r	Rudder Deflection Angle	deg

CHAPTER 1
INTRODUCTION

Simulation of flight is one of the most acceptable techniques in the aircraft flight test programs used by aviation industry. In order to use simulation as a useful tool to reduce the time and cost of designing and testing aircraft, a mathematical model is derived from the six degree of freedom equations of motion describing the dynamic behavior of a rigid body aircraft. The accuracy of the simulation results depends on the accuracy of the mathematical model used in the simulation.

In this study, a six degree of freedom simulation of aircraft motion is developed in MATLAB [10] and SIMULINK [11]. Using a mathematical model of fixed-wing aircraft, the model developed in this research is applied to an advanced jet training aircraft Aero L-39. The simulation is used to observe the longitudinal and lateral-directional responses of the aircraft following a pilot input in any of the control surfaces. The mathematical model is in state-space form and uses aircraft stability and control derivatives derived from the aircraft geometric data and aerodynamic characteristics. The simulation takes into account the change in speed and altitude due to pilot input. The results from the simulation are compared with the real flight performance characteristics from the flight manual of Aero L-39 [8] to validate the mathematical model used. The simulation is carried out for a range of airspeeds and altitudes within the flight envelop of the aircraft to examine the effect of changing speed and altitude on the aircraft dynamic response.

For the sake of using the whole range of speed and altitude, the simulation is developed and as nonlinear, so that it can be valid for all changes resulting from the dynamic response. The results obtained from the simulation then provide a basis for aircraft control system analysis and design process.

The mathematical model used in this work is in state-space form, where the states of the stability and control derivatives and states of the aircraft are represented in a set of matrices [1 and 2].

Stability derivatives represent the stability of the aircraft, while control derivatives represent its maneuverability, and they are obtained from geometric data and aerodynamic characteristics of the airplane. The stability and control derivatives relate the forces and moments acting on the aircraft axes to the aircraft states, such as angle of attack, sideslip angle, and angular rates. Stability and control derivatives of L-39 are obtained based on set of formulas presented in several references related to aircraft stability and control [1,2,3,4 and 5]. These stability and control derivatives are functions of aircraft speed, altitude, angle of attack, sideslip angle etc.

The model presented in this thesis mainly uses aircraft geometric data and aerodynamic characteristics. This was the major challenge in this work where stability and control derivatives or coefficients were not known for L-39. However, a flight test data of its longitudinal and lateral response at certain altitudes and speeds were given in the flight characteristics manual of the airplane. On the other hand, derivatives results from the simulation were compared with derivatives of an aircraft with the same category to check the stability and control coefficients [4]. These coefficients were then used to calculate a set of stability and control derivatives within the flight envelope of L-39. The flight envelope of L-39 is presented in the range of speed and altitude as a vector matrix in the code written as M-file that used to calculate aircraft stability derivatives and control coefficients.
The calculated derivatives are interpolated to determine the derivatives at a particular speed and altitude taking into accounts the changes.

The S-Function [12] is a tool of SIMULINK used in building the aircraft simulation model. An S-Function is a computer language description of a Simulink block written in “C” language. S-Function provides an interaction between SIMULINK solver and the blocks of the model. The model is simulated at any desired speed and altitude.

Because of pilot input, altitude and/or speed of the aircraft will change. Values of the new speed and/or altitude are fed-back to the model where stability and control derivatives are interpolated based on changes in altitude and/or airspeed

and the response of the aircraft is observed at the new speed and altitude. Then stability and control derivatives are updated at each time step of the simulation.

Finally, the simulation results are validated by comparing them with the results from aircraft flight characteristic manual. Such results can be used as a tool for flight test missions for this aircraft, also to improve flight performance or designing suitable autopilot and stability augmentation system for this aircraft. Even simulators can be developed based on such data.

CHAPTER 2
THEORETICAL BACKGROUND

The simulation of aircraft motion aims to observe the flight dynamic response following pilot input or any other input caused by atmospheric gust or similar effects. The simulation of aircraft motion helps control system engineers to examine the effect of pilot inputs or disturbances on the dynamic behavior of the aircraft. The accuracy of the simulation depends upon the mathematical model used in the simulation. If the mathematical model is correct and accurate, the simulation will produce the accurate and reliable dynamic behavior of the aircraft.

The mathematical model used in simulation is derived from the six degree of freedom (6DOF) rigid body differential equations of motion for aircraft [2].

The mathematical model used in this thesis is in the state space form. State-space models consist of an aircraft state equation and output equation [2], as it will be discussed in the following sections starting from general aircraft equations of motion.

2.1 Aircraft Equations of Motion

Aircraft dynamics can be expressed as a set of nonlinear ordinary differential equations (ODEs). The state equations of the model can be derived and they are valid for rigid bodies. They express the motions of the aircraft in terms of external forces and moments.

The contributions to the forces and moments from aerodynamics, thrust, and atmosphere will be considered here. In this section, the equations of motion will be presented along with all relevant force and moment equations.

There are six force and moment equations and six equations which determine the aircraft's attitude and position with respect to the earth.

The translational equations are expressed in terms of true airspeed V, angle of attack α, and sideslip angle β instead of the body axes velocity components u, v, and w.

The state equations for U, α, β, p, q, and r are valid only when the following restrictive assumptions are made:

1 - The airframe is assumed to be a rigid body in the motion under consideration.

2 - The airplane's mass is assumed to be constant during the time interval in which its motions are studied.

3 - The earth is assumed to be fixed in space, i.e. its rotation is neglected.

4 - The curvature of the earth is neglected.

The aerodynamic forces and moments primarily depend on angle of attack and side-slip angle. The angle of attack is associated with the longitudinal forces and moments, while the sideslip angle is associated with the lateral forces and moments. Lift, drag, and pitching moments depend on the angle of attack, whereas the side force, rolling moments and yawing moments depend on the sideslip angle. The angle of attack and the sideslip angle are described by the following equations:

$$\alpha = \tan^{-1}\frac{w}{U} \tag{2.1}$$

$$\beta = \sin^{-1}\frac{v}{U} \tag{2.2}$$

$$U = \sqrt{u^2 + v^2 + w^2} \tag{2.3}$$

2.1.1 Rigid Body Equations of Motion

The rigid body equations of motion of aircraft can be derived from Newton's second law, which states that the summation of all external forces acting on a body is equal to the time rate of change of the momentum of the body and that the summation of all external moments acting on the body is equal to the time rate of change of angular momentum. These equations can be expressed mathematically as follows: [1 and 2]

Force equation: $$\sum \vec{F} = \frac{d(m\vec{U})}{dt} \quad (2.4)$$

Moment equation: $$\sum \vec{M} = \frac{d(\vec{H})}{dt} \quad (2.5)$$

Where: m is mass, $\vec{U}$ is velocity and $\vec{H}$ is angular momentum of the aircraft.

Both the force and the moment have three components along the X, Y, and Z-axes (the body axes) of the aircraft. These components are as given below:

X-force component, $$F_x = \frac{d}{dt}(mu) \quad (2.6)$$

Y-force component, $$F_y = \frac{d}{dt}(mv) \quad (2.7)$$

Z-force component, $$F_z = \frac{d}{dt}(mw) \quad (2.8)$$

Rolling moment, $$L = \frac{d}{dt}(H_x) \quad (2.9)$$

Pitching moment, $$M = \frac{d}{dt}(H_y) \quad (2.10)$$

Yawing moment, $$N = \frac{d}{dt}(H_z) \quad (2.11)$$

The axis system and the nomenclature for forces, moments, linear and angular velocities are shown in Figure 2.1

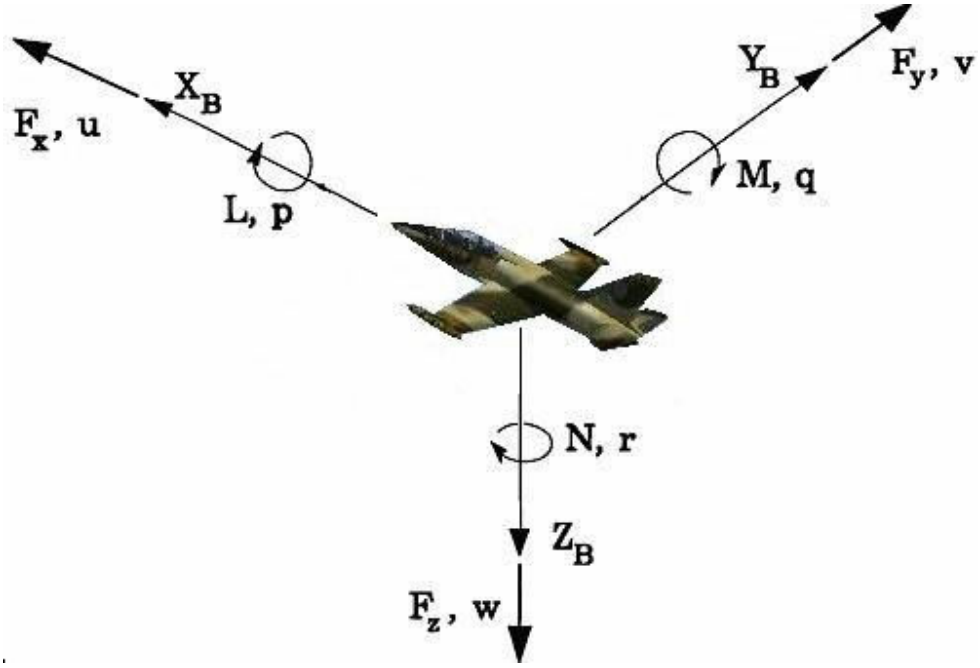

Figure 2.1: Forces, Moments, Velocities and Rotational Velocities on the Aircraft Body Axes Frame.

In these equations, H_x, H_y, and H_z are the components of angular momentum along the X, Y, and Z-axes, respectively.

To determine the force and moment equations of the aircraft, an elemental mass at a certain distance from the center of gravity and having a certain velocity relative to an inertial frame is considered. The external forces and the moments acting on the mass are then calculated using the above force and moment equations. The forces and the moments acting on the airplane are the integral of these elemental forces and moments integrated over the entire body of the aircraft, and are represented by the following equations [2].

$$F_x = m(\dot{u} + qw - rv) \tag{2.12}$$

$$F_y = m(\dot{v} + ru - pw) \tag{2.13}$$

$$F_z = m(\dot{w} + pv - qu) \tag{2.14}$$

$$L = I_x . \dot{p} - I_{xz} . \dot{r} + q . r (I_z - I_y) - I_{xz} . p . q \tag{2.15}$$

$$M = I_y \dot{q} + rp(I_x - I_y) - I_{xz}(p^2 - r^2) \tag{2.16}$$

$$N = -I_{xz} \dot{p} + I_z \dot{r} + pq(I_y - I_x) + I_{xz} q . r \tag{2.17}$$

These equations are non-linear, however they can be linearized by using small disturbance theory, so that they can be used for state space form equations [2].
Definition of forces, moments and velocity components in a body fixed frame are shown in Table 2.1

Table2.1 Forces, Moments and Velocity Components in Body Fixed Frame

	Roll Axis x	Pitch Axis y	Yaw Axis z
Angular Rates	p	q	r
Velocity Components	u	v	w
Aerodynamic Force Components	X	Y	Z
Aerodynamic Moment Components	L	M	N
Moment of Inertia About Each Axis	I_x	I_y	I_z
Product of Inertia	I_{yz}	I_{xz}	I_{xy}

2.1.2 Orientation and Position of the Aircraft

The position and orientation of the aircraft cannot be described relative to a non-inertial frame. The orientation and position of the aircraft can be defined in terms of a fixed frame of reference called Earth fixed frame as shown in Figure.2.2

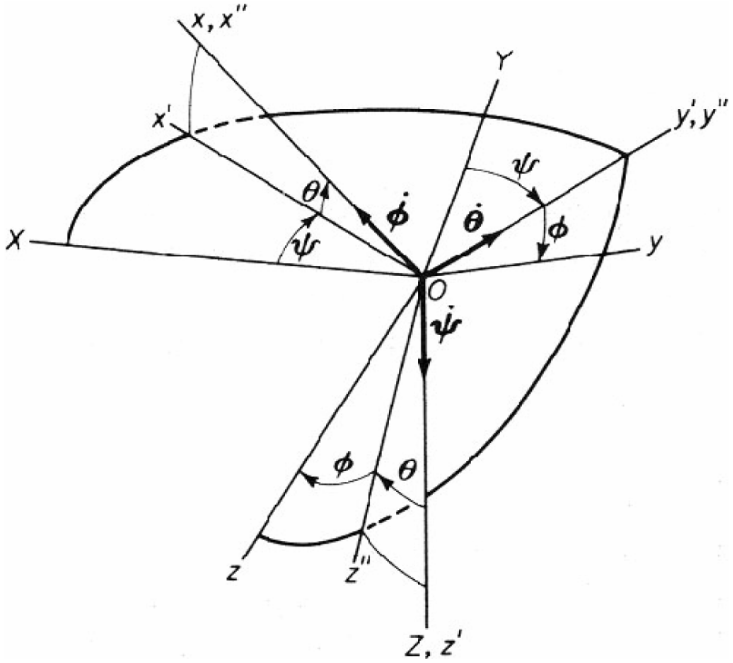

Figure 2.2 Euler Angels and Rotation Sequence.

The following transformations describe the motion of the aircraft relative to the inertial frame of reference [2].

I. Differential equations for the aircraft coordinates:

$$\dot{x} = \{u\cos\theta + (v\sin\phi + w\cos\phi)\sin\theta\}\cos\psi - (v\cos\phi - w\sin\phi)\sin\psi \tag{2.18}$$

$$\dot{y} = \{u\cos\theta + (v\sin\phi + w\cos\phi)\sin\theta\}\sin\psi - (v\cos\phi - w\sin\phi)\cos\psi \tag{2.19}$$

$$\dot{z} = -u\sin\theta + (v\sin\phi + w\cos\phi)\cos\theta \tag{2.20}$$

Where, θ, ϕ and ψ are called Euler angles which used to represent the attitude of the aircraft position and it is defined with respect to the earth-fixed reference frame.

II. Equations of the body-axes rotational velocities:

The relationship between the angular velocities in the body frame and the Euler rates can be determined from the following relations:

$$p = \dot{\phi} - \dot{\psi}\sin\theta \tag{2.21}$$

$$q = \dot{\theta}\cos\phi + \dot{\psi}\cos\theta\sin\phi \tag{2.22}$$

$$r = \dot{\psi}\cos\theta\cos\phi - \dot{\theta}\sin\phi) \tag{2.23}$$

III. Differential equations for the Euler angles:

Euler rates can be expressed in terms of body angular velocities in the following relations:

$$\dot{\theta} = q\cos\phi - r\sin\phi \tag{2.24}$$

$$\dot{\phi} = p + q\sin\phi\tan\theta + r\cos\phi\tan\theta \tag{2.25}$$

$$\dot{\psi} = (q\sin\phi + r\cos\phi)\sec\theta \tag{2.26}$$

By integrating above equations, the position and orientation of the aircraft relative to the inertial frame can be obtained. It is realized that the p, q and r are the angular velocities with respect to the body frame, on the other hand, $\dot{\theta}, \dot{\phi}$ and $\dot{\psi}$ are angular rates with respect to the Earth fixed frame.

2.1.3 Small Disturbance Theory

The motion of aircraft is assumed to consist of small deviations from the reference condition of steady flight. The use of this theory has been found to give good results, so that it can be used with sufficient accuracy for engineering purposes. In order to use small disturbance theory to solve non-linearity problems in flight dynamics, the values of all disturbances and their derivatives are assumed to be small.

This can be expressed in trigonometry form as following:

$$\sin(\theta_0 + \Delta\theta) = \sin\theta_0 \cos\Delta\theta + \cos\theta_0 \sin\Delta\theta$$
$$\cong \sin\theta_0 + \Delta\theta\cos\theta_0 \quad (2.27)$$
$$\cos(\theta_0 + \Delta\theta) = \cos\theta_0 \cos\Delta\theta - \sin\theta_0 \sin\Delta\theta$$
$$\cong \cos\theta_0 - \Delta\theta\sin\theta_0 \quad (2.28)$$

2.1.4 Linearization

The non-linear equations stated in the previous sections can be linearized in order to be used in state-space form, taking into account the assumption that the wind velocity is zero and by considering only the first order terms. Thus, the linear equations can be written as follows:

$$X_0 + \Delta X - mg(\sin\theta_0 + \Delta\theta\cos\theta_0) = m\Delta\dot{u} \quad (2.29)$$
$$Y_0 + \Delta Y + mg\phi\cos\theta_0 = m(\dot{v} + u_0 r) \quad (2.30)$$
$$Z_0 + \Delta Z + mg(\cos\theta_0 + \Delta\theta\sin\theta_0) = m(\dot{w} - u_0 q) \quad (2.31)$$

$$L_0 + \Delta L = I_x \dot{p} - I_{zx}\dot{r} \quad (2.32)$$
$$M_0 + \Delta M = I_y \dot{q} \quad (2.33)$$

$$N_0 + \Delta N = -I_{zx}\dot{p} + I_z \dot{r} \quad (2.34)$$
$$\Delta\dot{\theta} = q \quad (2.35)$$
$$\dot{\phi} = p + r\tan\theta_0, \qquad p = \dot{\phi} - \dot{\psi}\sin\theta_0 \quad (2.36)$$
$$\dot{\psi} = r\sec\theta_0 \quad (2.37)$$

$$\dot{x}_E = (u_0 + \Delta u)\cos\theta_0 - u_0\Delta\theta\sin\theta_0 + w\sin\theta_0 \quad (2.38)$$
$$\dot{y}_E = u_0\psi\cos\theta_0 + v \quad (2.39)$$
$$\dot{z}_E = -(u_0 + \Delta u)\sin\theta_0 - u_0\Delta\theta\cos\theta_0 + w\cos\theta_0 \quad (2.40)$$

Where, E refers to Earth Fixed frame.

2.1.5 Reference steady state

Reference flight condition can be considered if all of disturbances quantities set to be zero, as shown in the following relations:

$$X_0 - mg\sin\theta_0 = 0 \tag{2.41}$$

$$Y_0 = 0 \tag{2.42}$$

$$Z_0 + mg\cos\theta_0 = 0 \tag{2.43}$$

$$\dot{x}_{E_0} = u_0\cos\theta_0 \tag{2.44}$$

$$\dot{y}_{E_0} = 0 \tag{2.45}$$

$$\dot{z}_{E_0} = -u_0\sin\theta_0 \tag{2.46}$$

2.1.6 Contribution of Gravity Force

The gravity force acting on the aircraft supposed to act through its center of gravity, so no moment will be produced. The contribution to the external force on the aircraft will have components along the body axes as shown in Figure 2.3.

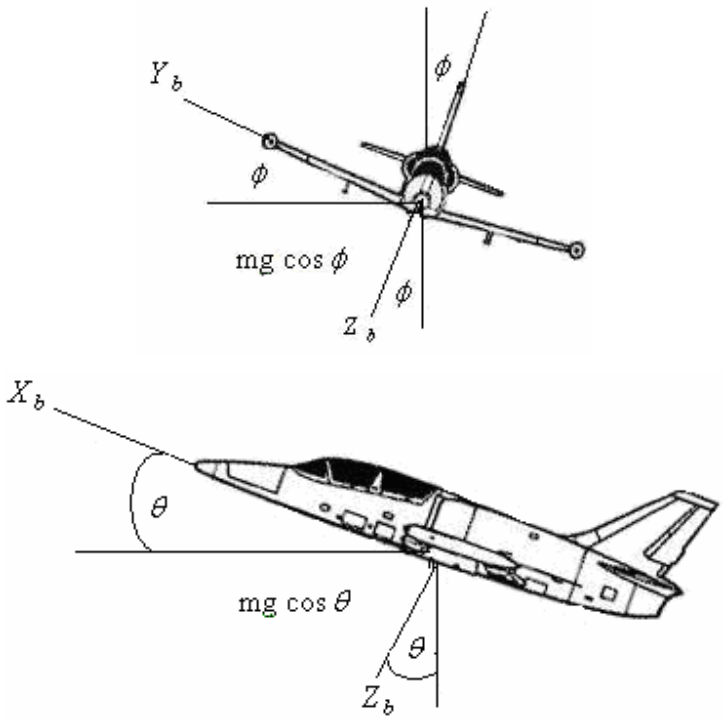

Figure 2.3 Components of Gravitational Force Acting Along the Body Axis.

The contribution of the aircraft weight W to the forces along the body-axes of the aircraft can be calculated if the Euler angles θ,ϕ and ψ are known.

$$(F_x)_{gravity} = -mg.\sin\theta \tag{2.47}$$

$$(F_y)_{gravity} = mg.\cos\theta.\sin\phi \tag{2.48}$$

$$(F_z)_{gravity} = mg.\cos\theta\cos\phi \tag{2.49}$$

2.1.7 Contribution of Thrust Force

The thrust force from the engine has components acting at each body axes. On the other hand, if the thrust is supposed to act along the center of gravity it will not cause any moment forces as shown in Figure 2.4.

Where,Y_T equals to zero for symmetrical thrust cases. An asymmetrical thrust case will produce a yawing moment, and Z_T is zero if thrust line and c.g. coincide.

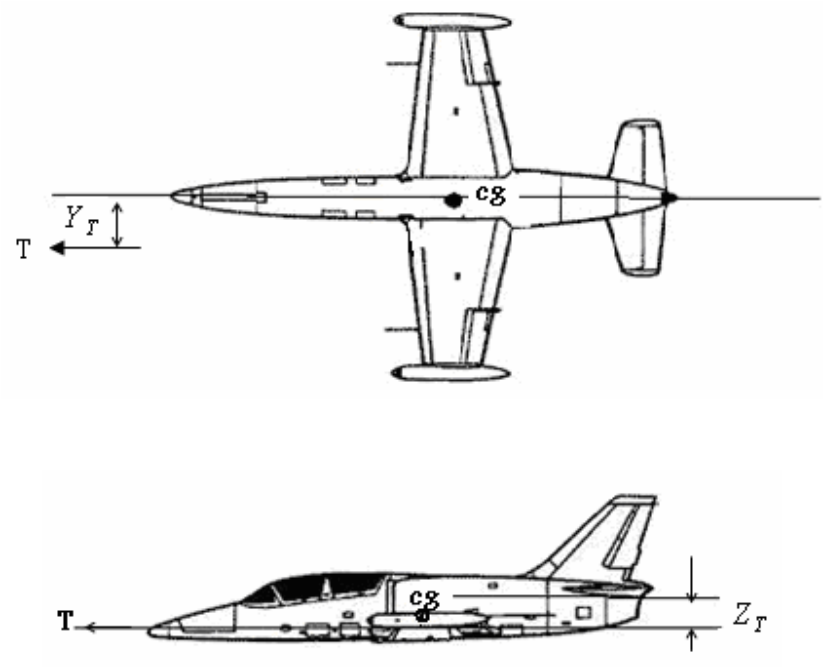

Figure 2.4 Forces and Moments due to Thrust Force.

If the thrust line is offset from the c.g., it will produce a pitching moment, the moments acting along the body axes due to the thrust force system can be expressed as follows:

$$M_T = Tz_T \tag{2.50}$$

$$N_T = Ty_T \tag{2.51}$$

In the same way, all the other forces and moments can be expressed in terms of the perturbation variables. Since three forces (X, Y, and Z forces) and three moments (L, M and N) are acting on the aircraft and the number of perturbation variables are large, a number of stability derivatives and coefficients exist.
The coefficients and derivatives that are relevant to the present thesis have been taken from Ref. [1, 2, 3 and 4] and they are included in the Appendix A

2.2 Longitudinal Equations of Motion

The longitudinal equations of motion of the aircraft can be expressed as following:

$$(\frac{d}{dx} - X_u).\Delta u - X_w.\Delta w + (g.\cos\theta_0).\Delta\theta = X_{\delta e}.\Delta\delta + X_{\delta T}.\Delta\delta_T \tag{2.52}$$

$$-Z_u.\Delta u + \left[\left(1 - Z_{\dot{w}}\right)\frac{d}{dt} - Z_w\right]\Delta w - \left[\left(u_0 + Z_q\right)\frac{d}{dt} - g.\sin\theta_0\right]\Delta\theta = Z_{\delta e}\delta_e + Z_\delta\Delta\delta_T \tag{2.53}$$

$$-M_u.\Delta u - \left(M_{\dot{w}}\frac{d}{dt} + M_w\right)\Delta w + \left(\frac{d^2}{dt^2} - M_q\frac{d}{dt}\right)\Delta\theta = M_{\delta e}.\Delta\delta_e + M_{\delta T}.\Delta\delta_T \tag{2.54}$$

2.3 Lateral-Directional Equations of Motion

The lateral equations of motion of the aircraft can be expressed as following:

$$\left(\frac{d}{dt} - Y_v\right).\Delta v - Y_p.\Delta p + \left(u_0 - Y_r\right).\Delta r - \left(s.\cos\theta_0\right).\Delta\phi = Y_{\delta r}.\Delta\delta_r \tag{2.55}$$

$$-L_v.\Delta v + \left(\frac{d}{dt} - L_p\right).\Delta p - \left(\frac{I_{xz}}{I_x}\frac{d}{dt} + L_r\right).\Delta r = L_{\delta a}.\Delta\delta_a + L_{\delta r}.\Delta\delta_r \tag{2.56}$$

$$-L_v.\Delta v + \left(\frac{d}{dt} - L_p\right).\Delta p - \left(\frac{I_{xz}}{I_x}\frac{d}{dt} + L_r\right).\Delta r = L_{\delta a}.\Delta\delta_a + L_{\delta r}.\Delta\delta_r \quad (2.57)$$

2.4 States of Aircraft

The state of aircraft can be described at a particular point of flight defined by a set of parameters [1 and 2]. These parameters are the angle of attack (α), sideslip angle (β), three translation velocities (u, v, and w), three angular rates (pitch rate p, roll rate q, and yaw rate r), and three Euler angles (pitch angle θ, roll angle ϕ, and yaw angle ψ).

The state of the aircraft can be easily described if theses parameters are known. The longitudinal response of the aircraft is described by changes in u, α, p, and θ, while the lateral response of the aircraft is described by changes in β, q, r, and ϕ.

2.5 Stability Derivatives and Coefficients

Stability derivatives are a means of linearizing the equations of motion of atmospheric flight vehicle so that conventional control engineering methods may be applied to assess their stability.

The dynamics of atmospheric flight vehicles is potentially very difficult to analyze, because the forces and moments on the vehicle are seldom simple linear functions of its states. In order to address this problem and to render the analysis of stability and the design of autopilots tractable, it is necessary to deal with linear approximations to the equations of motion. The analysis is then applied to a range of flight conditions.

A stability derivative is an incremental change in the aerodynamic forces or moments acting on the aircraft corresponding to an incremental change in one of the states. Thus, the aerodynamic forces and moments can be expressed by means of a Taylor series expansion of the perturbation variables about the reference equilibrium condition. For example, the change in force in the x-direction can be expressed as follows:

$$\Delta X\left(\mathrm{u},\dot{\mathrm{u}},.....,\delta_e,\dot{\delta}_e\right)=.\Delta u+\frac{\partial X}{\partial \dot{u}}.\Delta\dot{u}+.....\frac{\partial X}{\partial \delta_e}.\Delta\delta_e+H.O.T \tag{2.58}$$

The term $\frac{\partial X}{\partial u}$ is called the stability derivative and is evaluated at the reference flight condition. The contribution of the change in the velocity u in the X force is $\frac{\partial X}{\partial u}.\Delta u$.

The term can be expressed in terms of stability coefficient C_{xu} as follows:

$$\frac{\partial X}{\partial u}=C_{xu}.\frac{1}{u_0}Q.S \tag{2.59}$$

2.6 Control Derivatives and Coefficients

The control derivatives and coefficients represent the maneuverability of the aircraft. Control derivatives and coefficients relate the aircraft forces and moments to the deflection of the control surfaces. Since there are primarily three control surfaces and the throttle lever (elevator, throttle lever, aileron, and rudder), all the control derivatives and coefficients are functions of deflection of any of these control surfaces. The related control derivatives and coefficients used are included in Appendix A.

2.7 Damping and Natural Frequency

The damping and the natural frequencies of both short period and long period mode can be determined in terms of stability derivatives, and they describe the handling qualities of aircraft motion.

Both damping and frequency are functions of stability derivatives and, therefore, are functions of aircraft geometric and aerodynamic characteristics. The damping and frequency for the different modes of aircraft motion namely short-period mode, long-period or phugoid mode, roll mode, spiral mode, and dutch roll mode, are listed below:

2.7.1 Longitudinal Stability

I. Short-Period Mode

$$\text{Frequency,} \quad \omega_{nsp} = \sqrt{\frac{Z_\alpha M_q}{u_0} - M_\alpha} \tag{2.60}$$

$$\text{Damping ratio,} \quad \zeta = -\frac{M_q + M_{\dot{\alpha}} + \frac{Z_\alpha}{u_0}}{2\omega_{nsp}} \tag{2.61}$$

II. Long-Period Mode

$$\text{Frequency,} \quad \omega_{np} = \sqrt{\frac{-Z_u . g}{u_0}} \tag{2.62}$$

$$\text{Damping ratio,} \quad \zeta = \frac{-X_u}{2\omega_{np}} \tag{2.63}$$

2.7.2 Lateral Stability

I. Dutch Roll Mode

$$\text{Frequency,} \quad \omega_{nDR} = \sqrt{\frac{Y_\beta . N_r - N_\beta Y_r + u_0 . N_\beta}{u_0}} \tag{2.64}$$

$$\text{Damping ratio,} \quad \zeta_{DR} = -\frac{1}{2\omega_{nDR}}\left(\frac{Y_\beta + u_0 . N_r}{u_0}\right) \tag{2.65}$$

II. Spiral-Mode and Roll-Mode

Spiral-mode and roll-mode are non-oscillatory motions. The characteristic roots for these motions are as follows:

$$\lambda_{spiral} = \frac{L_\beta . N_r - L_r . N_\beta}{L_\beta} \tag{2.66}$$

$$\lambda_{roll} = L_p = -\frac{1}{\tau} \tag{2.67}$$

Where, τ is the roll time constant and L_p is the roll damping.

2.8 Aircraft Handling Qualities

It is mandatory that an aircraft shall be capable of being flown throughout its intended flight envelope, and in all but the severest of weather conditions by an average pilot. The pilot must be able to maneuver and to retain control of the aircraft at all times. In the rare event that the pilot loses control, for example in a stall or spin, a safe recovery must be possible. [15]

In order to examine the handling qualities of the aircraft, the simulation results are used to calculate damping ratios and natural frequencies as discussed earlier.

As a result of a considerable research, target values for damping ratios and frequencies have been set for all the flight levels and flight phase categories of aircraft classes [2].

Aircraft or flight phases with damping ratios and frequencies deviating from the target values are considered unsatisfactory.

Handling qualities are functions of damping and frequency, and these are functions of stability derivatives and, therefore, are functions of aircraft geometric and aerodynamic characteristics. However, geometry of aircraft can not de changed without effective consequence like increasing weight or reducing the performance.

The designers are faced with the challenge of providing an aircraft with optimum performance that is both safe and easy to fly. One of those challenges is to design an aircraft with high stability and high maneuverability at the same time, which is almost not possible because of the fact that both of them are opposite of each other. To achieve this, the designers need to know what degree of stability and maneuverability is required for the pilot to consider the aircraft safe and flyable.

CHAPTER 3
TECHNICAL APPROACH

The main objective of this thesis is to examine the aircraft motion and its response to input forces either by the pilot or atmospheric conditions. One of the most useful and acceptable tools used for aircraft performance evaluation is the simulation, where the motion of the aircraft is expressed in a mathematical model. Simulation of aircraft dynamics allows the designers to study the dynamic characteristics of the aircraft in advance, before carrying out any flight tests [14]. This significantly reduces the risk, cost and the time needed for automatic flight control system design and development and evaluation of new airplanes.

With the help of simulation, the design of control systems such as autopilot and Stability Augmentation System (SAS) will be easer and nearly actual before actual flight test or building subsystems hardware.

The aircraft used in this work is Aero L-39. Choosing the model was one of the most interesting stages of the research. The model, aircraft category and type, affects the nature of the results and then the requirements of design development and the design of control systems. What is fit for a jet airliner may not be suitable and reliable for fighter etc.

The mathematical model and solution method is independent of aircraft type, the difference is introduced with the model geometric data and stability derivatives.

Aero L-39 is a subsonic jet used as a trainer with high stability and as a fighter with high maneuverability, so it can give an impression of how the performance of an aircraft in the same category might be. However, there is no information published for the values of its stability and control derivatives, this thing was the first challenge facing this search. Evaluating stability and control derivatives of L-39 begin with collecting formulas, charts and equations from several references [1,2,3,4 and 5] regarding aircraft stability and control. In order to validate the values of stability and control derivatives, the results from L-39 were compared with an aircraft in the similar category and geometry Aermacchi M-311. The

specification of M-311 and its stability derivatives compared with those of L-39 are presented in appendix B. The results of the simulation are then validated based on data on the aircraft flight characteristics manual.

3.1 Aircraft Specification and Geometry

The aircraft used for this search is an advanced jet training aircraft, Aero L-39. The specifications and flight performance of Aero L-39 are shown in table 3.1.

Table 3.1 The Specifications and Flight Performance of L-39.

Manufacturer	Aero Vodochody - The Czech Republic
Type	Double seater in tandem – advanced jet training aircraft and ground supporter.
Length	12.13 m
Height	4.77 m
Wing span	9.12 m
Wing area	18.8 m^2
Wing aerodynamic chord	2.15 m
Wing sweepback angle at 25 % chord	1.75 deg.
Wing dihedral	2.5 deg.
Wing profile	NACA 64A012
Empty weight	3467 kg
Max. take-off weight	5600 kg
Max. fuel capacity	1400 l / 980 kg
Engine	Ivtchenko AI-25 TL
Thrust	1720 kg at sea level.
Rate of climb at sea level.	22 m/s
Max. speed	910 km/hr
Stalling speed	165 km/hr (with flaps fully extended)
Service ceiling	11,500 m
Range with internal fuel	1000 km.

The geometry of L-39 is shown in Figure 3.1

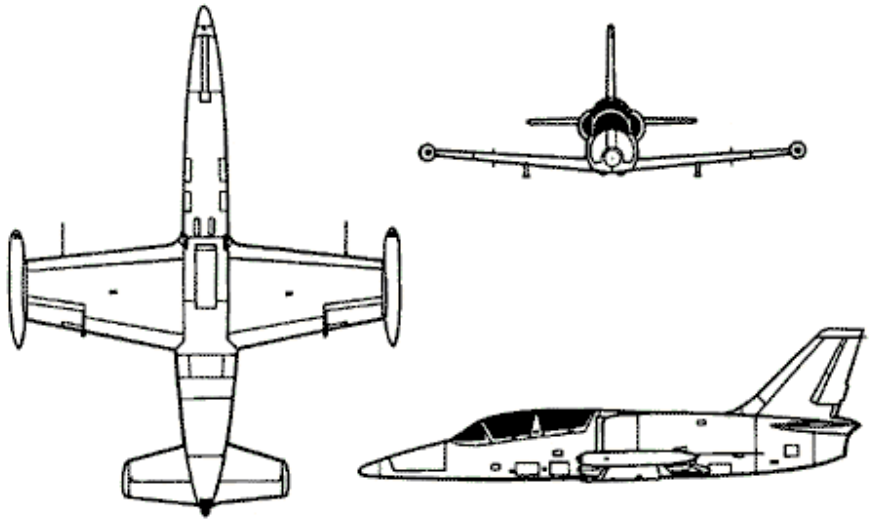

Figure 3.1 Geometry of L-39

3.2 Aircraft Mathematical Model

The accuracy of a simulation depends on the accuracy of the mathematical model. If the derived mathematical model is accurate, the simulation will give the desired reliable results. In an aircraft control system design, any changes in the mathematical model usually involve changes in the geometry, aerodynamic characteristics and performance of the aircraft. The mathematical model used in this thesis is the state-space model. The state-space model is represented by the following equations [1]:

State equation, $\dot{x} = Ax + B\eta 1$ (3.1)

Output equation, $\dot{y} = C.x + D.\eta 1$ (3.2)

where, A is the system matrix, B is the input matrix, C is the output matrix, D is the matrix to represent direct coupling between input and output, x is the vector

containing aircraft states $x = f\left(u, \alpha, q, \theta, \beta, p, r, \varphi\right)$, and $\eta 1$ is the input vector (δ_e, δ_T, δ_a, δ_r)

The non-linear simulation provided in this study is valid for any speed and altitude within the aircraft flight envelope expected while carrying on test flights. The non-linear simulation is different from linear simulations in that the linear simulation is performed with stability and control derivatives valid at only one speed and altitude. Therefore, it provides information at only one condition. In other words, the method considers the non-linearity of aircraft dynamic response at different speed and altitude. However, this method introduces a relatively simple approach for the non-linear simulation of aircraft motion.

Two data sets are prepared for the simulation. The first one is to define and calculate aircraft geometric and aerodynamic characteristics including the definition of atmosphere up to the altitude of aircraft service ceiling. The second set of data is the stability and control derivatives as a function of speed and altitude.

3.3 Linearization of Aircraft Model

The elements of the matrices forming the state-space model are linearized at each time step by using an interpolating routine used as a part of the simulation code. Both conditions of aircraft motion namely longitudinal and lateral-directional can be represented in state-space form, following systems are thus obtained [2]:

Linearized Longitudinal Model

$$\begin{bmatrix} \Delta\dot{u} \\ \Delta\dot{w} \\ \Delta\dot{q} \\ \Delta\dot{\theta} \end{bmatrix} = \begin{bmatrix} X_u & X_w & 0 & -g \\ Z_u & Z_w & u_0 & 0 \\ M_u + M_{\dot{w}}.Z_w & M_w + M_{\dot{w}}.Z_w & M_q + M_{\dot{w}}u_0 & 0 \\ 0 & 0 & 1 & 0 \end{bmatrix} . \begin{bmatrix} \Delta u \\ \Delta w \\ \Delta q \\ \Delta\theta \end{bmatrix} + \begin{bmatrix} X_{\delta e} & X_{\delta T} \\ Z_{\delta e} & Z_{\delta T} \\ M_{\delta e} + M_{\dot{w}}.Z_\delta & M_{\delta T} + M_{\dot{w}}.Z_{\delta T} \\ 0 & 0 \end{bmatrix} . \begin{bmatrix} \Delta\delta_e \\ \Delta\delta_T \end{bmatrix}$$

(3.3)

Linearized Lateral-Directional Model

$$\begin{bmatrix} \Delta\dot{\beta} \\ \Delta\dot{p} \\ \Delta\dot{r} \\ \Delta\dot{\phi} \end{bmatrix} = \begin{bmatrix} \frac{Y_\beta}{u_0} & \frac{Y_p}{u_0} & -\left(1-\frac{Y_r}{u_0}\right) & \frac{g.\cos\theta_0}{u_0} \\ L_\beta & L_p & L_r & 0 \\ N_\beta & N_p & N_r & 0 \\ 0 & 1 & 0 & 0 \end{bmatrix} . \begin{bmatrix} \Delta\beta \\ \Delta p \\ \Delta r \\ \Delta\phi \end{bmatrix} + \begin{bmatrix} 0 & \frac{Y_{\delta r}}{u_0} \\ L_{\delta a} & L_{\delta r} \\ N_{\delta a} & N_{\delta r} \\ 0 & 0 \end{bmatrix} . \begin{bmatrix} \Delta\delta a \\ \Delta\delta r \end{bmatrix} \qquad (3.4)$$

In each model, the A matrix consists of stability derivatives and the B matrix consists of control derivatives. The input vector in the longitudinal model consists of elevator and throttle deflections ($\Delta\delta e$, $\Delta\delta T$) respectively, while in the lateral-directional model the input vector consists of aileron and rudder deflections ($\Delta\delta a$, $\Delta\delta r$) respectively.

The model used in the present thesis combines both of these models into one, forming a single state-space model that represents both the longitudinal and the lateral-directional motions of the aircraft.

However, the combination of longitudinal and lateral-directional models into one model does not mean that these motions are coupled. The combination is done in such a way that the longitudinal and lateral-directional motions remain uncoupled, by solving longitudinal and lateral states separately in state-space matricides.

3.4 Stability and Control Derivatives and Coefficients

The stability and control derivatives and coefficients are simply the elements of the matrices of the state-space form, which can be calculated from a set of equations, parameters and charts collected from several references related to aircraft stability [1, 2, 3 and 4]. The equations used to calculate derivatives and coefficients are listed in appendix A

3.5 Programming of the Simulation

The aircraft geometry, atmosphere and derivatives and coefficients discussed in previous sections written as M-files and performed in MATLAB.

The flight envelope of L-39 is defined as a function of speed and altitude limits, the limits of speed are from 0.15 to 0.85 Mach, and the altitude range is from 0 to 11,500 m. The limits are presented as a vector matrix in the M-file code.

The derivatives in the look-up tables are interpolated to determine the derivatives at the desired altitude and speed. The interpolating program has been written in 'C' programming language and is included in appendix C. The simulation is performed using SIMULINK. The SIMULINK model utilizes an S-Function block [12] that works as the built-in state-space block and calculates the output using A, B, C, and D matrices.

For the purpose of the present thesis, C matrix is taken as an identity matrix of the size of the A matrix. The S-function block needs to be programmed in C language. This is then compiled using the Mex facility in MATLAB, also performing the required interpolation and giving the different outputs at each time step of simulation. Each output belongs to a different altitude and/or speed.

The SIMULINK model and subsystems are shown in the following Figures:

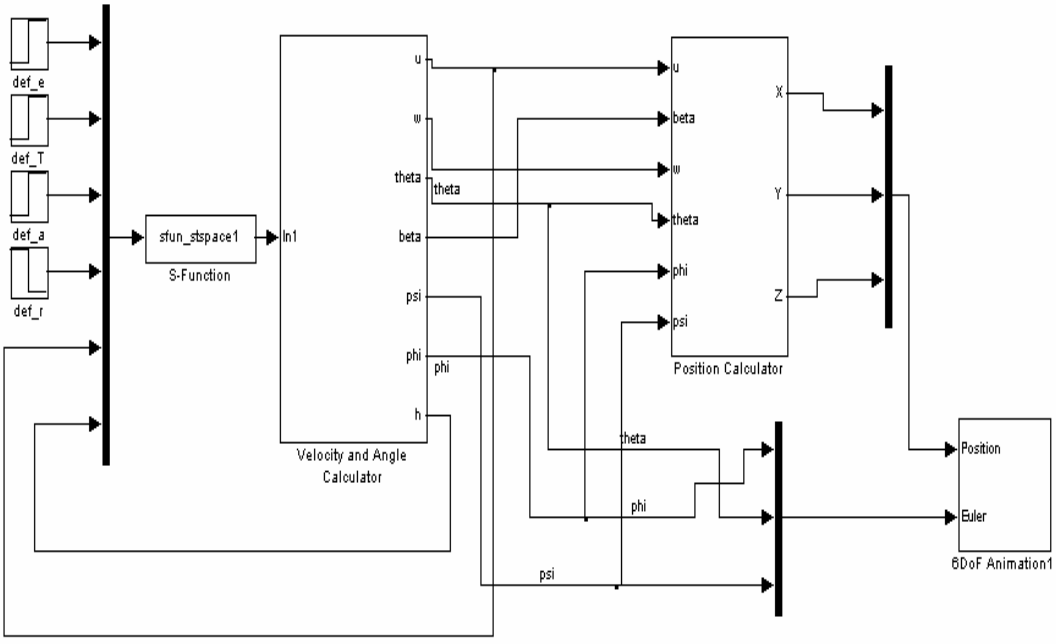

Figure 3.2 SIMULINK Model.

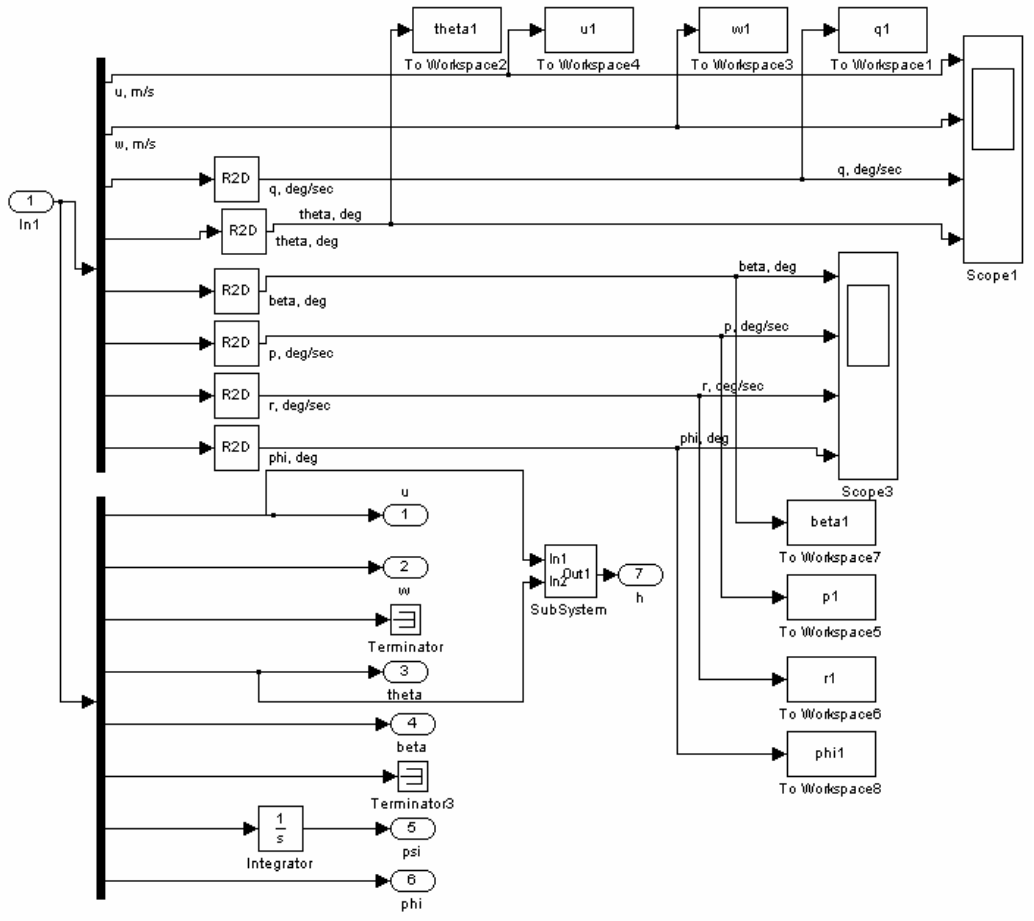

Figure 3.3 A Subsystem to Calculate Speed and Altitude.

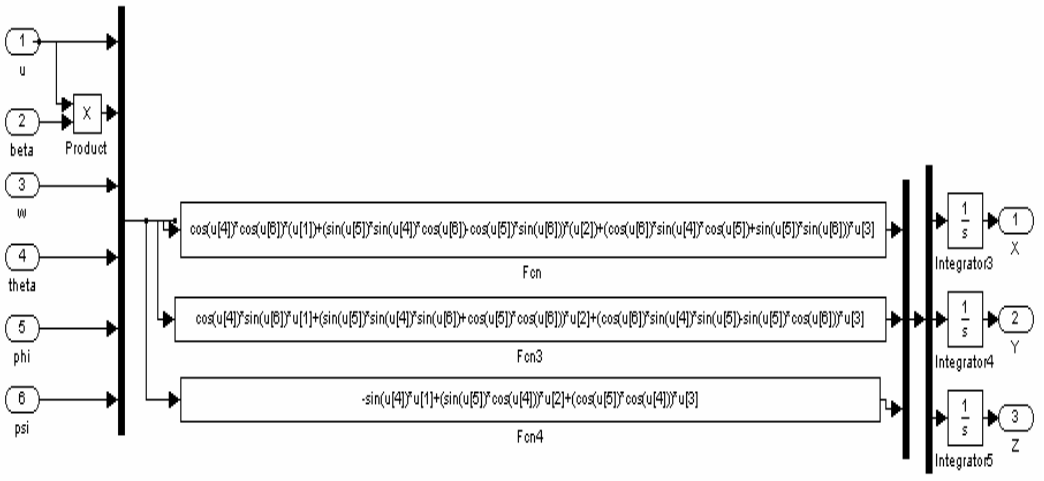

Figure 3.4 A Subsystem to Calculate Aircraft Position.

3.6 Virtual Flight Test

Carrying out virtual flight test by simulation can be started by inserting the initial flight conditions. These are mainly the speed and altitude. Some other parameters can be considered also as initial such as aircraft mass, air temperature and density.

The response of the aircraft will start to appear after pilot input on (elevator, rudder, aileron, or throttle lever deflection), and will manifest itself as a change in altitude and/or speed. Changes in speed and/or altitude are fedback to the model. The S-function calculates the new speed and altitude and performs the required interpolation to find the derivatives at the new speed and the altitude. The response of the aircraft varies accordingly.

Simulation of the aircraft motion can be observed in the scope plots and animation picture. The plots show the dynamic behaviors of the aircraft at each simulation step. The dynamic behavior displayed in the plots includes the behavior of the aircraft speed, angle of attack, pitch rate, pitch angle, sideslip angle, roll rate, yaw rate and roll angle with respect to time following a pilot input. The animated picture shows the six-degree-of-freedom motion of the aircraft with respect to the inertial frame.

The results of simulation can be saved in the MATLAB work space so that it can be used and analyzed where needed.

CHAPTER 4
RESULTS AND DISCUSSION

As discussed earlier, performing a simulation aims at showing the dynamic response of aircraft to pilot input or other inputs such as atmospheric gusts. Thus, the effect of those inputs on the aircraft dynamic response can be determined before building the first prototype. The satisfactory response of the aircraft on simulation implies that the derived mathematical model is representative of the aircraft motion. Since the mathematical model used depends on geometric and aerodynamic characteristics, a satisfactory response of the aircraft in a validated simulation also provides a good prediction of the acceptability of airplane design. Simulation results can be used to predict the handling qualities of the aircraft as well.

Simulation results are classified in two categories, longitudinal flight and lateral flight results, and are shown in the scope plots and/or in a visual animation 3D model.

The flowchart presented in Figure 4.1 shows all simulation conditions carried out by the simulation program.

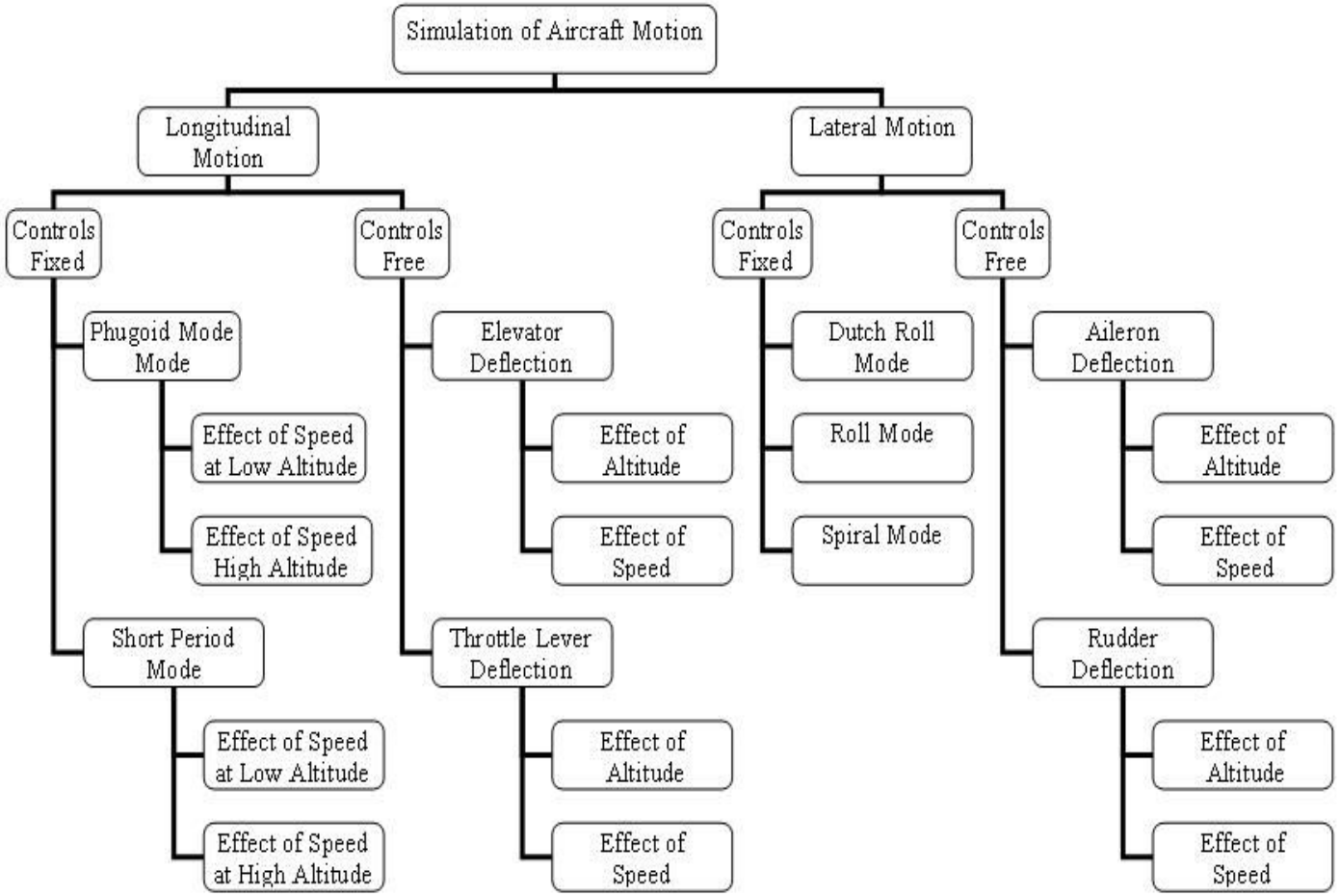

Figure 4.1 Flowchart of Simulation Conditions

The results will be discussed in two cases according to the types of controls as following:

Case I: Controls Fixed; in this case, the aircraft is considered to be disturbed from an initial flight condition, with the controls locked in position. Thus η is zero or constant. All of response periods in this case are found by solving the eigenvalues of the stability matrix.

In order to validate simulation results, the results obtained for this case are compared with results from aircraft characteristics manual.

It can be seen that, in the following plots the range of Mach number used is not the same for all cases because it is the range given by the manufacturer for those cases.

Case II: Controls Free; in this case, the control is presumed to be free as in ‘’hands off”’ by the pilot. This case is of interest primarily manually controlled aircraft as in the case of L-39.

In both cases, the effect of altitude and speed on the aircraft dynamic response will be examined, with all kinds of control inputs for lateral and longitudinal motion.

4.1 Simulation of Longitudinal Motion Modes

In this section the longitudinal motion of the model will be examined for both stick fixed and stick free condition.

4.1.1 Stick Fixed Longitudinal Motion

In the stick fixed case, the values of mode periods are plotted for the whole range of speed and altitude envelope, so that the simulation will give a good prediction for the response performance at any speed and altitude.

4.1.1.1 Phugoid – Long period Modes

a. Phugoid mode at low altitude (500 m)

As shown in Figure 4.2, the simulation results of the aircraft performance follow the results of the aircraft flight characteristics manual. As predicted by Lanchester theory, phugoid period increases with speed and decreases with altitude

at fixed Mach number [1]. The increase in phugoid period with increasing Mach number is mainly due to loss of true static stability, especially at transonic regime when C_{m_u} become negative, as in the case of L-39. With increasing Mach number, C_{m_u} will decrease which will leads to decrease in the term $(M_u + M_{\dot{w}}.Z_w)$ in equation (3.3). The aft shift of aerodynamic center is counted positive. Shifts with Mach number can be determined theoretically [4] or from wind tunnel. This will lead to the fact that at higher Mach numbers, the aircraft has a tendency to put the nose down. This phenomenon is referred to as transonic 'tuck' [3]. In other words, moment due to forward speed M_u will increase with increasing Mach number which will lead the phugoid period to increase with Mach number. All related equations of stability derivatives are presented in appendix A.

The simulation diverges slightly from flight data at high Mach numbers, probably because of compressibility effects becoming significant.

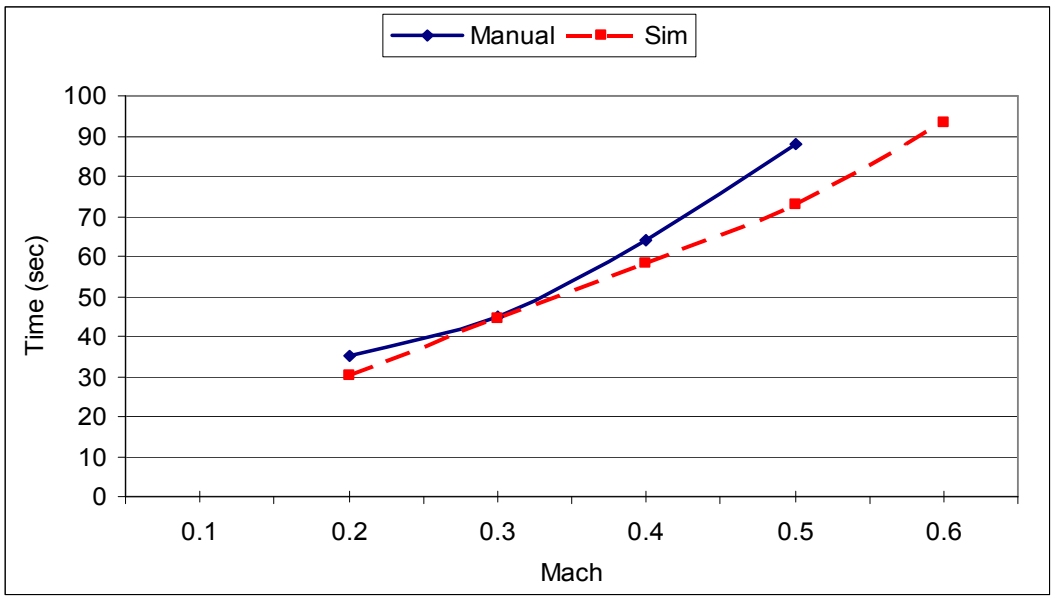

Figure 4.2 Aircraft Response for Longitudinal Stability – Phugoid at 500m.

b. Phugoid mode at high altitude (10,000 m)

At high altitude of 10,000 m which is almost the ceiling of aircraft operation, the period increases with increasing speed as at low altitude. However, it is noted that the period is slightly less for higher altitude, because of the effect lower density at higher altitudes which will lead the value of the dynamic pressure to decrease and as a result the value of M_u will be negative, with taking into account the same reasons in the case of low altitude response. However the response will increase steeply at transonic speeds because of decreasing stability at higher Mach numbers. The range of Mach number shown in Figure 4.3 is the range of available data given in aircraft manual.

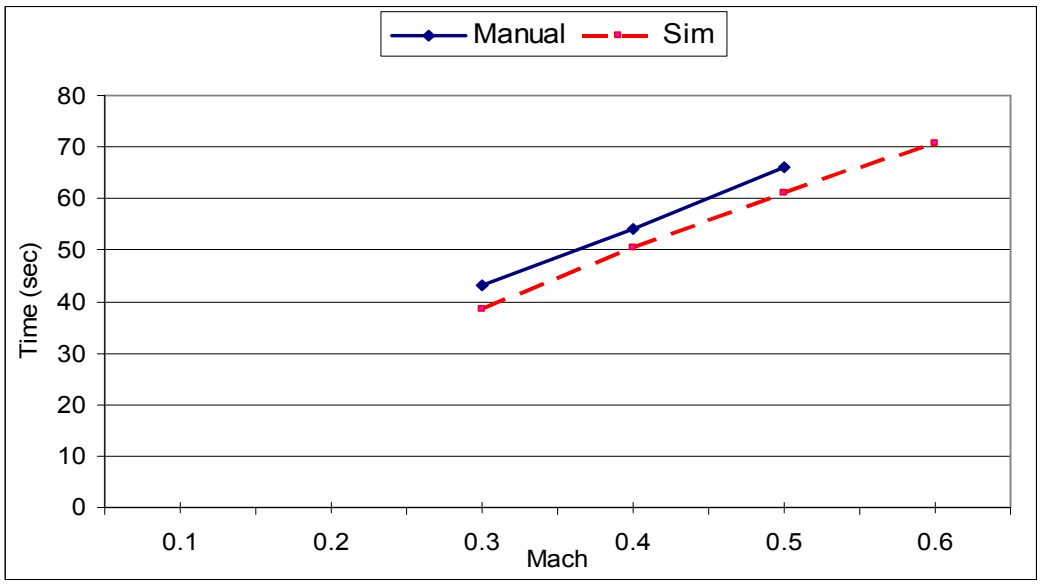

Figure 4.3 Aircraft Response for Longitudinal Stability – Phugoid Mode Damping Time at 10000m

c. Phugoid mode damping to the half at low altitude (500m)

As shown in Figure 4.4, the dynamic response of the aircraft show reduction in damping to the half period with increasing speed which is opposite of the behavior of phugoid mode response. The reason for this behavior can be explained mathematically from the following equation:

$$t_{1/2} = \frac{0.69}{|\eta|} \tag{4.1}$$

$$\eta = -\zeta\omega_n \tag{4.2}$$

Damping to the half can be obtained once the eigenvalues of the characteristic equation are known. The term η in the above equations is the real part of eigenvalues, ζ and ω_n are defined in equations (2.62) and (2.63). The dominant parameter in this case is X_u, the aircraft forward force per unit change in speed, which increase with speed and leads the damping to the half to reduced, as shown in Figure 4.4.

Again, the simulation diverges slightly from flight data at high Mach numbers, probably because of compressibility effects becoming significant.

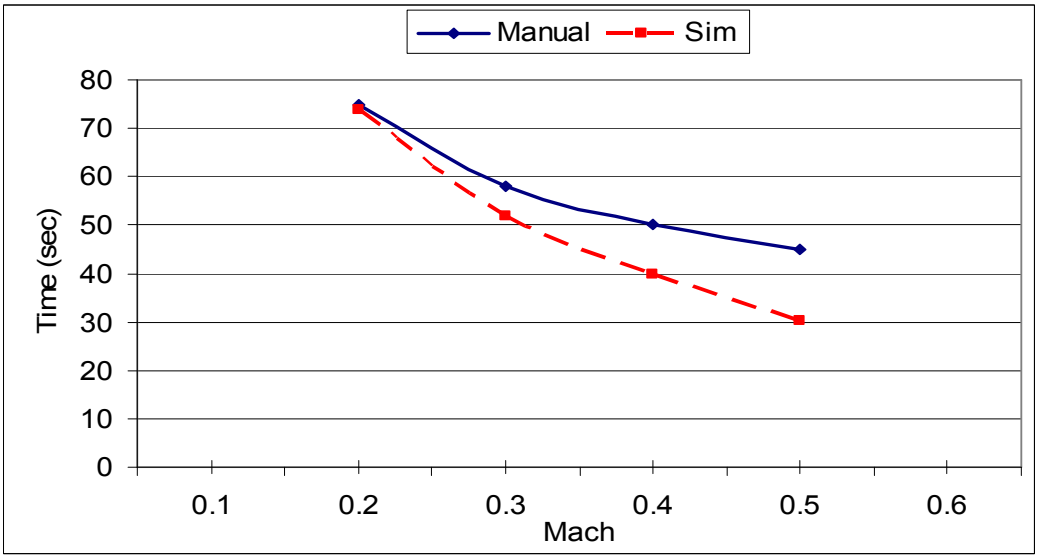

Figure 4.4 Aircraft Response for Longitudinal Stability – Phugoid Mode – Damping to the Half at 500m.

d. Phugoid mode damping to the half at high altitude (10,000m)

As for phugoid mode period at high altitude, and as shown in Figure 4.5, the period of damping to the half tends to increase with increasing speed. Surprisingly the response is opposite to that of low altitude case, because of decreasing X_u with increasing speed at high altitudes, where the low density at that altitude produces lower drag coefficient However, the period will decrease with getting in transonic region, where the drag force shows rapid increase in the value. The response of the transonic region is not supplied by the flight characteristics manual [8].

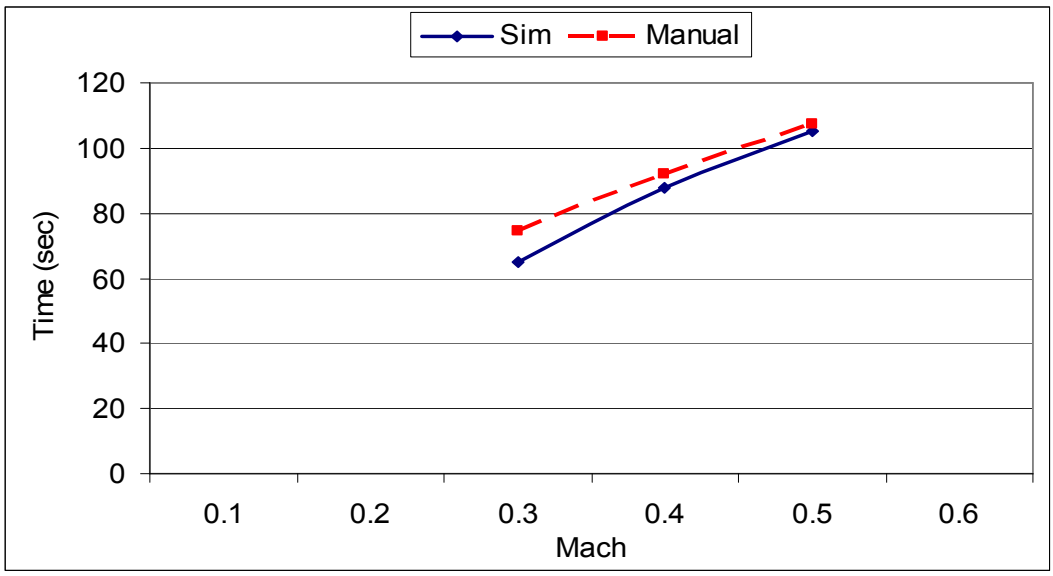

Figure 4.5 Aircraft Response for Longitudinal Stability – Phugoid Mode – Damping to the Half at 10,000 m.

4.1.1.2 Short Period Modes

a. Short period mode at low altitude (500 m)

The short period mode does the opposite behavior of long period mode, decreasing with speed and increasing with altitude [1], the most dominant parameter governing this behavior is the term $M_{\dot{\alpha}} + M_q$, in equation (2.61) where $M_{\dot{\alpha}}$ is change in pitching moment due to rate of change of angle of attack, and M_q is the change in pitching moment due to the pitch rate. Decreasing of this term decreases the

damping by increasing speed equations shown in appendix A. Figure 4.6 show the effect of speed on short period damping.

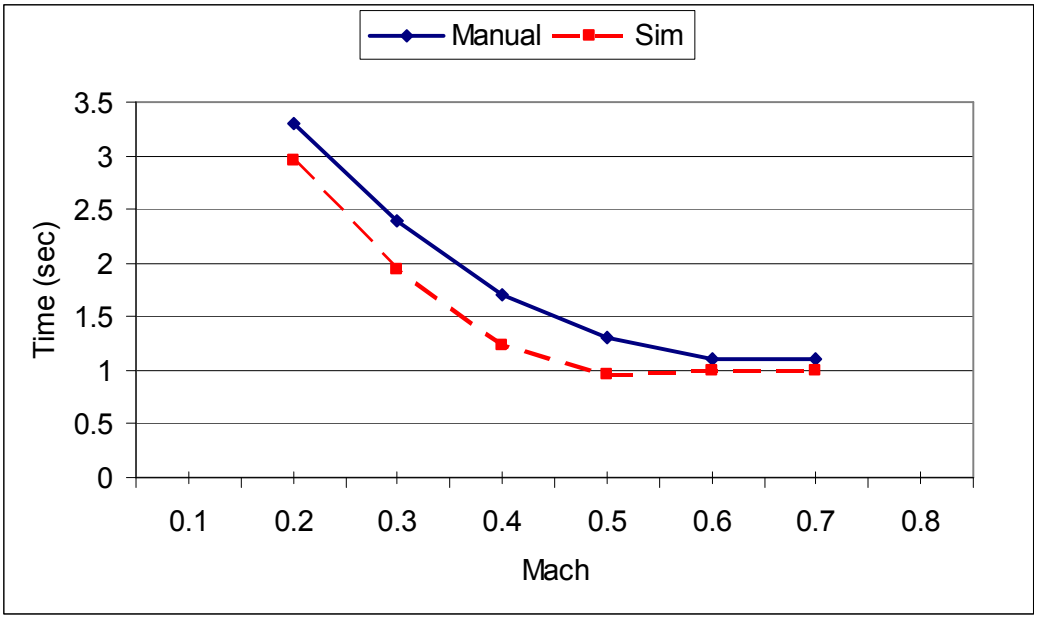

Figure 4.6 Aircraft Response for Longitudinal Stability – Short Mode at 500m.

b. Short period mode at high altitude (10,000 m)

The period of the short mode at high altitude behaves in the same manner of the behavior at low altitude. As shown in Figure 4.7. However, the period will increase with entering the transonic region, because compressibility factor become significant in transonic regime with less drag force at high altitude.

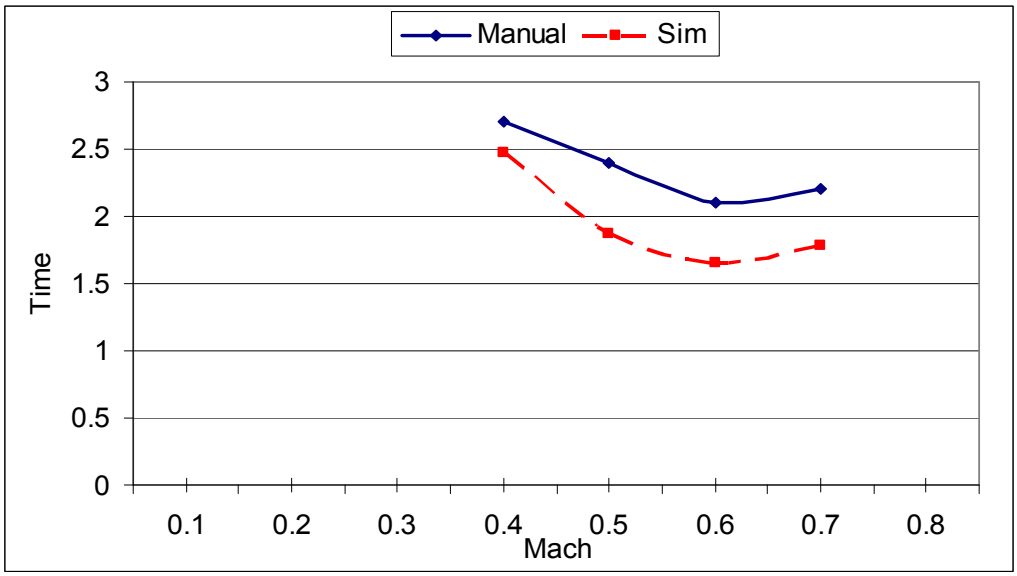

Figure 4.7 Aircraft Response for Longitudinal Stability – Short Period Mode at 10,000 m.

c. Short period mode damping to the half at low altitude (500m)

As in the case of phugoid mode, from equations (4.1) and (4.2), damping to the half can be obtained once the eigenvalues of characteristics equation are known. The real part of eigenvalues of characteristics equation is $\eta = -\zeta\omega_n$, where ω_n and ζ are defined in equations (2.60) and (2.61). The dominant parameter in this case is again the term $(M_{\dot{\alpha}} + M_q)$, which increase with speed and leads to the damping to the half reduce. It can be noted that, the short period mode is not affected directly by the amount of drag force that increases with increasing Mach number, as shown in Figure 4.8.

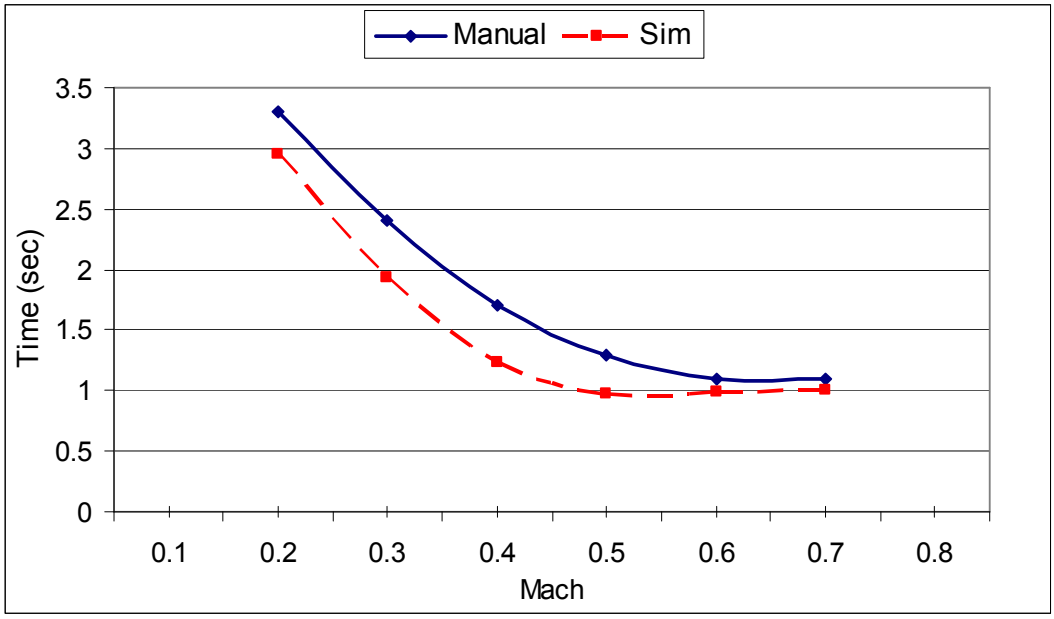

Figure 4.8 Aircraft Response for Longitudinal Stability – Short Period Mode – Damping to the Half at 500m.

d. Short period mode damping to the half at high altitude (10,000m)

As for short period mode at low altitude, the period of damping to the half tends to decrease with increasing speed. As shown in Figure 4.9. This is because short period mode is not affected directly by the amount of drag force that increases with increasing Mach number. However, the period is significantly higher at high altitude than of low altitude. This means that the damping is higher at lower altitudes, and that is why the aircraft shows much better performance at low altitudes at higher rates of density.

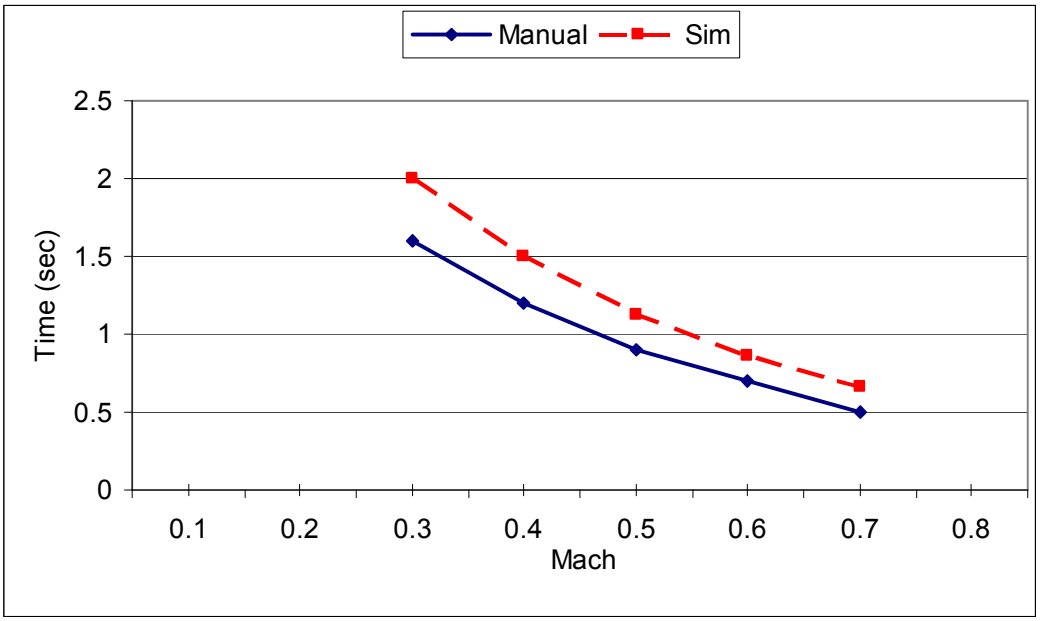

Figure 4.9 Aircraft Response for Longitudinal Stability – Short Period -Damping to the Half at 10,000 m.

4.1.2 Stick Free Longitudinal Motion

The dynamic responses of the longitudinal motion of the aircraft following a pilot input includes changes in the forward speed, vertical speed, pitch rate, pitch attitude, angle of attack, and altitude. The pilot input in this category is step input in elevator or/and throttle lever. Since it is called stick free, the control stick is left free after the input is applied.

4.1.2.1 Aircraft Response Following Elevator Deflection

The pilot input here is deflection of the elevator by amount of one degree step. The simulation is divided into two cases at which the effect of altitude and the effect of airspeed were examined.

Case I. Effect of altitude

In this case the simulation is run twice for two different altitudes, at 10,000m and at 500m at a fixed speed of 500 km/hr (138.8 m/sec).the results are shown in Figures 4.10 - 4.13.

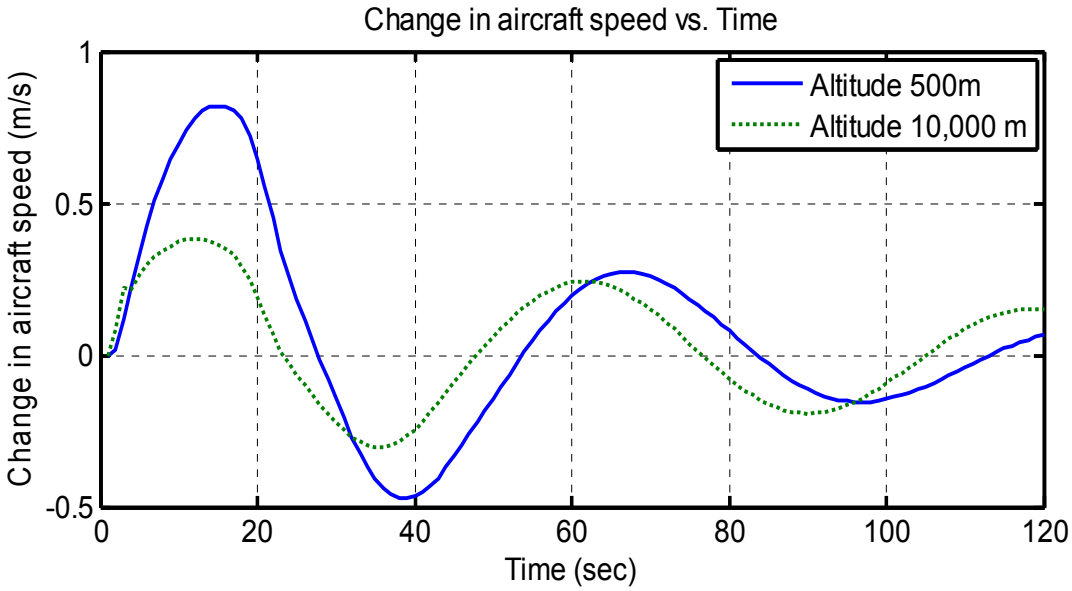

Figure 4.10 Aircraft Speed Response to 1 Degree Step Input in Elevator Deflection at Speed of 500 km/hr and Altitudes of 500m and 10,000m.

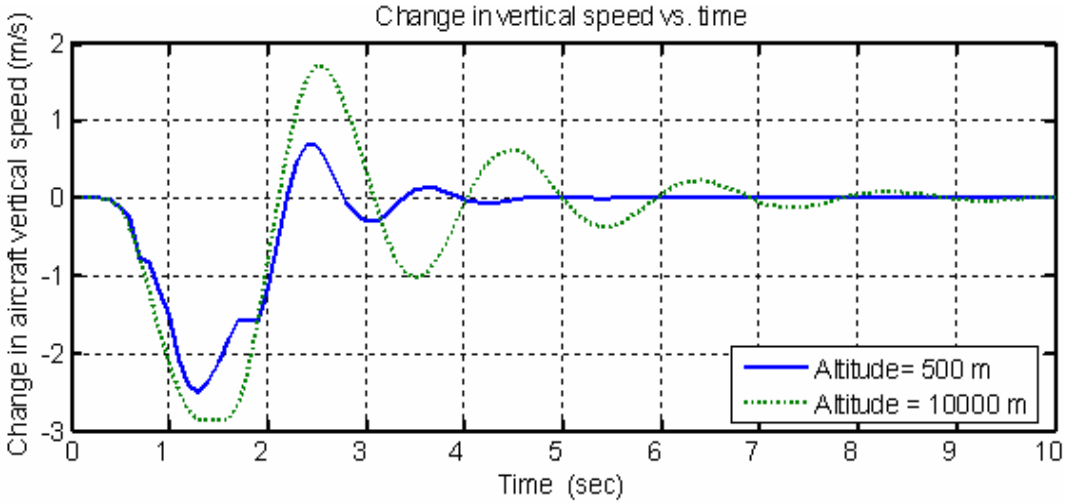

Figure 4.11 Aircraft Vertical Speed Response to 1 Degree Step Input in Elevator Deflection at Speed of 500 km/hr and Altitudes of 500m and 10,000m.

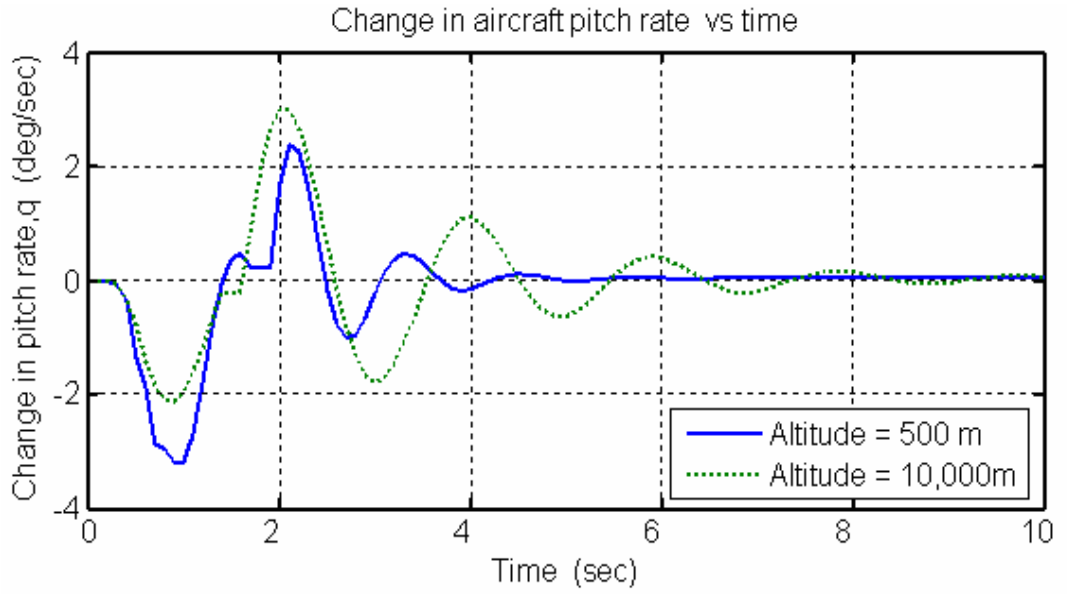

Figure 4.12 Aircraft Pitch Rate Response to 1 Degree Step Input in Elevator Deflection at Speed of 500 km/hr and Altitudes of 500m and 10,000m.

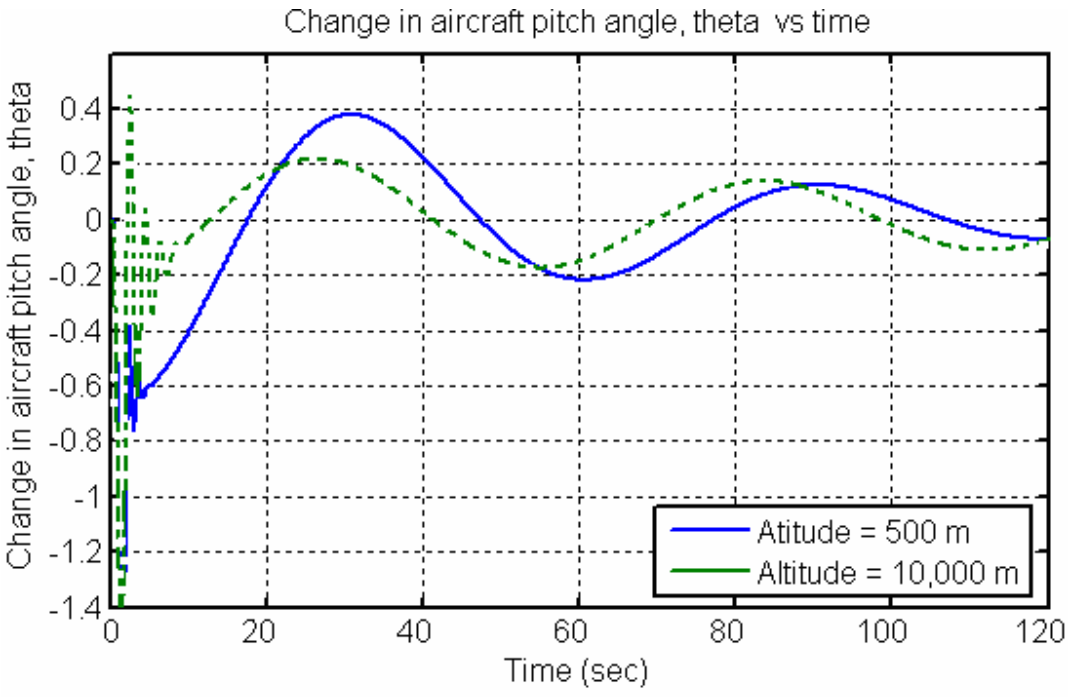

Figure 4.13 Aircraft Pitch Angle Response to 1 Degree Step Input in Elevator Deflection at Speed of 500 km/hr and Altitudes of 500m and 10,000m.

As shown in the previous Figures, dynamic response shows heavy damping and high amplitude at low altitude. The reason is that the magnitude of the aerodynamic forces is higher at low altitude at which the dynamic pressure and density are at their highest levels. However, the situation is the opposite at high altitudes. Mathematically, the forces and moments effecting aircrafts response became low at high altitude because of decreasing density and drag force at the same speed. All equations are presented in appendix A. Practically, the aircraft will show sluggish response at high altitude, that is why this altitude is not recommended for flying L-39.

Case II. Effect of airspeed

In this case the simulation is run twice for two different airspeeds, high speed at 750 km/hr and low speed at 300 km/hr at fixed altitude of 3000m. Those values were chosen because 3000m is the best altitude for L-39 for carrying out aerobatics and maneuvers, 750 km/hr is the maximum cruising speed and 300km/hr is minimum speed at which the aircraft still shows satisfactory handling qualities. The responses are shown in Figures 4.14-4.17:

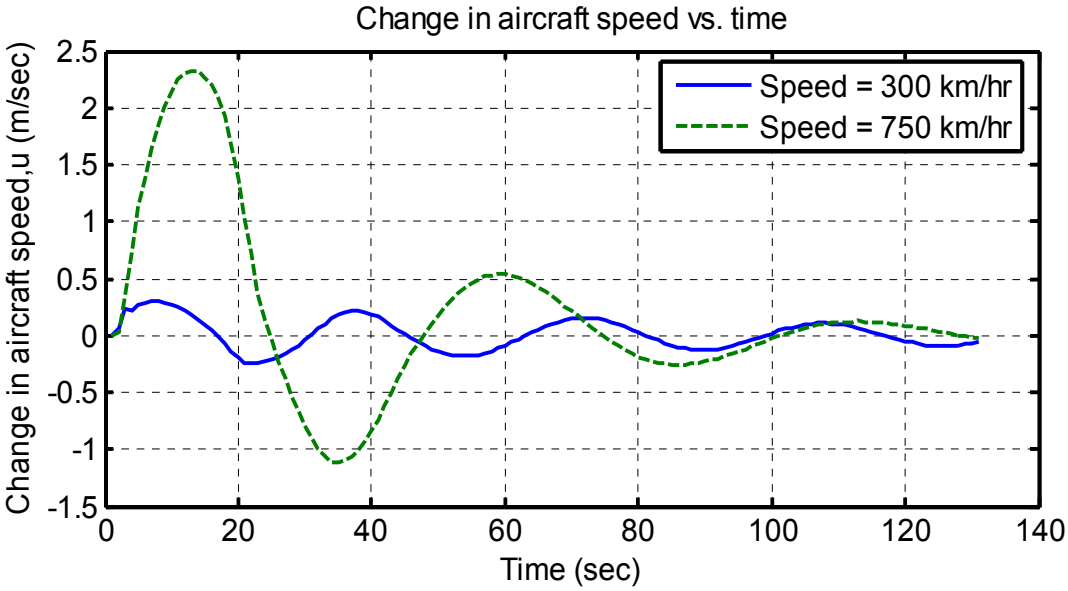

Figure 4.14 Aircraft Angle of Attack Response to 1 Degree Step Input in Elevator Deflection at Altitude of 3000 m. and Speed of 300km/hr and 750 km/hr.

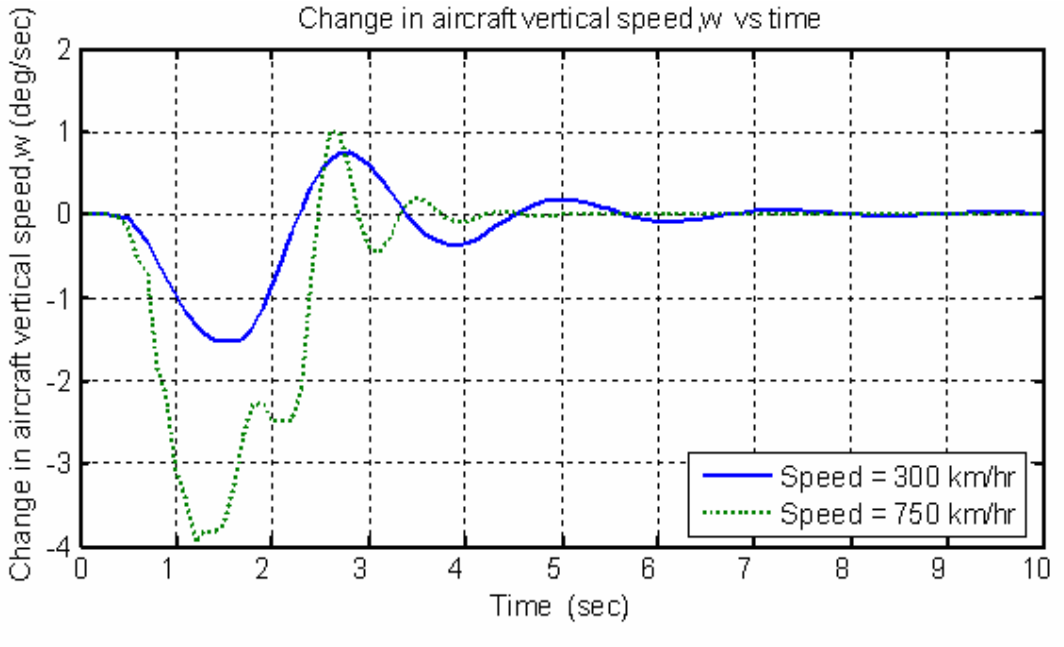

Figure 4.15 Aircraft Vertical Speed Response to 1 Degree Step Input in Elevator Deflection Altitude of 3000 m, and Speed of 300km/hr and 750 km/hr.

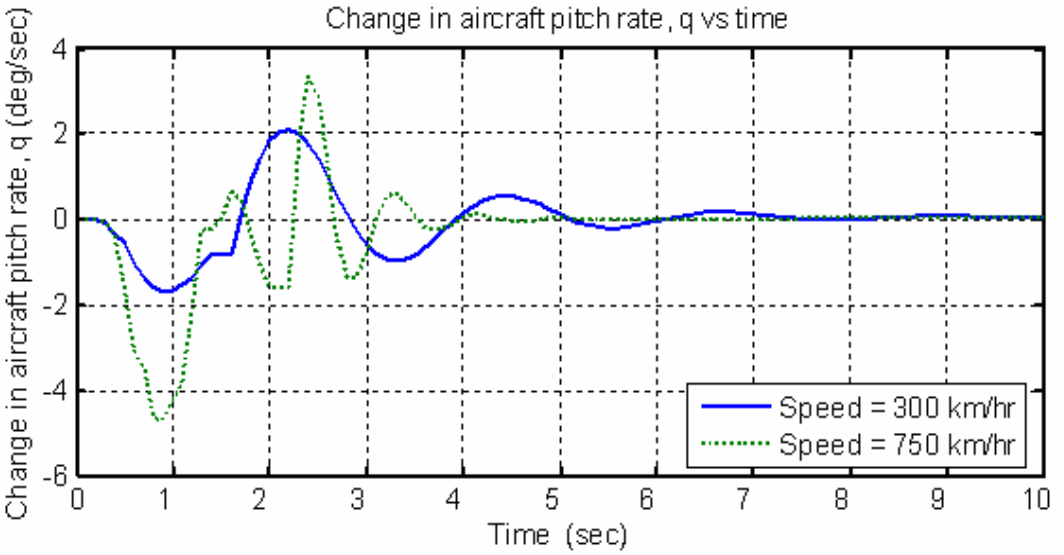

Figure 4.16 Aircraft Pitch Rate Response to 1 Degree Step Input in Elevator Deflection at altitude of 3000 m. and Speed of 300km/hr and 750 km/hr.

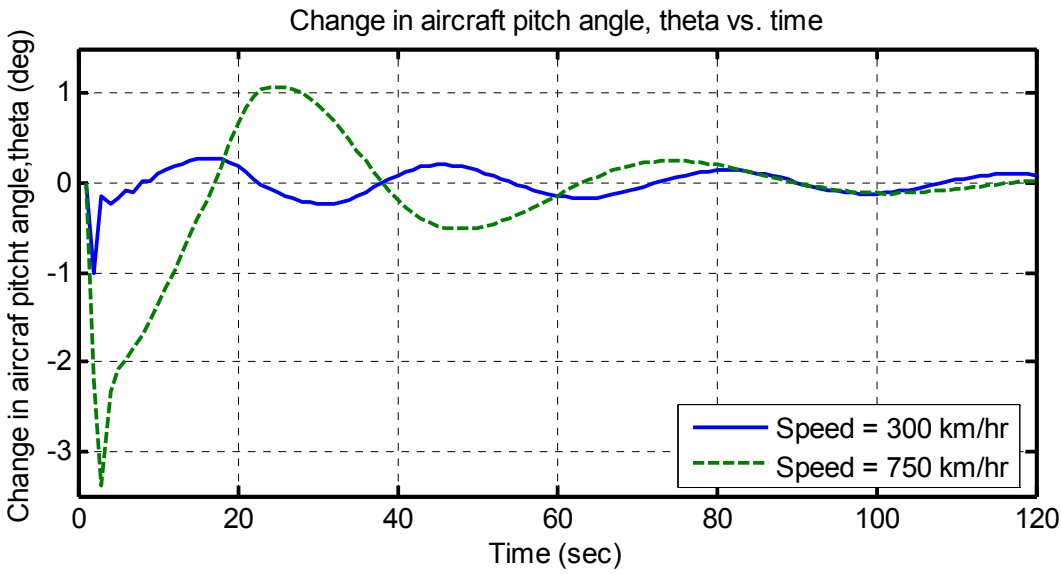

Figure 4.17 Aircraft Pitch Angle Response to 1 Degree Step Input in Elevator Deflection Altitude of 3000 m. and Speed of 300km/hr and 750 km/hr.

The effect of speed on aircraft stability shows high amplitude at high speed and higher damping ratio. However, the time taken to attain original state is almost the same with small differences for the two speeds as plotted and discussed in stick fixed case. This leads to the fact that, settling time is fairly independent of aircraft speed. However, it has a great effect on damping ratio and amplitude of the response. In general, the reason for high value of amplitude, hence the response at high speeds is because of the compressibility factor becoming significant in transonic regime, also with greater aerodynamic forces.

4.1.2.2 Aircraft Response Following Throttle Lever Deflection

The pilot input here is deflecting the throttle lever by amount of 5 degrees step input. The simulation is divided into two cases at which the effect of altitude and the effect of airspeed were examined. The effect of throttle lever deflection shows significant changes at deflection of more than one degree that is why it is taken as 5 deg. The throttle lever movement range is shown in Figure 4.18

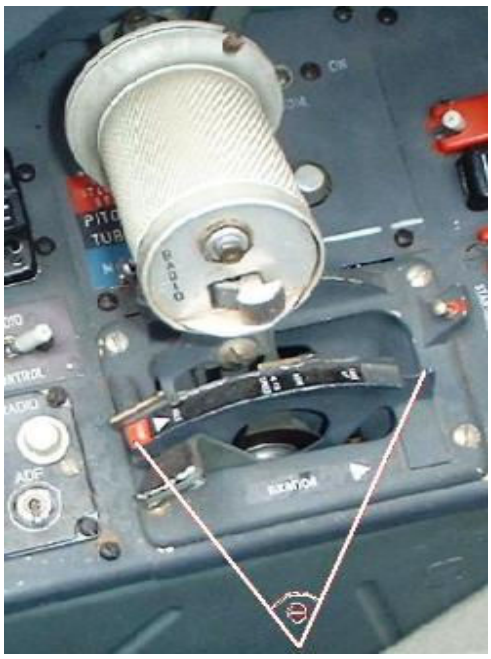

Figure 4.18 Throttle Lever Setting Rang in L-39 Left Side Panel.

To calculate the thrust control derivative ($X_{\delta T}$), it is assumed that the variation in engine thrust vs. throttle setting is linear. The deflection range is 45 deg from idle to maximum RPM, with thrust change from 135 kg at idle position to 1720 kg at maximum position at sea level condition, as shown in Figure 4.19

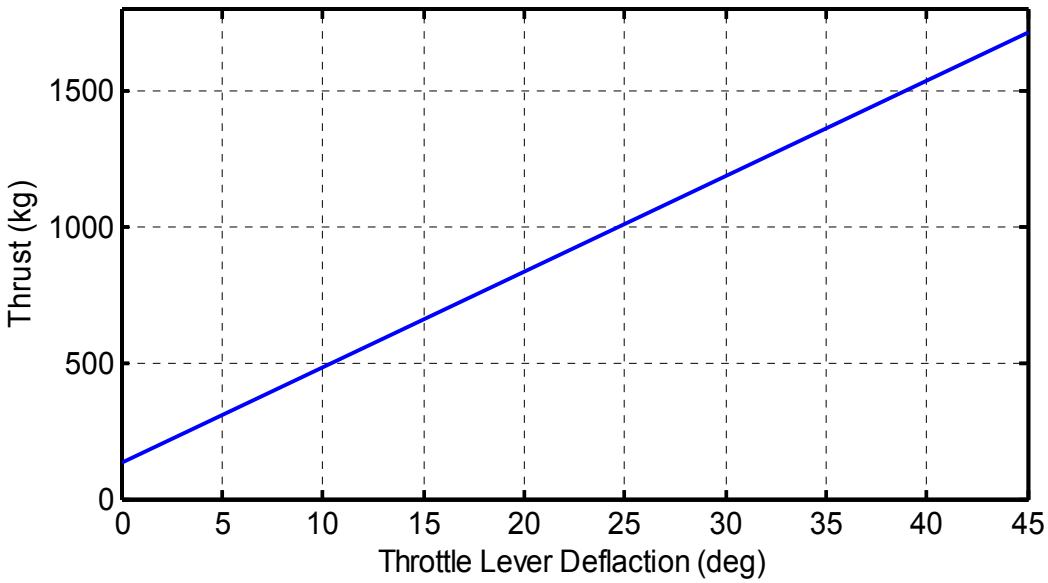

Figure 4.19 Variation of Engine Thrust vs. Throttle Lever Setting.

As it seen in Figure 4.19, the relation between thrust and position of throttle lever can be assumed as a linear. The slope of this curve is thrust control derivative ($X_{\delta T}$), which is calculated to be 2018 kg/rad as follows:

$$X_{\delta T} = \frac{\partial T}{\partial \delta T} = \frac{T_{\max} - T_{idle}}{\delta T_{\max} - \delta T_{idle}}$$
$$= \frac{(1720 - 135)}{45 - 0} = 35.22 kg / \deg$$
$$= 2018.23 kg / rad \div 4200 kg = 0.48(1/rad)$$

Case I. Effect of altitude

In this case, the simulation is performed twice for two different altitudes, at 10,000m and at 500m at fixed speed of 500 km/hr (138.8 m/sec). the results are shown in Figures 4.20 – 4.23:

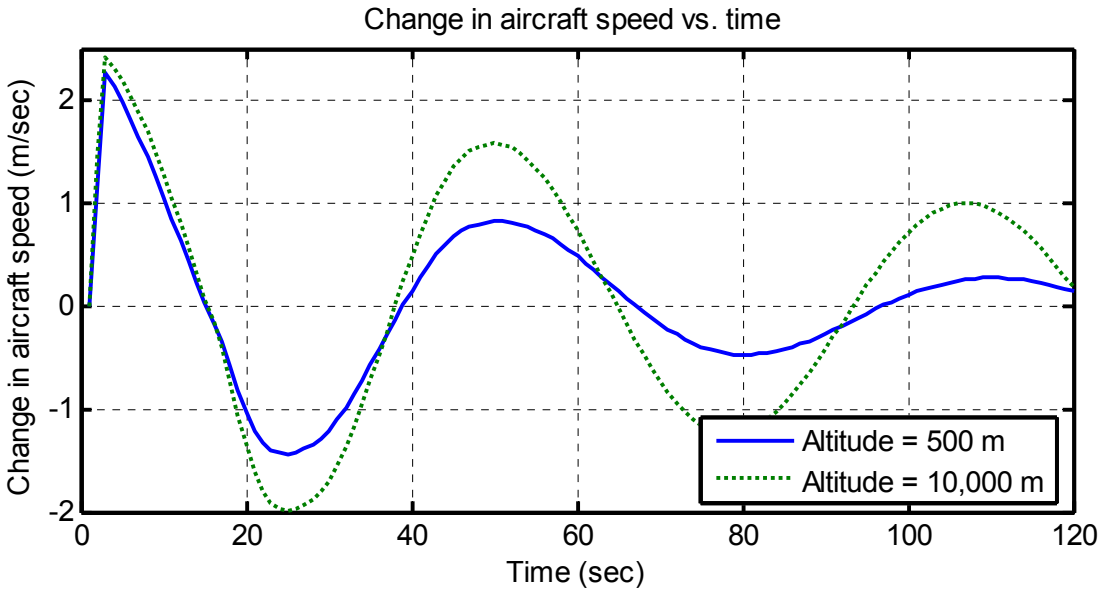

Figure 4.20 Aircraft Airspeed Response to 5 Degree Step Input in Throttle Deflection at Speed of 500 km/hr and Altitudes of 500m and 10,000m.

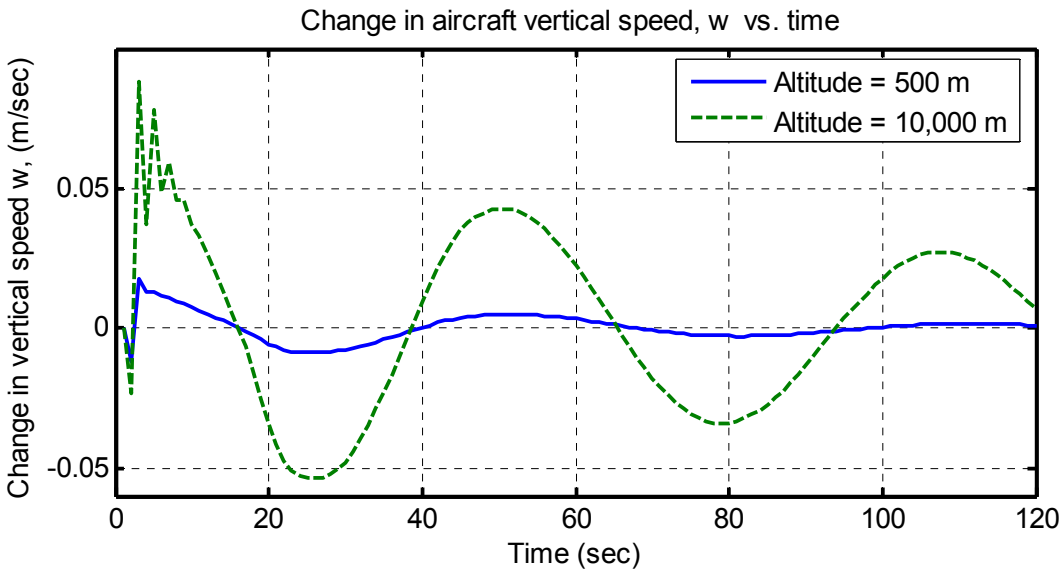

Figure 4.21 Aircraft Vertical Speed Response to 5 Degree Step Input in Throttle Deflection at Speed of 500 km/hr and Altitudes of 500m and 10,000m

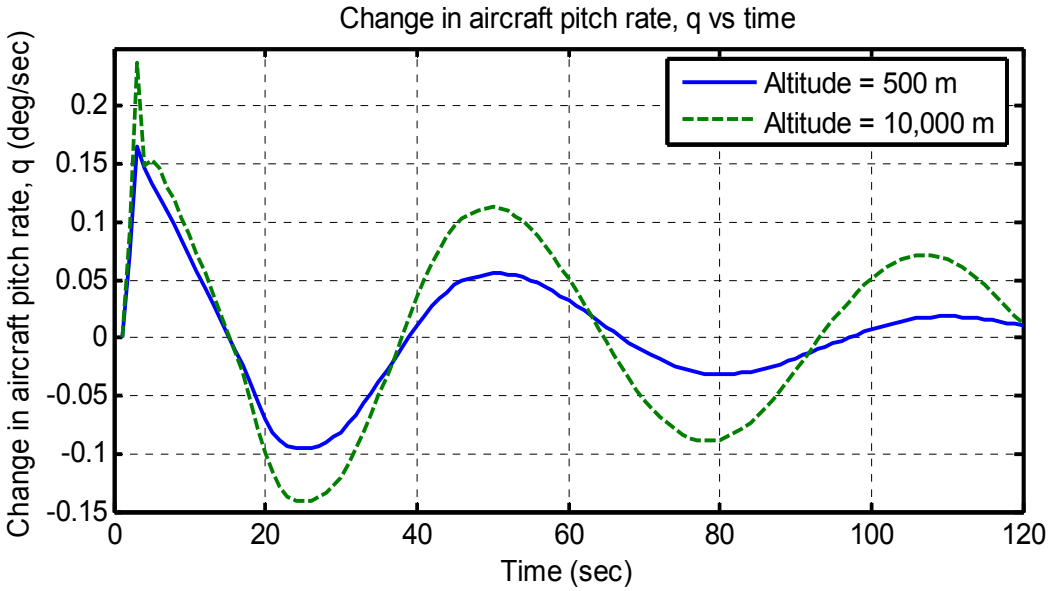

Figure 4.22 Aircraft Pitch Rate Response to 5 Degree Step Input in Throttle Deflection at Speed of 500 km/hr and Altitudes of 500m and 10,000m

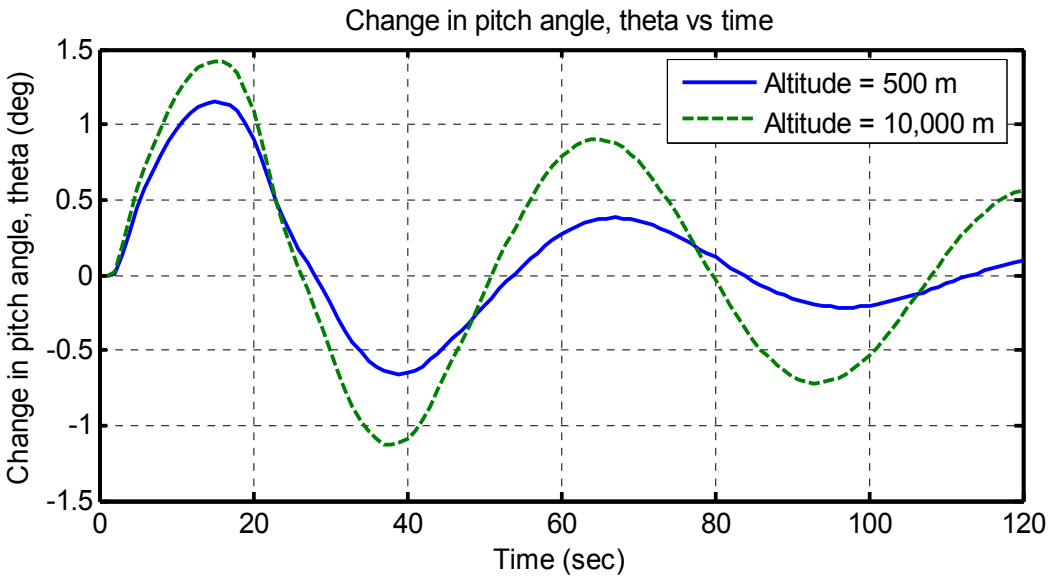

Figure 4.23 Aircraft Pitch Angle Response to 5 Degree Step Input in Throttle Deflection at Speed of 500 km/hr and Altitudes of 500m and 10,000m.

As shown in the previous Figures, and as for the case of elevator deflection, the response shows heavy damping at low altitude, the reason for this case is the same for the case of elevator deflection, however the effect of throttle lever deflection, thus the thrust force is less in effect than that of the elevator in longitudinal motion, that is why it is neglected sometimes for the sake of simplifying the simulation.

Case II. Effect of airspeed

In order to check the effect of speed on throttle lever deflection response, simulation is performed twice for two different airspeeds, as in the case of elevator deflection. The responses are shown in Figures 4.24 – 4.27

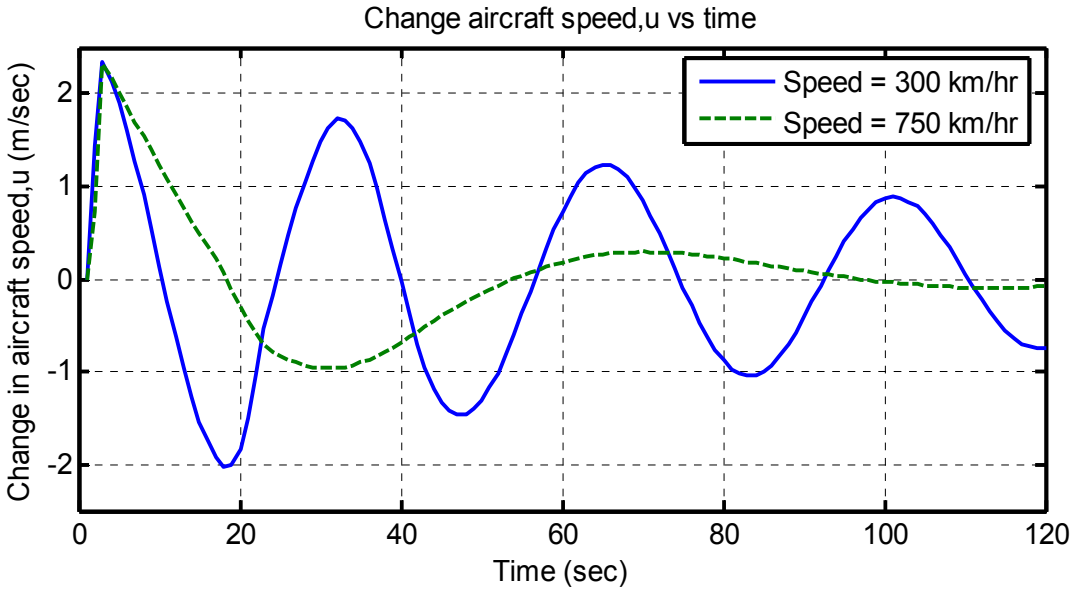

Figure 4.24 Aircraft Speed Response to 5 Degree Step Input in Throttle Lever Deflection Altitude of 3000 m. and Speed of 300km/hr and 750 km/hr.

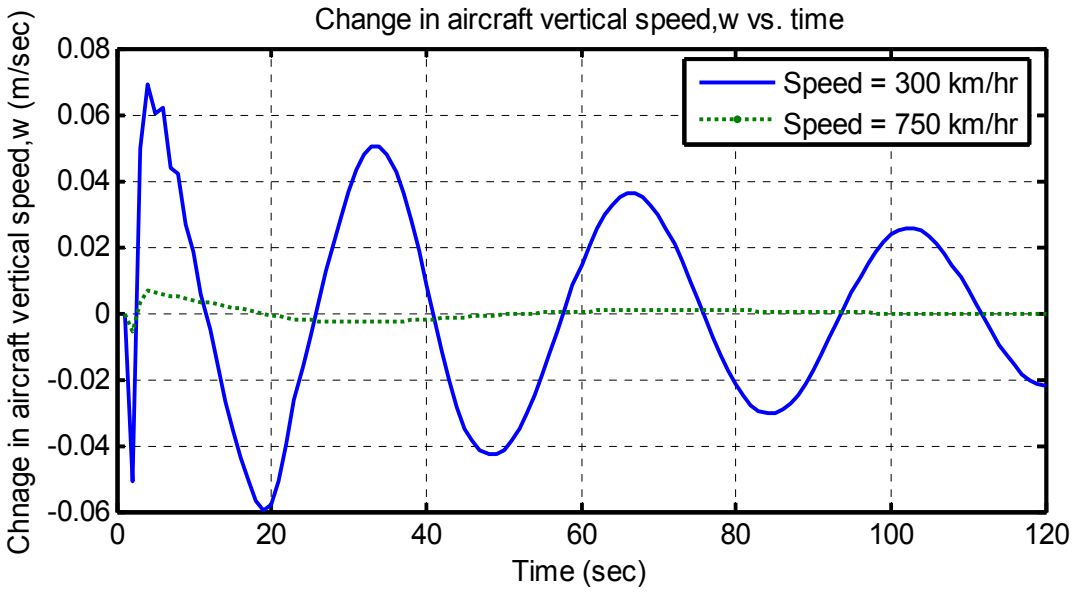

Figure 4.25 Aircraft Vertical Speed Response to 5 Degree Step Input in Throttle Lever Deflection Altitude of 3000 m. and Speed of 300km/hr and 750 km/hr.

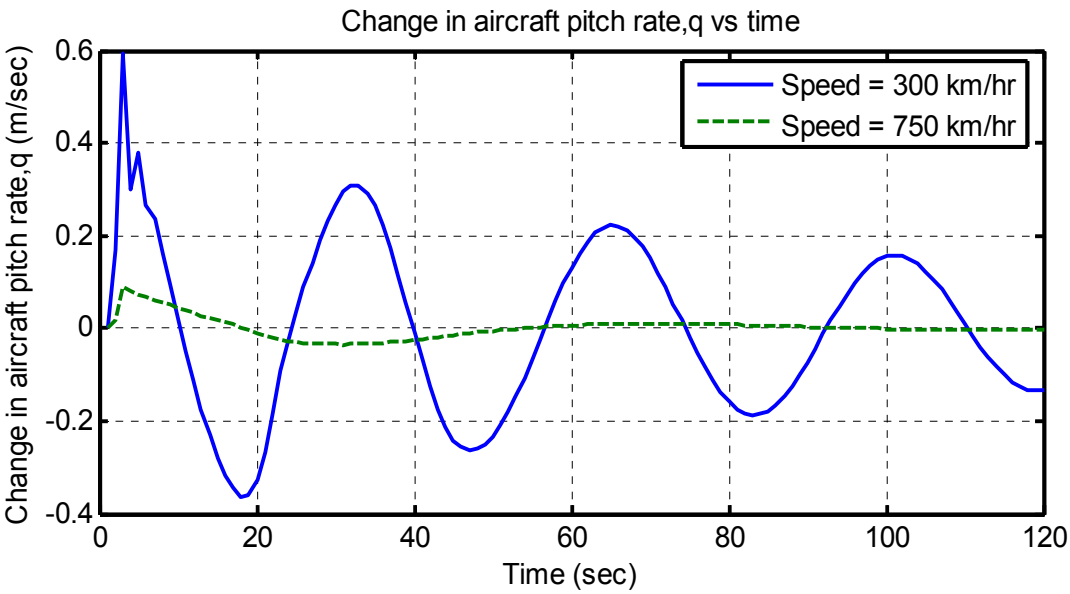

Figure 4.26 Aircraft Pitch Rate Response to 5 Degree Step Input in Throttle Lever Deflection Altitude of 3000 m. and Speed of 300km/hr and 750 km/hr.

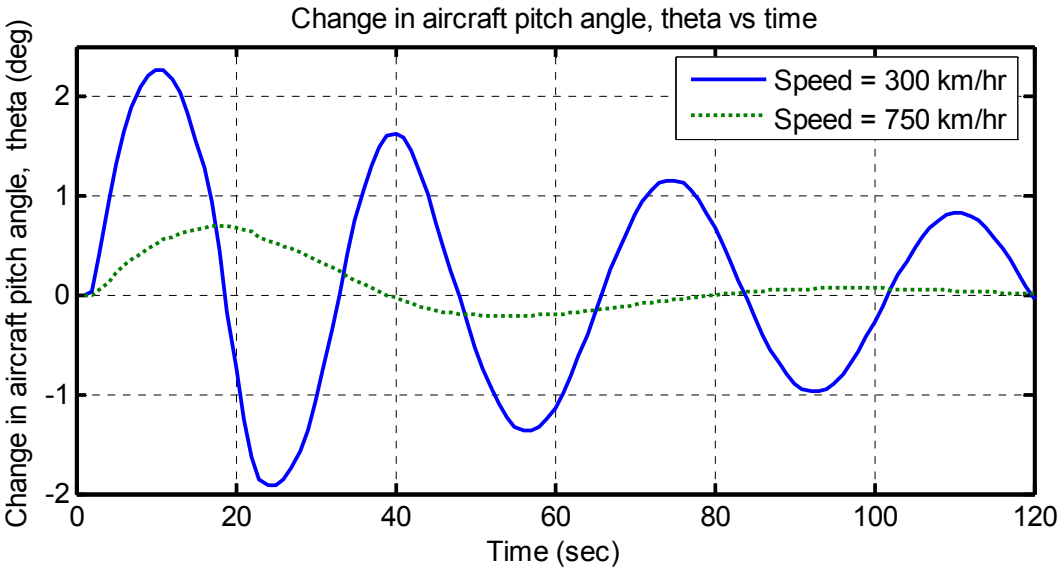

Figure 4.27 Aircraft Angle of Attack Response to 5 Degree Step Input in Throttle Lever Deflection Altitude of 3000m and Speed of 300km/hr and 750 km/hr.

As shown in the previous Figures, the effect of airspeed shows significant difference between high and low speed. The reason of high damping ratio at high speed is because of great effect of dynamic pressure and aerodynamic forces in general. In the case of low speed, the amplitude of the oscillatory motion is high and damping ratio is low because of less dynamic pressure, thus less resistance of aircraft response which leads to longer time to attain its reference flight condition for the aircraft.

4.2 Simulation of Lateral-Directional Motion Modes

In general, the variation of lateral modes with speed and altitude is not simple, because of lateral stability derivatives being dependent on the lift coefficient in complex ways, and also the cross coupling between roll and yaw motions.

Increasing C_L will increase theC_{l_β}, the variation of aircraft rolling moment coefficient with angle of sideslip, [2]. Those effects appear most strongly at low speed and high altitude both of which require high C_L.

In this section, the lateral-directional motion of the model will be examined for both stick fixed and stick free conditions.

4.2.1 Stick Fixed-Lateral Motion

In the stick fixed case, the values of mode periods are plotted for the whole range of speed envelope so that it can give a good prediction for the response performance at any speed and altitude. The initial altitude used here is 3000 m, with aircraft mass of 4000 kg. So that the results can be validated using the flight characteristics manual.

4.2.1.1 Dutch Roll mode Response

The only lateral mode compared with results from the flight manual is the dutch roll mode, because it is the mode supplied by flight characteristics manual. As shown in the next two Figures 4.28 and 4.29.

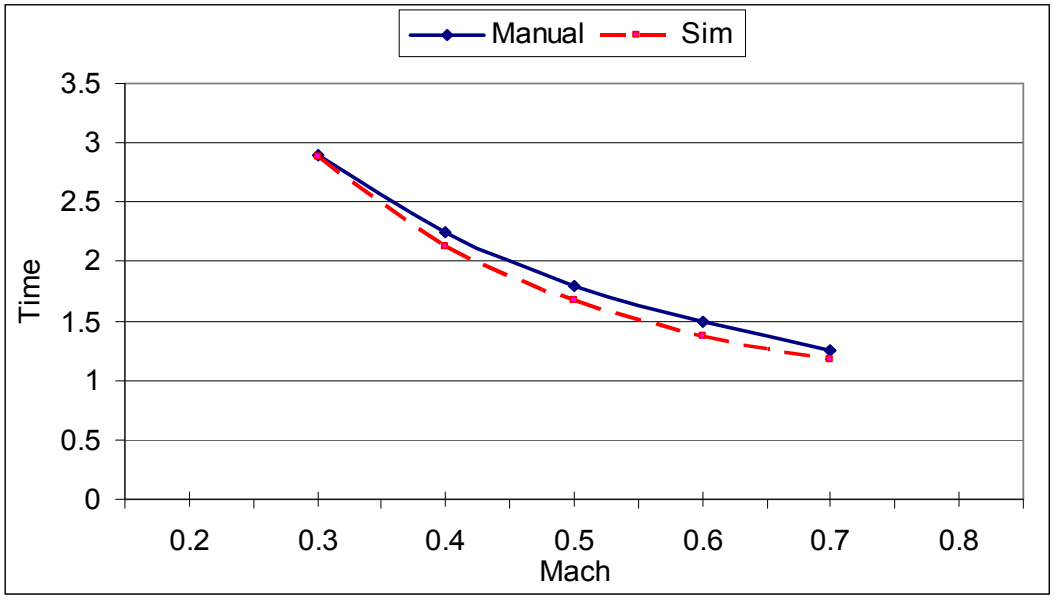

Figure 4.28 Aircraft Lateral Stability Response- Dutch Roll at 3000m.

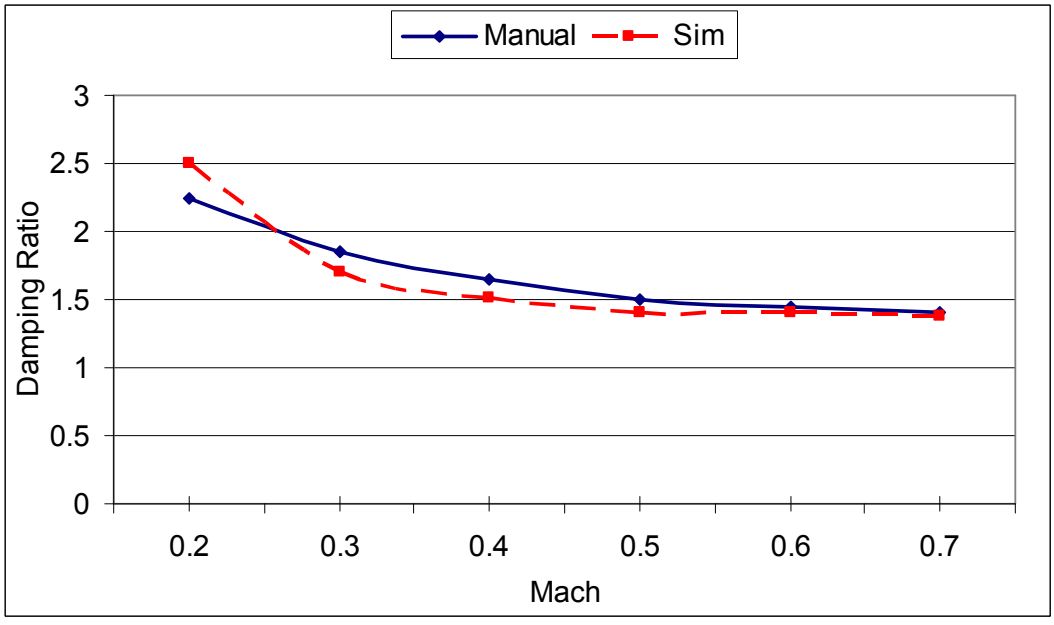

Figure 4.29 Aircraft Lateral Stability Response, Dutch Role Mode Damping Ratio for Two Successive Amplitudes at 3000 m.

Dutch roll mode period decreases with increasing speed. As expected the damping is weak at low speed and increased with as the speed increases. The reason for this can be seen from equations (2.64) and (2.65), at which the angular and lateral

acceleration will increase with speed, leading to the damping time decrease. All equations related to lateral stability coefficients are listed in appendix A.

Even though there are no plots that show the behavior of L-39 in both roll and spiral modes, it is found that, showing them will add wider perspective for lateral motion behavior for this aircraft. Only, damping to the half can be calculated for these cases since these modes are not oscillatory, they are pure convergence (or divergence) modes.

4.2.1.2 Roll Mode Response

The rolling mode response is damped at all speeds, however the damping will increase with speed as shown in Figure 4.30. The reason for this is that, the magnitude of the roll damping derivative L_p, variation with rolling moment with roll rate, which increases with speed.

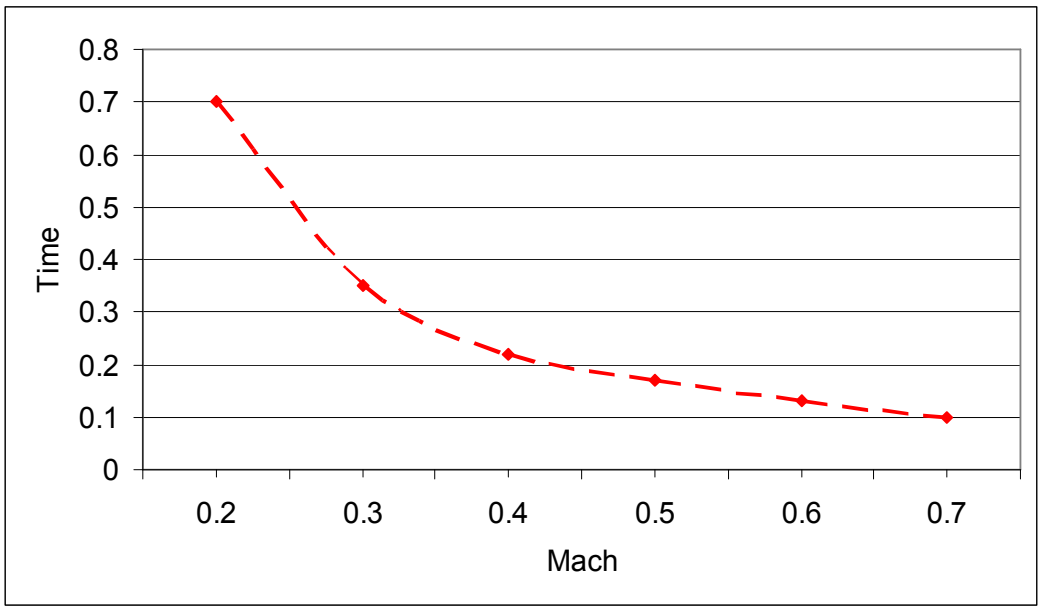

Figure 4.30 Aircraft Lateral Stability Response- Roll Mode Damping to the Half at 3000m

4.2.1.3 Spiral mode response

The spiral mode is frequently unstable over most of the speed range, as shown in Figure 4.31, the damping period keep on increasing as the speed increases. This is probably due to complex variation of C_{l_β} with C_L and Mach number. From equation (2.66) the stability derivative L_β (dihedral effect) and N_r (yaw rate damping), are usually negative. On the other hand, N_β (directional stability) and L_r (roll moment due to yaw rate) are positive, thus, $L_\beta.N_r - L_r.N_\beta \geq 0$, which is not the case for L-39.

However, spiral mode stability can be improved by increasing dihedral effect L_β. For this reason, designing a yaw damper is highly recommended for L-39.

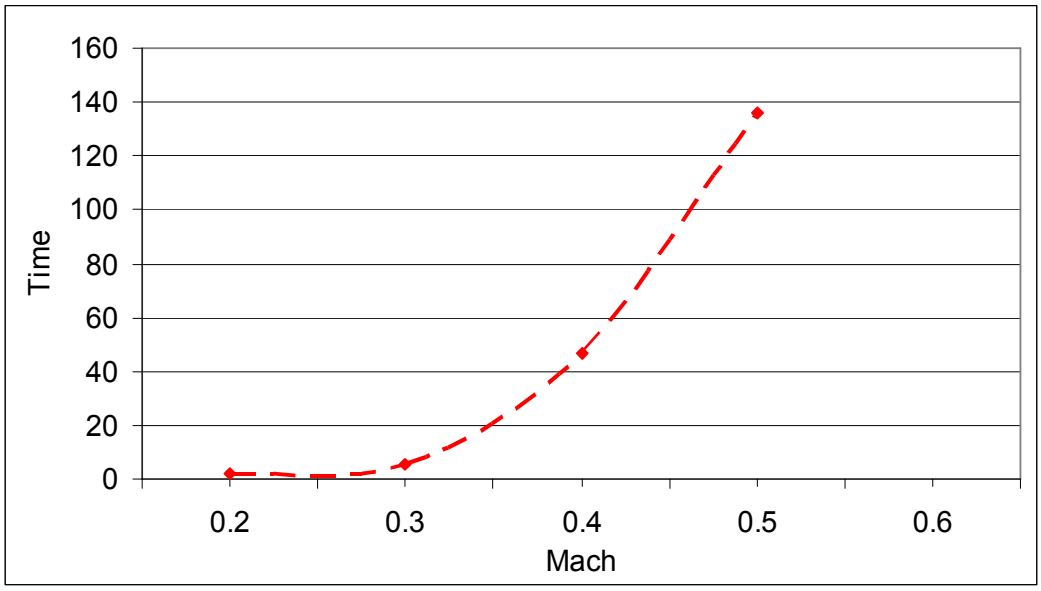

Figure 4.31 Aircraft Lateral Stability Response- Spiral Mode Damping to the Half at 3000m

4.2.2 Stick Free Lateral-Directional Motion

The dynamic responses of the lateral-directional motion of the aircraft following aileron and/or rudder deflection by the pilot cause the values to change in the airplane sideslip angle, roll rate, and yaw rate and bank-roll angle.

The dynamic response of aircraft to lateral motion is observed at some initial speed, altitude, and elevator and rudder deflection angles. The results of these simulations are presented in the following sections.

4.2.2.1 Aircraft Response Following Aileron Deflection

The pilot input here is deflecting the aileron by amount of one degree for duration of one second. The simulation is divided into two cases at which the effect of altitude and the effect of airspeed were examined, in order to examine the effect of altitude and speed changes aircraft response following control inputs.

Case I. Effect of altitude

In this case, the simulation is run twice for two different altitudes, high at 10,000m and low at 500m at fixed speed of 500 km/hr (138.8 m/sec). The results are shown in Figures 4.32 – 4.35.

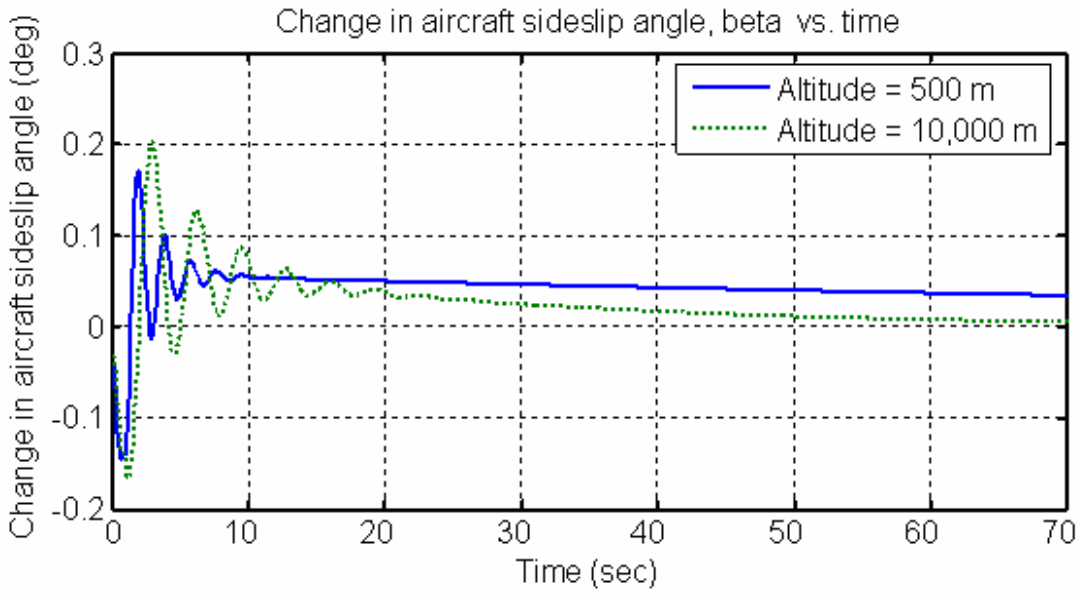

Figure 4.32 Aircraft Sideslip Response to 1 Degree Step Input in Aileron Deflection at Speed of 500 km/hr and Altitudes of 500m and 10,000m.

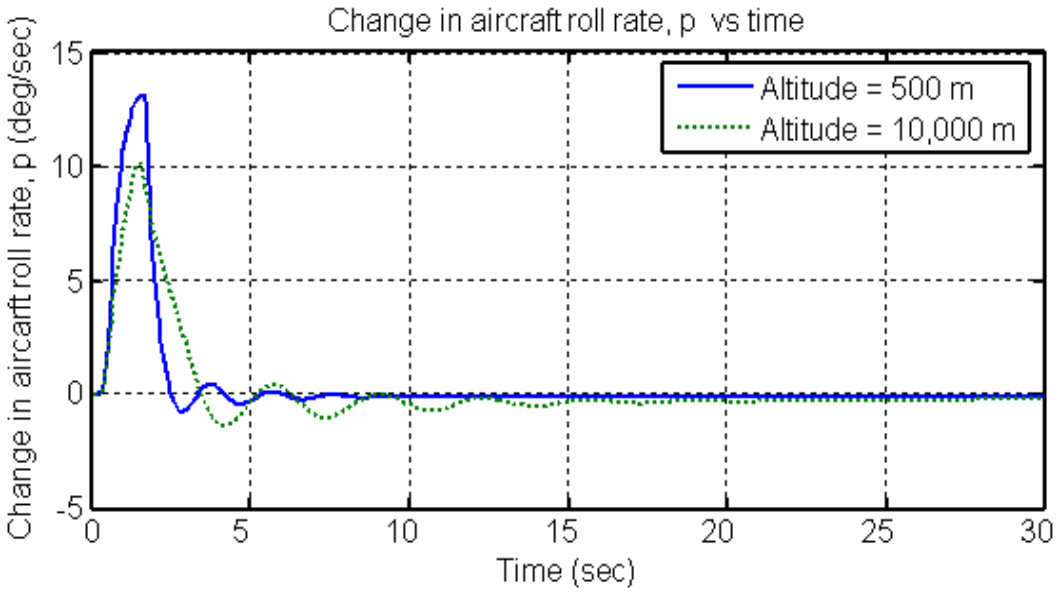

Figure 4.33 Aircraft Roll Rate Response to 1 Degree Step Input in Aileron Deflection at Speed of 500 km/hr and Altitudes of 500m and 10,000m.

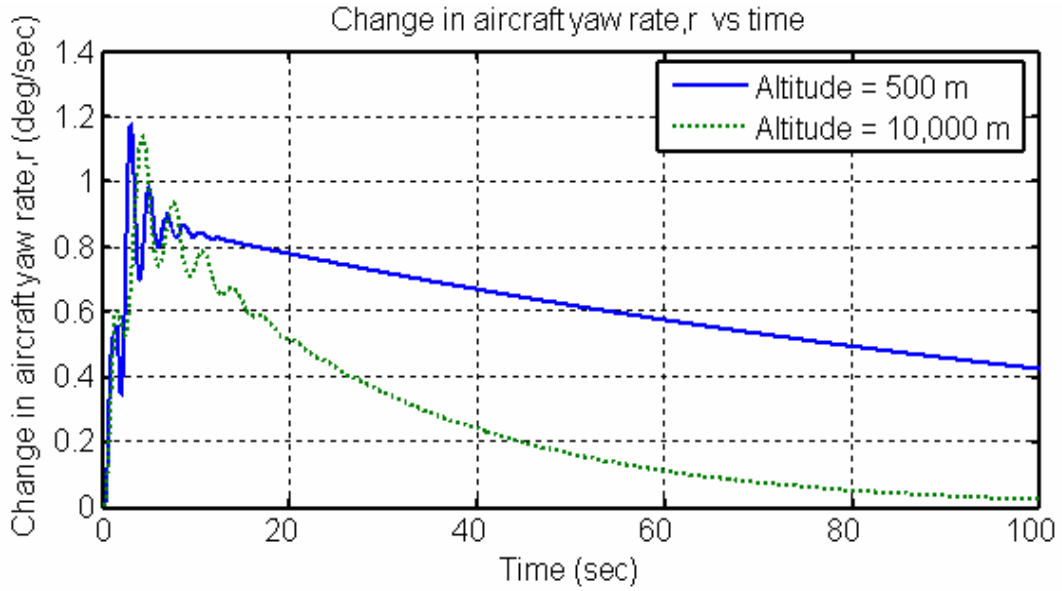

Figure 4.34 Aircraft Yaw Rate Response to 1 Degree Step Input in Aileron Deflection at Speed of 500 km/hr and Altitudes of 500m and 10,000m.

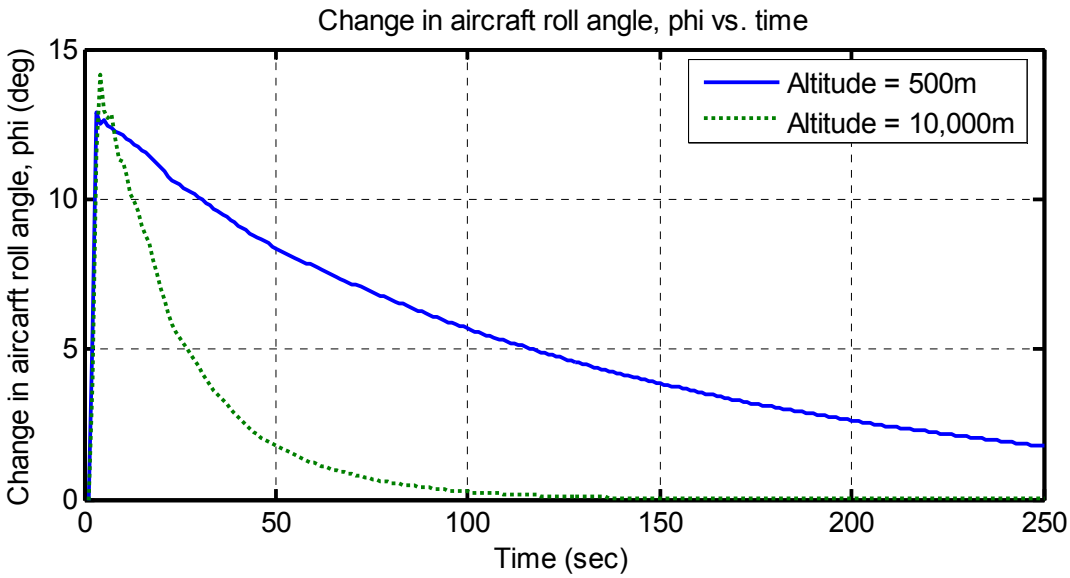

Figure 4.35 Aircraft Roll Response to 1 Degree Step Input in Aileron Deflection at Speed of 500 km/hr and Altitudes of 500m and 10,000m.

As shown in the previous Figures, there is difference in the response of aircraft due to aileron deflection at high and low altitudes, it is clear that the reaction to the aileron deflection is much less at high altitude that leads the aircraft to attain its original attitude faster. However the damping is higher at high altitude because of the lower effect of aerodynamic forces.

Case II. Effect of airspeed

In this case, the simulation is performed twice for two different airspeeds, at 750 km/hr and at 300 km/hr at fixed altitude of 3000m, in the sake of examining the effect of speed on aircraft response following a control input in aileron. Those values were chosen because 3000m is the best altitude for L-39 for carrying out aerobatics and maneuvers, 750 km/hr is the maximum cruising speed and 300 km/hr is minimum speed at which aircraft is still show satisfied controllability. The responses are shown in Figures 4.36 – 4.39

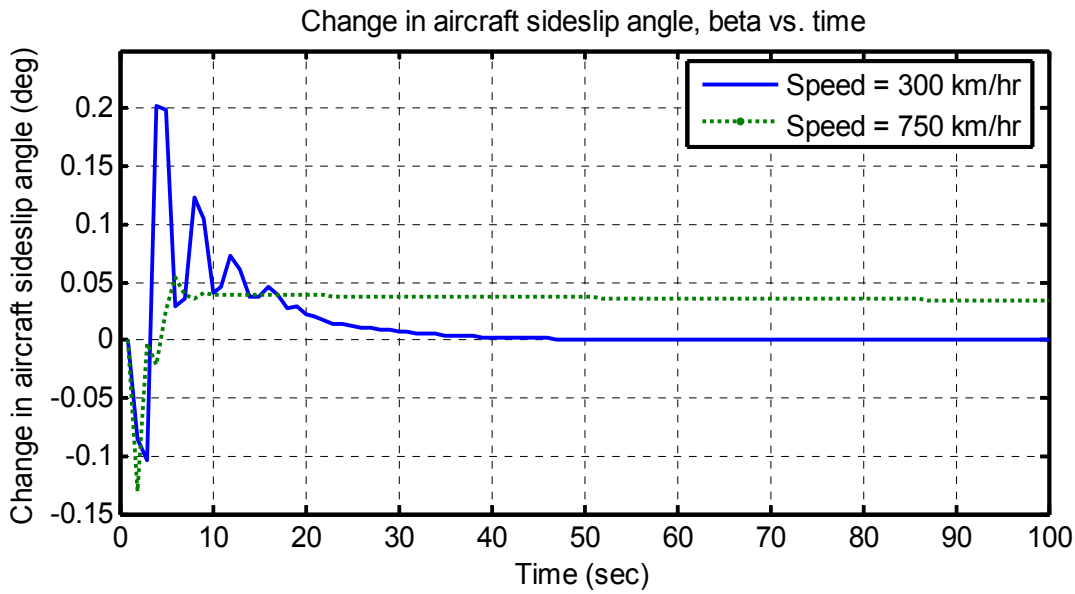

Figure 4.36 Aircraft Sideslip Angle Response to 1 Degree Step Input in Aileron Deflection at Altitude of 3000 m. and Speed of 300km/hr and 750 km/hr.

.

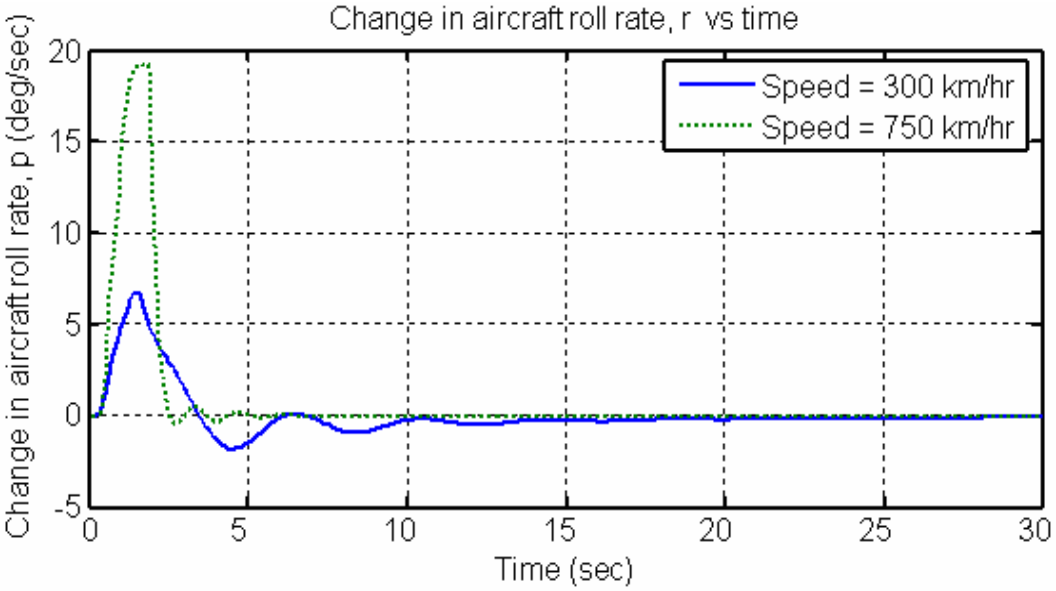

Figure 4.37 Aircraft Roll Rate Response to 1 Degree Step Input in Aileron Deflection Altitude of 3000 m. and Speed of 300km/hr and 750 km/hr.

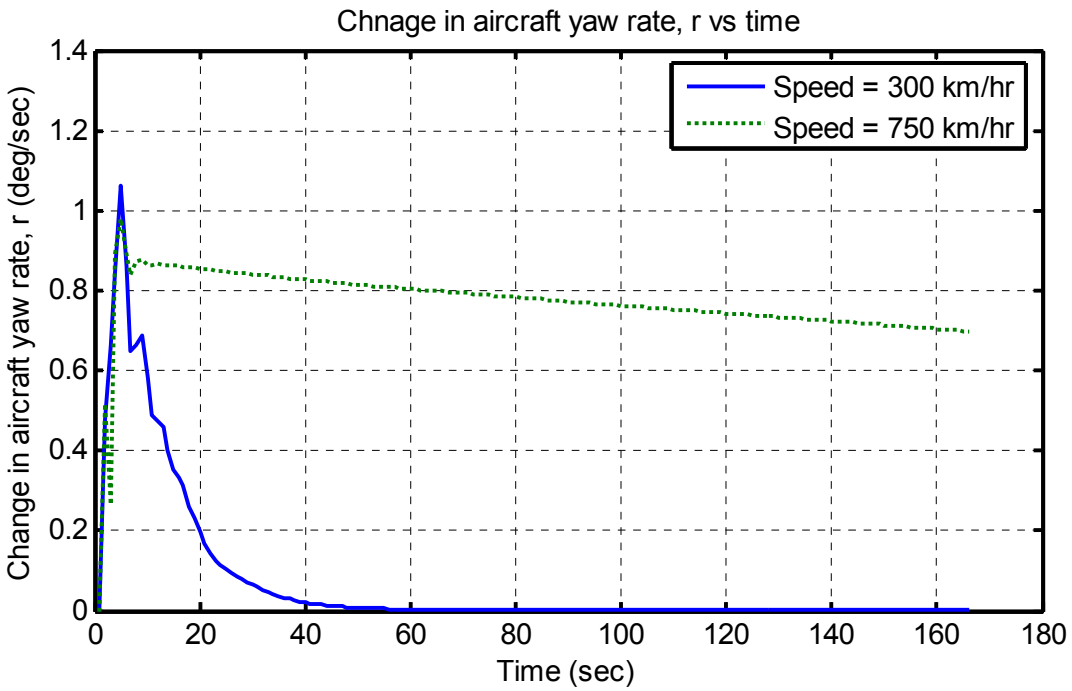

Figure 4.38 Aircraft Yaw Rate Response to 1 Degree Step Input in Aileron Deflection at Altitude of 3000 m. and Speed of 300km/hr and 750 km/hr.

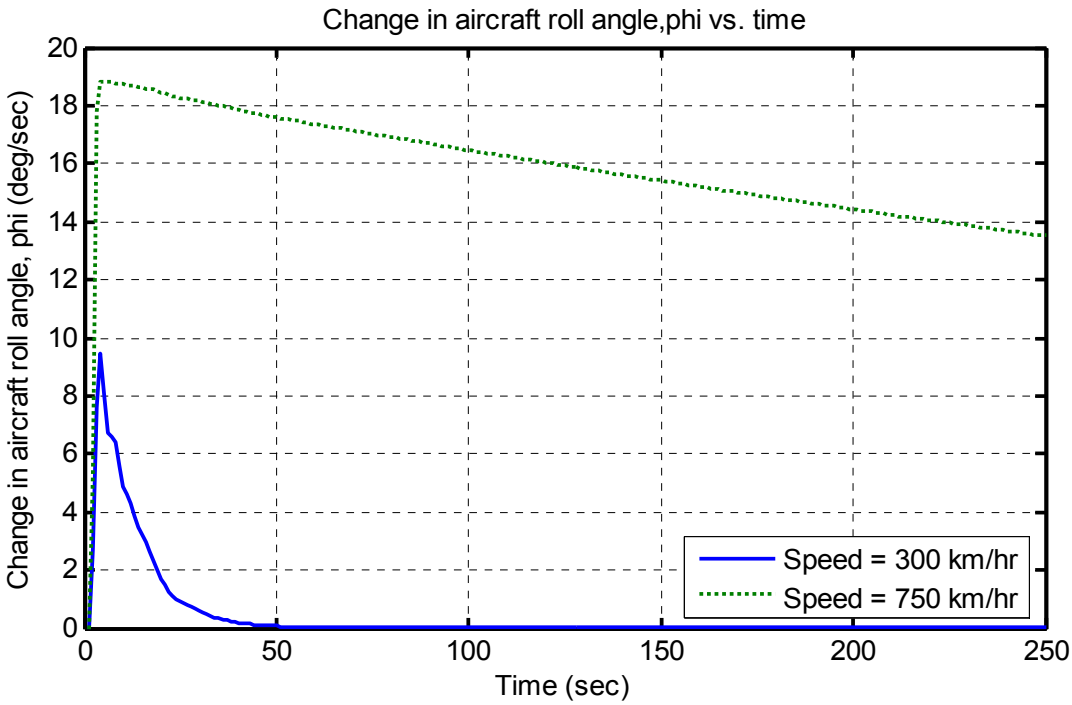

Figure 4.39 Aircraft Roll Angle Response to 1 Degree Step Input in Aileron Deflection Altitude of 3000 m. and Speed of 300km/hr and 750 km/hr.

As seen in the previous plots, the aircraft shows bad behavior at high speed for the lateral stability for aileron step input, as discussed in spiral mode case, the aircraft is almost unstable at high speed and it takes long period to return to reference condition due to the effects of yaw moments and dihedral effect, applying any input at high speed may bring the aircraft out of stability margin. However in previous case the aircraft shows weak stability by settle down to original position in relatively long time, which is not well acceptable in fighters. This is one of the reasons of limiting the maximum cursing speed of L-39 at 750 km/hr.

4.1.2.2 Aircraft Response Following Rudder Deflection

The pilot input in this case is the rudder deflection by amount of one degree for a period of one second. As for the previous cases, the simulation is divided into two cases at which the effect of altitude and the effect of airspeed were examined.

Case I. Effect of altitude

In the same manner in the longitudinal motion, the simulation performed twice for two different altitudes, 10,000 m and 500 m at fixed speed of 500 km/hr (138.8 m/sec). The results are shown Figures 4.40 – 4.43.

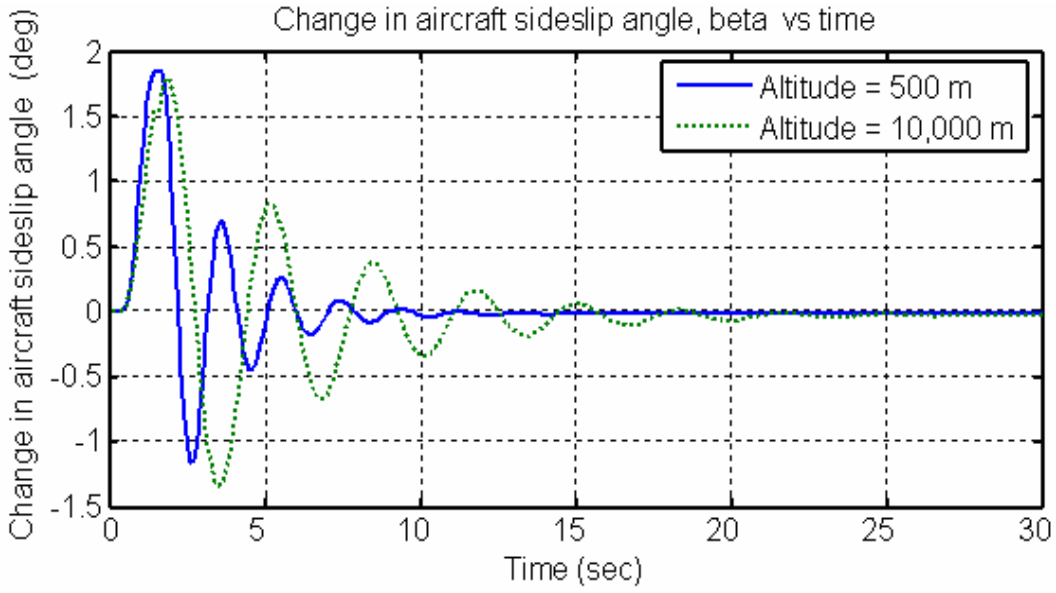

Figure 4.40 Aircraft Sideslip Response to 1 Degree Step Input in Rudder Deflection at Speed of 500 km/hr and Altitudes of 500m and 10,000m.

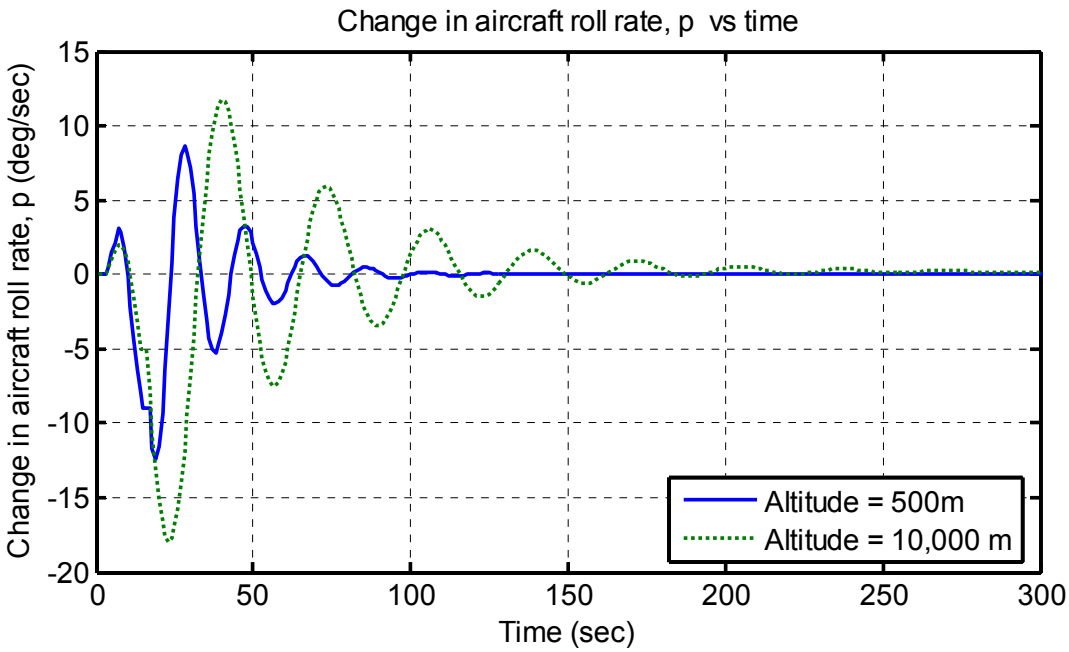

Figure 4.41 Aircraft Roll Rate Response to 1 Degree Step Input in Rudder Deflection at Speed of 500 km/hr and Altitudes of 500m and 10,000m

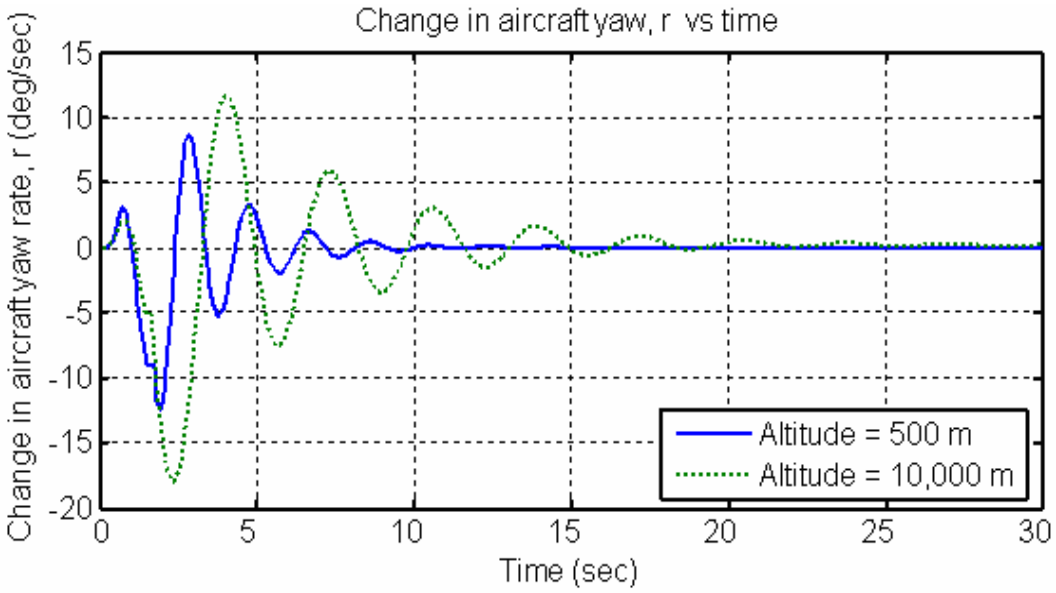

Figure 4.42 Aircraft Yaw Rate Response to 1 Degree Step Input in Rudder Deflection at Speed of 500 km/hr and Altitudes of 500m and 10,000m.

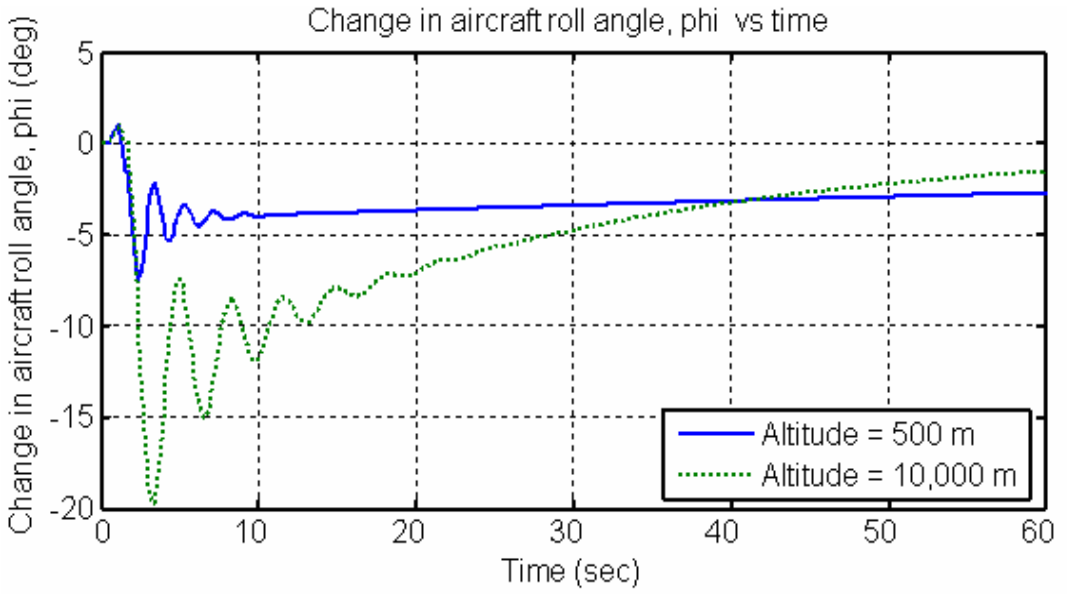

Figure 4.43 Aircraft Roll Angle Response to 1 Degree Step Input in Rudder Deflection at Speed of 500 km/hr and Altitudes of 500m and 10,000m

As shown in the previous plots, and as for the case of aileron deflection the response of aircraft following rudder deflection shows higher amplitude for the response of all cases at high altitude, however, the damping is slower at high altitude, the most effective parameters for this is yaw angular acceleration N_r, which decrease with increasing altitude, in addition to the other derivatives with have mutual relation with yawing and rolling moments. As a result, the aircraft will show slow and sluggish response at such a high altitude.

Case II. Effect of airspeed

In the same manner, in this case the simulation is performed twice for two different airspeeds, at 750 km/hr and 300 km/hr at fixed altitude of 3000m.

The responses are shown in Figures 4.44 – 4.47

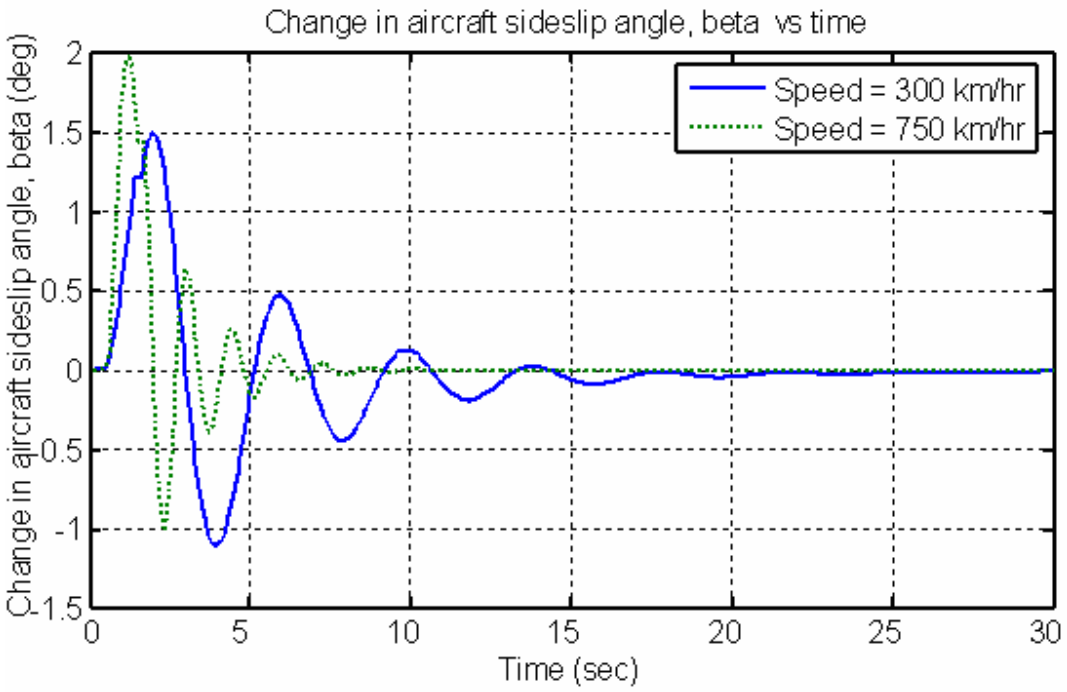

Figure 4.44 Aircraft Sideslip Response to 1 Degree Step Input in Rudder Lever Deflection Altitude of 3000 m. and Speed of 300km/hr and 750 km/hr.

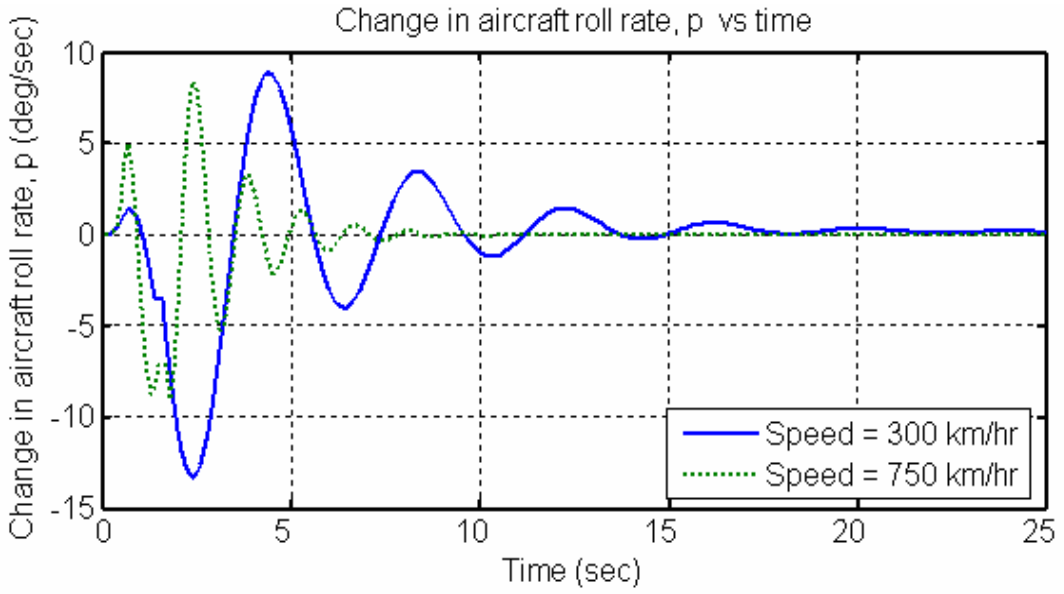

Figure 4.45 Aircraft Roll Rate Speed Response to 1 Degree Step Input in Rudder Lever Deflection Altitude of 3000 m. and Speed of 300km/hr and 750 km/hr.

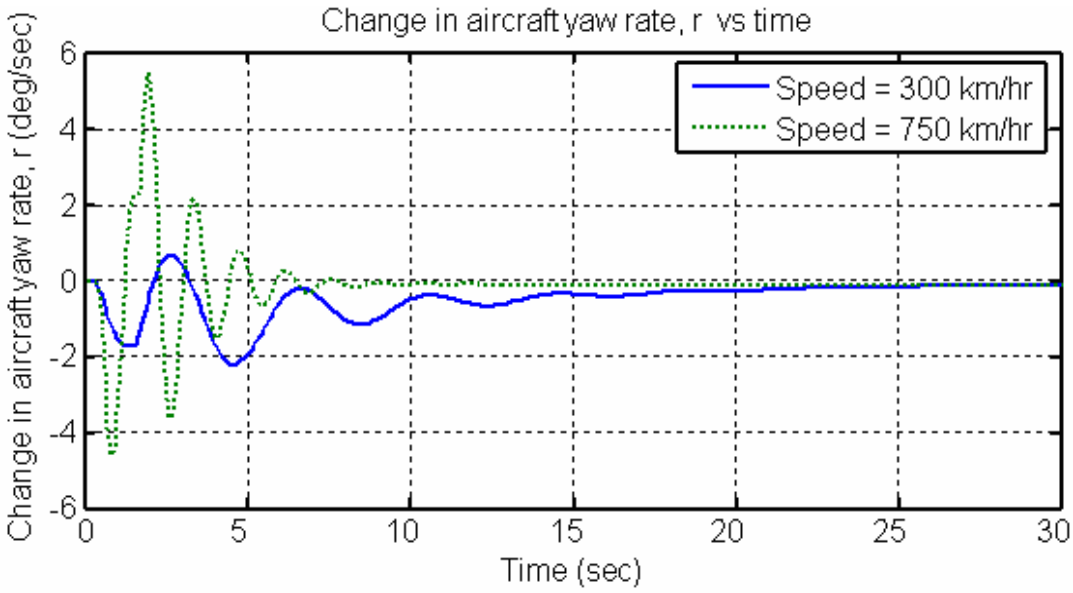

Figure 4.46 Aircraft Yaw Rate Response to 1 Degree Step Input in Rudder Lever Deflection Altitude of 3000 m. and Speed of 300km/hr and 750 km/hr.

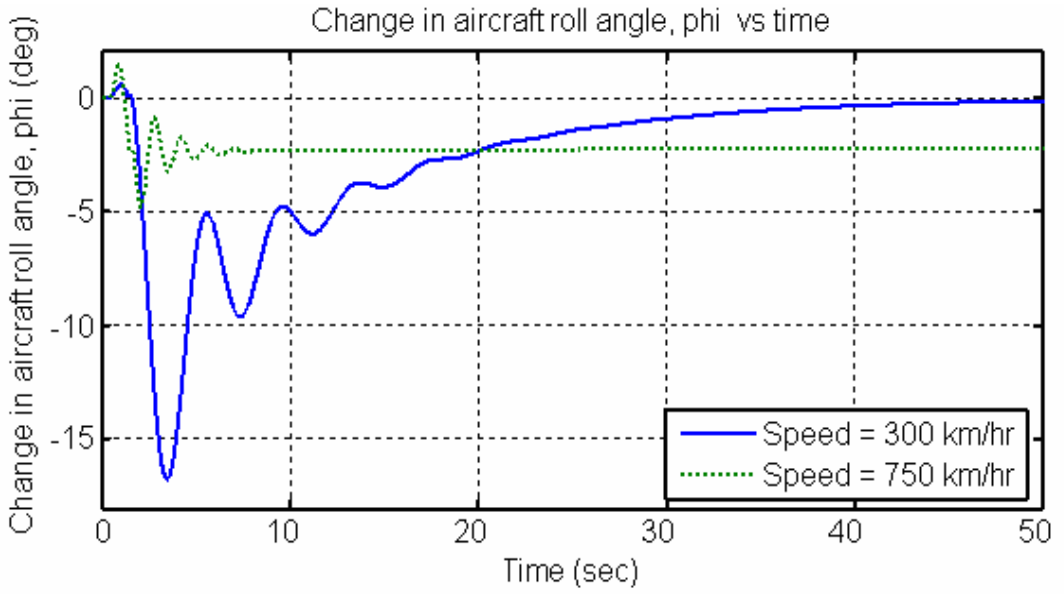

Figure 4.47 Aircraft Roll Angle Response to 1 Degree Step Input in Rudder Lever Deflection Altitude of 3000 m. and Speed of 300km/hr and 750 km/hr.

As shown in the previous Figures, responses show significant difference between high and low speeds performance. At high speed, the response is highly damped because of compressibility factor, so the aircraft will not return to its original attitude in short time as in the case of aileron deflection, the reasons are almost the same by taking into account yawing moments and derivatives instead of rolling derivatives. Even though the damping divergence is very slow at high speed, the aircraft is still stable. However, stability at speeds more than 750 km/hr is not guaranteed.

The lateral motion of an aircraft is a complicated combination of rolling, yawing and sideslipping motions. The aircraft produces both yawing and rolling moments due to sideslip, this interaction between roll and yaw produces the coupled motion. These facts make the physics and nature of lateral stability differ from longitudinal stability where there is no coupled motion.

In general, the results obtained from simulations are of significant importance to aircraft control system designers. The significance of these results lie in the fact that the aircraft handling qualities vary with the variation in the speed and altitude. Thus, the handling qualities will be estimated in the following section.

4.3 Estimation of L-39 Handling Qualities

Because of the importance of the aircraft handling qualities discussed in section 2.6, this section will give good impression of L-39 handling qualities at altitude of 3,000 m and speed of 500 km/hr which are considered as the optimum speed and altitude for this trainer regarding to its controllability.

This estimation is done for the stick fixed longitudinal and lateral characteristics. The damping and frequency of both short and phugoid period modes were determined in terms of aerodynamic stability derivatives [2].

The handling qualities of the aircraft can be estimated according to its class and flight phase, and then it can be specified in terms of one of three levels.

The following tables show a definition of aircraft classes, flight phases and levels [15].

Table 4.1 Aircraft Classes

CLASS	I	II	III	IV
Description	Light Small, aircraft. Maximum mass 5700 kg	Medium weight, Low-to-medium Maneuverability aircraft. Mass between 5700 and 30000 kg	Large, heavy, low-to-medium maneuverability aircraft. Mass greater than 30000 kg.	High maneuverability aircraft
Examples of role and aircraft.	-Light utility. -Primary trainer. -Light observation. Cessna Caravan. Pilatus Islander. Piper Tomahawk. Tucano. Turboporter. Optica.	Heavy utility/search and rescue. Light or medium transport /cargo/tanker. Early warning electronic countermeasures/ airborne command, control or communications relay. Anti-submarine. Assault transport. Reconnaissance Tactical bomber. Heavy attack. Trainer for CLASS II. Lockheed C130 BAE-146. Boeing 737. Douglas DC9. Grumman E2.	Heavy Transport /cargo/ tanker. Heavy bomber. Patrol/early warning/electronic counter-measures/ airborne command control, or communications relay. Trainer for CLASS III. Airbus A-300, Douglas DC-10, Boeing B-52, Boeing 747, Boeing 707.	Fighter/ interceptor. Attack. Tactical reconnaissance Observation. Trainer for CLASS IV. Lockheed-Martin F16. Panavia Tornado. General Dynamics F111. BEA Hawk. Yakovoliev Yak 50. Zlin 50L. Blackburn Buccaneer.

Table 4.2 Flight Phases

Phases	A	B	C
Description	Rapid maneuvering, precision tracking or precise flight path control.	Gradual maneuvers without precision tracking. Accurate flight path control may be required	Normal gradual maneuvers and usually precise flight path control.
Typical examples of tasks	Air-to-air combat. Ground attack. Weapon delivery/Launch. Reconnaissance. Air-to-air refueling. Terrain following. Maritime search and support. Aerobatics. Close formation flying.	Climb. Cruise. Loiter. Air-to-air refueling. Descent. Aerial delivery.	Take-off. Approach (includes instrument approaches). Overshoot. Landing (includes arrested landing).

Table 4.3 Flying Qualities Levels

LEVEL	1	2	3	ABOVE 3
Task.	Task achieved without excessive pilot workload	Some degradation in task effectiveness or increase in pilot workload or both.	Airplane can be controlled but with severe task degradation. The total workload of the pilot is approaching the limit of his capacity.	Inability to complete task required. Allowed only in special circumstances.

According to previous table L-39 can be considered as:

Class: IV

Flight Phase: A

Moreover, there is additional estimation for the rating of handling qualities based on pilot opinion, in this rating the pilot give a rate out of ten called Pilot Rating in addition to flying quality level. As shown in the following flow chart:

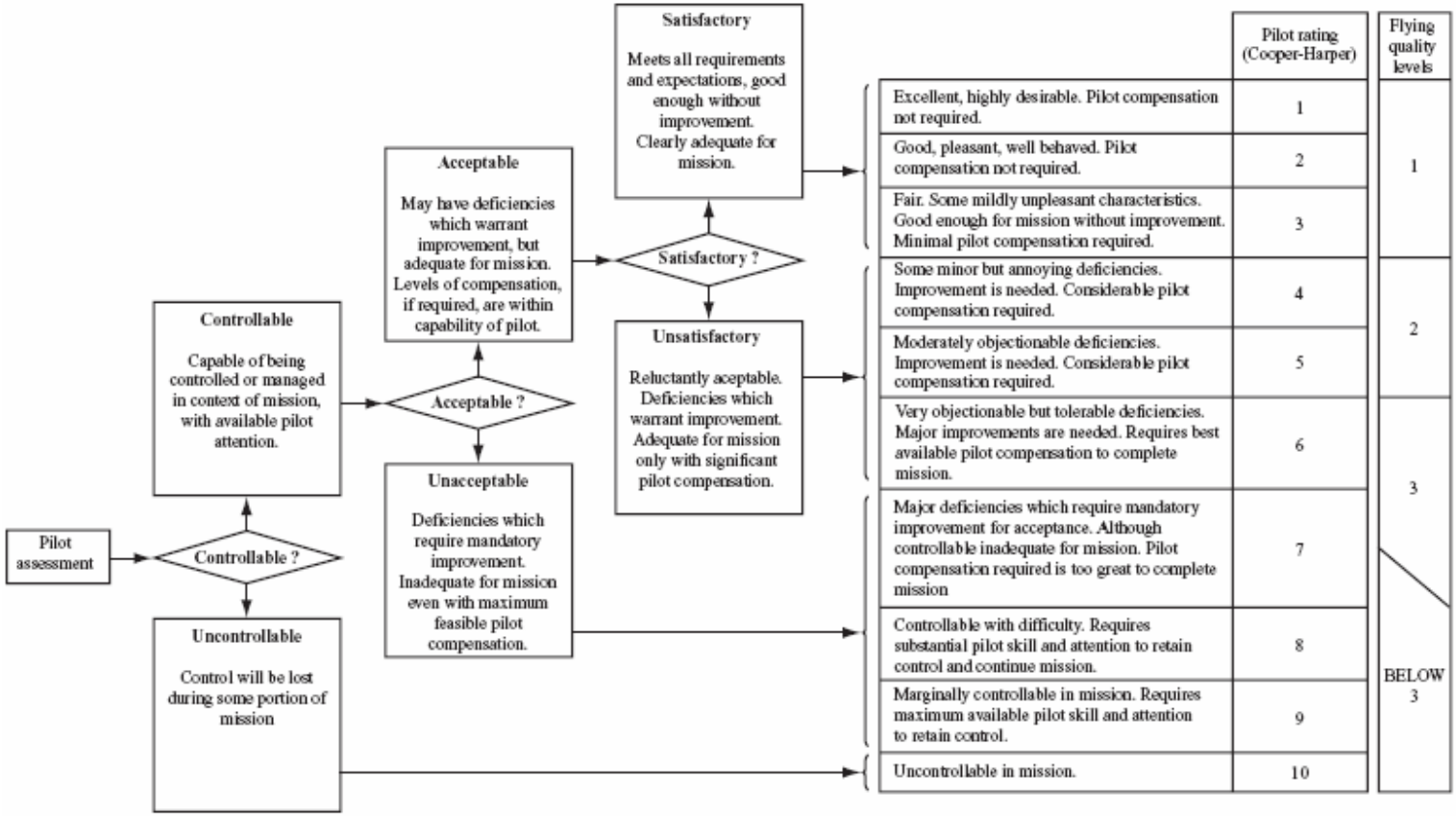

Figure 4.48 Pilot Assessment rating of flying qualities (Cooper-Harper)

4.3.1 Longitudinal Flying Qualities

Damping and frequency limits for longitudinal flying qualities are presented in both phugoid and short period mode in the following tables

Table 4.4 Phugoid Damping Ratio (ζ_p) Limits

LEVEL	1	2	3
Characteristics	ζ_p at least 0.04	ζ_p at least 0.0	An undamped oscillatory mode with $t_{1/2}$ of at least 55 seconds.

Table 4.5 Short Period Damping Ratio (ζ_{sp}) Limits

FLIGHT PHASE CATEGORY	LEVEL 1		LEVEL 2		LEVEL 3	
	Min ζ_{sp}	Max ζ_{sp}	Min ζ_{sp}	Max ζ_{sp}	Min ζ_{sp}	Max ζ_{sp}
A	0.35	1.3	0.25	2.0	0.1	-
B	0.30	2.0	0.20	2.0	0.1	-
C	0.50	1.3	0.30	2.0	0.25	-

L-39 longitudinal handling qualities can be calculated using (damp) command in MATLAB, by finding damping ratio and frequency for matrix (Along). According to previous tables handling qualities is summarized in the following table:

Table 4.6 Handling Qualities of Longitudinal Motion

Flight Condition	Speed = 500 km/hr (139 m/s), Altitude = 3000 m, Mass = 4200kg	
Phugoid Mode	ζ_p = 0.139	LEVEL 1
Short Period Mode	ζ_{sp} = 0.23	LEVEL 3

It can be seen from previous table that the handling quality of short period mode is LEVEL 3 however, and as tabulated in table 4.1 , the rate can be level 2 because it much closer to the value 0.25 than 0.10 , especially when we take into consideration the fact that ,this value may decrease with increasing altitude [esdu].

4.3.2 Lateral-Directional Flying Qualities

Lateral flying qualities requirement are listed in Tables 4.7, 4.8 and 4.9. The definition of aircraft class and category were presented in Tables 4.1 and 4.2.

4.3.2.1 Roll Mode Flying Qualities

Acceptable values of the roll mode time constant, t_R , are given in Table 4.7.

Table 4.7 Maximum Values of Roll Mode Time Constant, t_R :

CLASS	FLIGHT PHASE CATEGORY	t_R (sec)		
		LEVEL 1	LEVEL 2	LEVEL 3
I, IV	A	1.0	1.4	Insufficient evidence to define an upper limit. Limited evidence suggests a value of 6 to 8 seconds for all flight phases and aircraft classes.
II, III	A	1.4	3.0	
All Classes	B	1.4	3.0	
I, IV	C	1.0	1.4	
II , III	C	1.4	3.0	

4.3.2.2 Spiral Mode Flying Qualities

Spiral mode acceptability is assessed in terms of the minimum time to double the bank angle for an airplane initially in trimmed level flight with zero yaw and stick free but following a disturbance in bank of up to 20°. Minimum values are given in Table 4.8.

Table 4.8 Minimum Time to Double Bank Angle, t_2 (sec):

FLIGHT PHASE CATEGORY	LEVEL 1	LEVEL 2	LEVEL 3
A, C	12	8	5
B	20	8	5

4.3.2.3 Dutch Roll Mode Flying Qualities

Minimum Dutch Roll frequency and damping requirements are given in Table 4.9

Table 4.9 Minimum Values of Natural Frequency and Damping Ratio for the Dutch Roll Oscillation:

CLASS FLIGHT PHASR CATEGORY		Minimum values								
		LEVEL 1			LEVEL 2			LEVEL 3		
		ζ_D	$\zeta_D\omega_D$ (rad/s)	ω_D (rad/s)	ζ_D	$\zeta_D\omega_D$ (rad/s)	ω_D (rad/s)	ζ_D	$\zeta_D\omega_D$ (rad/s)	ω_D (rad/s)
IV	A	0.4	-	1.0	0.02	0.05	0.5	0.0	-	0.4
I,IV	A	0.19	0.35	1.0	0.02	0.05	0.5	0.0	-	0.4
II,III	A	0.19	0.35	0.5	0.02	0.05	0.5	0.0	-	0.4
All Classes	B	0.08	0.15	0.5	0.02	0.05	0.5	0.0	-	0.4
I, IV	C	0.08	0.15	1.0	0.02	0.05	0.5	0.0	-	0.4
II, III	C	0.08	0.10	0.5	0.02	0.05	0.5	0.0	-	0.4

As for longitudinal motion, L-39 lateral-directional handling qualities can be calculated using (damp) command in MATLAB, by finding damping ratio and frequency for matrix (Alat). According to previous tables handling qualities is summarized in the following table:

Table 4.10 Handling Qualities of Lateral-Directional Motion

Flight Condition	Speed = 500 km/hr (139 m/s), Altitude = 3000 m, Mass = 4200kg	
Roll Mode	t_R = 0.329	LEVEL 1
Spiral mode	t_2 = 58.97 sec	LEVEL 1
Dutch Roll Mode	ζ_D =0.14, ω_D =2.93(red/s), $\zeta_D \omega_D$ =0.41 (red/s).	LEVEL 2

In general, the handling qualities mainly depend on the aircraft geometry, and having some improvement in the aircraft handling qualities requires an increase in the area of horizontal stabilizer to improve longitudinal handling qualities and increase area of vertical stabilizers to improve lateral handling qualities in addition to other things. Increasing the area results in more drag, the result is that the aircraft performance will worsen and the airplane will be heavier. Therefore, some sort of stability augmentation system that will enhance the aircraft handling qualities at all altitudes and speeds could be implemented [1, 2 and 9].

CHAPTER 5
CONCLUSION

In the present thesis, development of a six degree of freedom simulation of aircraft motion to predict the longitudinal and the lateral-directional motion following a pilot input have been studied. The model developed takes into account the change in speed and altitude due to pilot input and is capable of simulating aircraft response over the entire defined flight envelope. Simulation can be used to observe the effect of changing speed and altitude on the aircraft dynamic response. Moreover, aircraft handling qualities have been found for the sake of estimating its controllability. This capability of the model will facilitate the control engineers in designing autopilots and stability augmentation systems, where they can take into consideration the effect of changing altitude and speed.

The MATLAB - SIMULINK tools have been used to simulate the motion of the model developed. The ability to perform a simulation of aircraft motion has significantly reduced the time, cost and risk involved with aircraft control system design. To a great extent, this ability has allowed flight dynamic engineers as well as control engineers to observe the dynamic response of an aircraft prior to building the real aircraft [14]. However, despite many advantages, the simulation has few limitations as well. The basis of any simulation is a mathematical model developed from equations of motion. The mathematical model is not always precisely representing the aircraft motion. The model developed for the aircraft longitudinal and lateral-directional motion is not free from some inaccuracies, especially in the transonic regime.

In general, this will limit the reliability and validity of simulation. The response of the aircraft observed in simulation will not be exactly the same as the response obtained from the real flight tests. This is due to the fact that a number of assumptions have been made and a number of parameters are estimated or neglected while developing the mathematical model. Furthermore, the mathematical model, in most cases, is a linearized model while the actual aircraft motion is non-linear.

The mathematical model primarily consists of aircraft stability derivatives and control coefficients. The derivatives used here are taken from several related references [1, 2, 3, 4 and 5].

Some of the parameters used for the equations were estimated based on several facts and assumptions regarding real flight conditions. Thus, these are just approximate equations. Despite this fact, the simulation of the aircraft motion that is performed using some assumptions, still gives accurate results when validated with flight test data, the accuracy of about 90 % has been obtained in average, over the majority of the flight envelope.

This work clearly shows that, the simulation of aircraft dynamic response changes as functions of speed and altitude. The simulations performed for both longitudinal and lateral motions, and for both stick fixed and stick free cases.

In longitudinal motion, the effect of changing altitude shows that the performance of aircraft at low levels is better than that of high altitude, because of low effect of aerodynamic forces at high altitude. The effect of speed on aircraft response at the same altitude shows that, the response of the aircraft to any control input is higher at high speed than that of low speed, surprisingly the period needed by both speeds to attain original attitude is almost the same, which leads to the fact that, oscillation time is independent mainly on aircraft speed. However, it has a great effect on damping ratio and amplitude of the response.

In lateral motion, the coupled motion makes the prediction of response characteristics difficult due to number of parameters involved. However, the results were satisfactory. The effect of altitude on lateral stability support the result of longitudinal stability , that the aircraft response at low altitude is better than of that at high altitude for the same reasons. The effect of speed on lateral stability shows of lateral motion response at high speed at which the aircraft is very close to be unstable, because of being close to leave the stability margin.

These results significantly helps flight control systems designers to take into account the effects of this non-linearity while designing a stability augmentation system (SAS) or control augmentation system (CAS) [6].

CHAPTER 6
RECOMMENDATIONS

The dynamic response of an aircraft following a pilot input can easily be obtained by the simulation of the aircraft motion using tools such as MATLAB and SIMULINK, as is shown in the this thesis. Flight control systems engineers can observe the motion of a proposed aircraft using design specifications prior to building the real aircraft. This reduces the need for building a physical prototype and performing flight tests to see if the performance is satisfactory or not. However, further research shall be carried out in order to fully validate the results of this simulation accurately.

Firstly, the mathematical model used in the simulation does not always represent the real aircraft motion. This is partly due to many assumptions made during building of the model and partly due to the use of linearization process of the equations at each step time of the simulation. This thesis was an attempt to reduce the error in aircraft simulation due the linearization of equations of motion. The only way to make the model more reliable is to conduct more research and to avoid the assumptions and approximations as possible as it can be.

Secondly, the mathematical model developed for the simulation of aircraft motion does not always include the effect of atmospheric disturbances, such as gust, turbulence, etc., neither does the present model. Taking atmospheric disturbances will give more reality to the simulation.

Thirdly, as the model used in this work (Aero L-39) doesn't have an auto pilot, using simulation results that give good prediction of the values of stability and control derivatives at any flight condition can be considered as a good start for autopilot design compatible with this aircraft.

Fourth, though the flight test is beyond the scope of this thesis, the best method to validate the results of simulation is to conduct a flight test, especially for estimating flying handling qualities where pilot opinion is one the most significant parameters of estimation. Also, using simulation before conducting any regular

functional-check-flight (FCF) will give good prediction for the test pilot of how the response of the aircraft would be according to initial flight conditions. The data obtained from the flight test can then be used to compare the results from simulation.

Finally, the Simulation program in this study can be used as an educational tool for undergraduate students to learn about the effect of any tiny parameter in the huge amount of parameters and equations in the whole simulation process.

REFERENCES

[1] Etkin, Bernard, Dynamics of Flight: Stability and Control, John Wiley & Sons, New York, 1996.

[2] Nelson, Robert C, Flight Stability and Automatic Control, McGraw-Hill Company, 1989.

[3] Roskam, Jan, Airplane Flight Dynamics and Automatic Flight Controls Part I, Design, Analysis, and Research Corporation, Lawrence, Kansas, 1995.

[4] Roskam, Jan, Airplane Design Part VI, Preliminary Calculation of Aerodynamic Thrust and Power Characteristics. Design, Analysis, and Research Corporation, Lawrence, Kansas, 1990.

[5] Roskam, Jan, Airplane Design Part VII: Determination of Stability, Control and Performance Characteristics: FAR and Military Requirements, Design, Analysis, and Research Corporation, Lawrence, Kansas, 2002

[6] Schmidt, Louis, Introduction to Aircraft Flight Dynamics, AIAA Education Series, Inc., Reston, Virginia, 1998

[7] Hodgkinson, John, Aircraft Handling Qualities, AIAA Educating Series, Inc., Reston, Virginia, 1999.

[8] Flight Characteristics of L-39 ZO Aircraft, Aero Vodochody, 1978.

[9] Brian L. Stevens and Frank L. Lewis, Aircraft Control and Simulation, John Wiley & Sons, New Jersey, 2003.

[10] Using MATLAB, The Mathworks Company, Inc., Natic, Massachusetts, Version 7.0.

[11] Using SIMULINK, The Mathworks Company, Inc., Natic, Massachusetts, Version 7.0.

[12] Writing S-Functions, The Mathworks Company, Inc., Natic, Massachusetts, Version 3.

[13] Using Aerospace Blockset, The Mathworks Company, Inc., Natic, Massachusetts, Version 1.

[14] Clark, W., Role of Simulation in Support of Flight Tests, National Conference Publication - Institution of Engineers, Australia, v 1, n 93 pt 6, 1993, p 13-18.

[15] A Background to the Handling Qualities of Aircraft, ESDU 92006a, The Royal Aeronautical Society, England, 2003.

[16] Estimation of sideforce, yawing moment and rolling moment derivatives due to rate of roll for complete aircraft at subsonic speeds, ESDU 85010, The Royal Aeronautical Society, England, 1985.

APPENDIX A

STABILITY AND CONTROL DERIVATIVES

Longitudinal Stability Derivatives

Derivatives and coefficients due to the change in forward speed, u

• The X force derivative and coefficient:

Change in X-force with change in forward speed, $X_u = \dfrac{-(C_{D_u} + 2C_{D_0})QS}{mu_0}$

• The Z-force derivative and coefficient:

Change in Z-force with change in forward speed, $Z_u = \dfrac{-(C_{L_u} + 2C_{L_0})QS}{mu_0}$

• The pitching moment derivative and coefficient:

Change in pitching moment with change in forward speed, $M_u = C_{m_u} \dfrac{QS\bar{c}}{u_0 I_y}$

• The Z-force derivative and coefficient:

Change in Z-force with change in angle of attack, $Z_\alpha = u_0 Z_w$

Where, $Z_w = \dfrac{-(C_{L_\alpha} + C_{D_0})QS}{mu_0}$

• The pitching moment derivative and coefficient:

Change in pitching moment with change in angle of attack, $M_\alpha = u_0 M_w$

Where, $M_w = C_{m_\alpha} \dfrac{QS\bar{c}}{u_0 I_y}$

Derivatives and coefficients due to the time rate of change of the angle of attack, $\dot{\alpha}$

• The Z-force derivative and coefficient:

Change in Z-force with time rate of change of angle of attack, $Z_{\dot{\alpha}} = u_0 Z_{\dot{w}}$

Where, $Z_{\dot{w}} = C_{z_{\dot{\alpha}}} \dfrac{\bar{c}QS}{2mu_0^2}$

• The pitching moment derivative and coefficient:

Change in pitching moment with rate of change of angle of attack,

$M_{\dot{\alpha}} = u_0 M_{\dot{w}}$

Where, $M_{\dot{w}} = C_{m_{\dot{\alpha}}} \frac{\bar{c}}{2u_0} \frac{QS\bar{c}}{u_0 I_y}$

Derivatives and coefficients due to the Pitching Velocity, q

• The Z-force derivative and coefficient:

Change in Z-force with change in pitch rate, $Z_q = C_{z_q} \frac{\bar{c}QS}{2u_0 m}$

• The pitching moment derivative and coefficient:

Change in pitching moment with change in pitch rate, $M_q = C_{m_q} \frac{\bar{c}}{2u_0} \frac{QS\bar{c}}{I_y}$

Longitudinal Control Derivatives

Derivatives and coefficients due to the deflection of the elevator, δe

• The Z-force derivative and coefficient:

Change in Z-force due to elevator deflection, $Z_{\delta_e} = C_{z_{\delta e}} \frac{QS}{m}$

Where, $C_{z_{\delta_e}} = -\frac{S_t}{S} \eta_h \frac{dC_{L_t}}{d\delta_e}$

• The pitching moment derivative and coefficient:

Change in pitching moment due to elevator deflection, $M_{\delta_e} = C_{m_{\delta e}} \frac{QS\bar{c}}{I_y}$

Where, $C_{m_{\delta_e}} = -\eta_h V_H \frac{dC_{L_t}}{d\delta_e}$

Lateral Stability Derivatives

Derivatives and coefficients due to the change in sideslip angle, β

• The Y-force derivatives and coefficients

Change in Y-force with change in sideslip angle, $Y_\beta = \frac{QSC_{y\beta}}{m}$

• The yawing moment derivative and coefficient:

Change in yawing moment with change in sideslip angle, $N_\beta = \frac{QSbC_{y_p}}{2I_x u_0}$

• The rolling moment derivative and coefficient:

Change in rolling moment with change in sideslip angle, $L_\beta = \frac{QSbC_{l_\beta}}{I_x}$

Derivatives and coefficients due to the roll rate, p

• The Y-force derivative and coefficient:

Change in Y-force with change in roll rate, $Y_p = \frac{QSbC_{y_p}}{2mu_0}$

• The yawing moment derivative and coefficient:

Change in yawing moment with change in roll rate, $N_p = \frac{QSb^2C_{n_p}}{2I_z u_0}$

• The rolling moment derivative and coefficient:

Change in rolling moment with change in roll rate, $L_p = \frac{QSC_{l_p}}{2I_x u_0}$

Derivatives and coefficients due to the yawing rate, r

• The Y-force derivative and coefficient:

Change in Y-force with change in yaw rate, $Y_r = \frac{QSbC_{y_r}}{2mu_0}$

• The yawing moment derivative and coefficient:

Change in yawing moment with change in yaw rate, $N_r = \frac{QSb^2C_{n_r}}{2I_z u_0}$

• The rolling moment derivative and coefficient:

Change in rolling moment with change in yaw rate, $L_r = \frac{QSb^2 C_{l_r}}{2I_x u_0}$

Lateral Control Derivatives

Derivatives and coefficients due to the deflection of aileron, δa

• The yawing moment derivative and coefficient:

Change in yawing moment due to aileron deflection, $N_{\delta_a} = \frac{QSC_{n_{\delta a}}}{I_z}$

• The rolling moment derivative and coefficient:

Change in rolling moment due to aileron deflection, $L_{\delta_a} = \frac{QSC_{l_{\delta a}}}{I_x}$

Derivatives and coefficients due to the deflection of rudder, δr

• The Y-force derivative and coefficient:

Change in Y-force due to rudder deflection, $Y_{\delta_r} = \frac{QSC_{y\,\delta r}}{m}$

• The yawing moment derivative and coefficient:

Change in yawing moment due to rudder deflection, $N_{\delta_r} = \frac{QSC_{y\,\delta r}}{m}$

• The rolling moment derivative and coefficient:

Change in rolling moment due to rudder deflection, $L_{\delta_r} = \frac{QSbC_{l_{\delta_r}}}{I_x}$

APPENDIX B

STABILITY AND CONTROL DERIVATIVES, GEOMETRY AND SPECIFICATIONS OF AERO L-39 AND AERMACCHI M-311

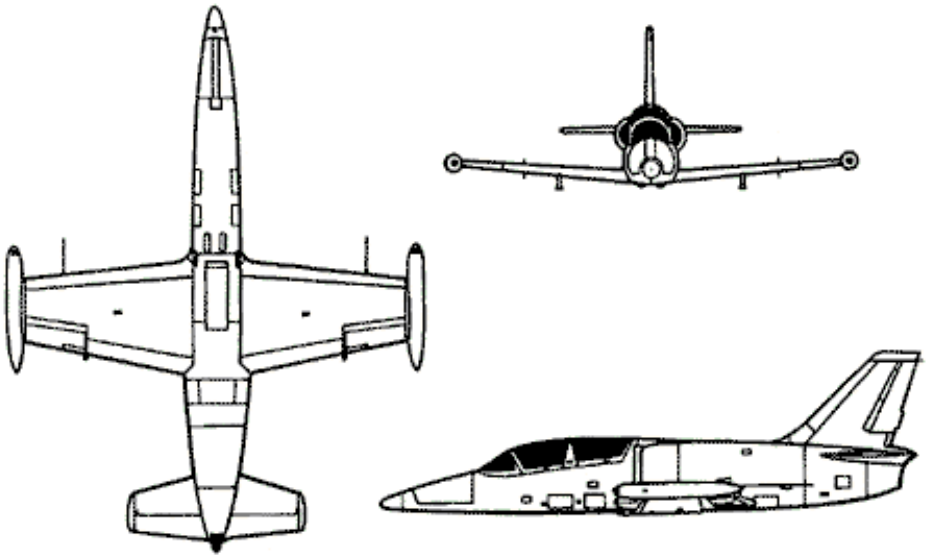

Figure A.1: Geometry of L-39

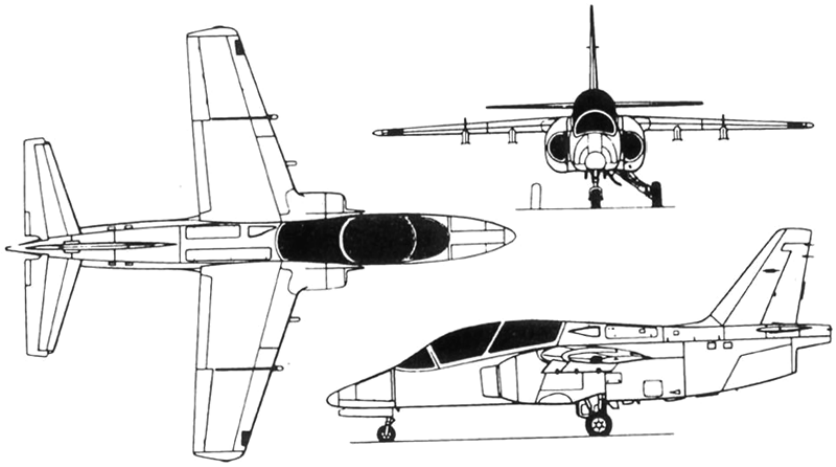

Figure A.2 Geometry of M-311

Table A.1: L-39 and M-311 Specifications and Geometry

Manufacturer	Aero vodochody - The Czech Republic	Aermacchi - Italy
Type	Double seater – jet advanced training aircraft and ground supporter.	Double seater – jet advanced training aircraft and ground supporter
Length (m)	12.13	9.53
Height (m)	4.77	3.73
Wing span (m)	9.12	8.51
Wing area (m^2)	18.8	12.6
Wing aerodynamic chord (m)	2.15	-
Wing sweepback angle at 25 % chord (deg)	1.75	-
Wing dihedral (deg)	2.5	-
Wing profile	NACA 64A012	-
Empty weight (kg)	3467	1850
Max. take-off weight (kg)	5600	3720
Max. fuel capacity (l/ kg)	1400 / 980	890 / 696
Engine	Ivtchenko AI-25 TL	Pratt & Whitney JT1 5D-5C
Thrust at sea level (kg)	1720	1447
Rate of climb (m/s)	22	26
Max. speed (km/hr)	910	766
Stalling speed (with flaps fully extended) (km/hr)	165	163
Service ceiling (m)	11,500	12,200
Range with internal fuel (km)	1000	1390

Table A.2 Stability and Control Derivatives Comparison of L-39 and M-311

Flight Condition	**L-39**	**M-311**
Speed (m/s)	186	186
Altitude (m)	7622	7622
Mach Number	0.6	0.6
C.G. Position	0.246	0.25
Mass (kg)	4,100	1,800
Longitudinal Stability and Control Derivatives		
C_{D_0}	0.057	0.0205
C_{D_u}	0.032	0.05
C_{D_α}	0.126	0.12
C_{L_0}	0.22	0.149
C_{L_α}	2.47	5.5
C_{m_u}	-0.015	0
C_{m_α}	-0.115	-0.24
$C_{m_{\dot{\alpha}}}$	-2.62	-9.6
C_{m_q}	-6.05	17.7
$C_{L_{\delta e}}$	0.423	0.38
$C_{m_{\delta e}}$	-0.90	-0.88
Lateral Stability and Control Derivatives		
C_{l_β}	-0.13	-0.11
C_{l_β}	-0.42	-0.39
C_{l_r}	0.21	0.28
C_{y_β}	-0.946	-1.0
C_{y_p}	-0.413	-0.14
C_{y_r}	0.88	0.61
C_{n_β}	0.091	0.170
C_{n_p}	0.028	0.090
C_{n_r}	-0.21	-0.26
$C_{l_{\delta a}}$	0.16	0.10
$C_{l_{\delta r}}$	0.103	0.050
$C_{y_{\delta r}}$	0.266	0.028

APPENDIX C

MATLAB AND 'C' CODES

FILE NAME: AB_Matrix.m

CALCULATION OF AIRCRAFT GEROMETRY STABILITY AND CONTROL DERIVATIVES

```
%============================================================
%Aircraft geometric data
%============================================================
lf = 12.13; %Fuselage length (m)
b = 9.12; %Wing span (m)
S = 18.8;  %Wing panform area (m^2)
Sh = 5.1;  %Horizontal tail area (m^2)
Sv = 5.35; %Vertical tail area (m^2)
Sf = 9;  %Fuselage area (m^2)
S0 = 2.1;  %Fuselage cross section area (m^2)
Se = 1.7;  %Elevator area (m^2)
Cr = 2.75; %Wing root chord (m)
Ct = 1.4; %Wing tip chord (m)
cbar = 2.35; %Mean Aerodynamic Chord
b_h = 4.1; %Horizontal tail span (m)
b_v = 2.35; %Vertical tail span (m)
lcg = 6.4; %Distance from nose to the center of gravity (m)
%h1 = 1.35; %Fuselage height at 0.25*lf (m)
%h2 = 1.47; %Fuselage height at 0.75*lf (m)
%h = 1.28; %Fuselage average height (m)
Sfs = 15; %Fuselage projected side area (m^2)
Wf = 1.53; %Maximum fuselage width (m)
KN = 0.00025; %Empirical factor related to the sideslip derivative for fuselage and
        fuselage-wing interference (per radian)
lh = 5; %Distance from a/c center of gravity to the horizontal tail quarter chord (m)
lv = 4.25; %Distance from a/c center of gravity to the vertical tail aerodynamic center (m)
Zv = 2; %Distance from center of pressure of vertical tail to fuselage center line (m)
y1 = 2.55; %Distance of inboard aileron edge from the wing root (m)
y2 = 3.7; %Distance of outboard aileron edge from the wing root (m)
Zw = -0.58; %Distance, parallel to the z axis, from wing root quarter chord to fuselage
        centerline (m)
d = 1.9; %Maximum fuselage depth or diameter (m)
P_Xcg = 0.246; %Distance from wing leading edge to center of gravity in percentage of
        chord
e = 0.87; %Oswald's span efficiency factor
GAMMA = 0.043; %Wing dihedral angle (rad)
LAMBDA = 0.0355; %Wing half chord sweep angle (rad)
```

```
LAMBDAh = 0.349; %Horizontal tail half chord sweep angle (rad)
LAMBDAv = 0.61; %Vertical tail half chord sweep angle (rad)

%=========================================================
% Aircraft & Test Initial Values
%=========================================================
m =4000;  %Mass of the aircraft (kg)
T0 =288; %Sea level temperature (deg k)
%U =230;% Initial speed (m/s)
%h1 =3000; % Initial altitude (m)

%=========================================================
%Atmospheric Constants
%=========================================================
gamma1 = 1.4; %Ratio of Specific Heats
R = 287.05; %Gas constant (N.m/kg.k)
rho0 = 1.225; %Density at sea level (kg/m^3)
LR = -0.0065; %Lapse rate [deg k/m)
mu0 = 1.79e-5; %Absolute Viscosity (N.s/m^2)
g = 9.81; %Acceleration due to gravity (m/s^2)

%=========================================================
% Height and Velocity (Flight envelop)
%=========================================================
h1=[0 11500]; % L39 Altitude range (m)
T = T0 + LR*h1; %Temperatures at the desired altitudes
a = sqrt(gamma1*R*T); %Speed of sound at the desired altitude
U = [.15*a(1) 0.85*a(2)]; %L39 velocity range (m/s)
n = length(U); %Length of velocity vector
l = length(h1); %Length of altitude vector

%=========================================================
%Atmospheric temperature at the desired altitudes (deg k)
for i = 1:l
T(i) = T0 + LR*h1(i);
end
%Density of air at the desired altitudes (kg/m^3)
for i = 1:l
rho(i) = rho0*(T(i)/T0).^-(1+g/(R*LR));
end
%Viscosity of the air at desired altitudes (kg.s/m^2)
mu=((T/T0).^0.75)*mu0;
Rx=0.266;
Ry=0.346;
Rz=0.38;
e1= (b+lf)/2;
Ix = m*(Rx*b/2)^2; %Moment of inertia about x axis (kg m^2)
Iy = m*(Ry*lf/2)^2; %Moment of inertia about y axis (kg m^2)
Iz = m*(Rz*e1/2)^2; %Moment of inertia about z axis (kg m^2)
%eta for the calculation of K(Empirical Factor for Cndeltaa Estimation)
eta = y1/(b/2);
```

```
%Wing Taper Ratio
lambda = Ct/Cr;
%Wing aspect ratio
AR = b^2/S;
%Horizontal Tail Aspect Ratio
ARh = b_h^2/Sh;
%Horizontal Tail Aspect Ratio
ARv =b_v^2/Sv;
%Control surface area/lifting surface area
a1= Se/Sh;
%Flap effictiveness parameter
%tau = 0.283;
W = m*g; %Weight of the aircraft (kg)
%Flight mach number
M = U./sqrt(gamma1*R*T);
%Compressibility Correction factor
Beta= sqrt(1-M.^2);
%Distance from wing leading edge to center of gravity (m)
Xcg = P_Xcg*cbar;
%Lift coefficient at low speed
CL0 = 0.22;
%Airfoil lift curve slop at zero Mach number (1/deg) (Roskam VI T8.1b)
CLalpha0 = 0.12;
%Airfoil lift curve slop (1/deg)(Roskam VI 8.1)
for i = 1:n
CLalphaM(i) = CLalpha0/Beta(i);
end
for i = 1:n
% Ratio of airfoil lift curve slop to 2pi
k(i)= 57.3*CLalphaM(i)*Beta(i)/(2*pi);
end
%Wing Lift Curve Slope (Roskam VI 8.22 p248)
for i = 1:n
CLalphaw(i) =
        (2*pi*AR)/(2+sqrt((AR^2*Beta(i)^2/k(i)^2)*(1+(((tan(LAMBDA))^2)/Beta(i)^2)+
        4)));
end
kh=0.94;
%Horizontal Tail Lift Curve Slope
for i = 1:n
CLalphah(i) =
        (2*pi*ARh)/(2+sqrt((ARh^2*Beta(i)^2/kh^2)*(1+(((tan(LAMBDAh))^2)/Beta(i)^2
        )+4)));
end
%Vertical Tail Lift Curve Slope
for i = 1:n
CLalphav(i) =
        (2*pi*ARv)/(2+sqrt((ARv^2*Beta(i)^2/k(i)^2)*(1+(((tan(LAMBDAv))^2)/Beta(i)^
        2)+4)));% eq3.8
end
kwf = 1+(0.025*(d/b))-(0.25*(d/b)^2);
```

```
for i = 1:n
CLalphawf(i) = kwf*CLalphaw(i);
end
for i = 1:n
Cmalphaf(i) = CLalphawf(i)*lcg/cbar;
end
%Change in rolling moment due to side slip (1/rad)
deltaClbeta = 0;
%Flight dynamic pressure (kg/m^2)
for i = 1:n
for j = 1:l
Q(i,j) = 0.5*rho(j)*U(i)^2;
end
end
%Reynold's Number
for i = 1:n
for j = 1:l
Re(i,j) = rho(j)*U(i)*cbar/mu(j);
end
end
%Fuselage Reynold's Number
for i = 1:n
for j = 1:l
Ref(i,j) = rho(j)*U(i)*lf/mu(j);
end
end
%Drag coefficient at zero lift angle of attack
for i = 1:n
if    M(i) < 0.5
   CD0(i) = 0.048;
elseif M(i) > 0.5
   CD0(i) = (0.0976*M(i)^2)-(0.057*M(i))+ 0.0565;
end
end
%Change of drag coefficient with forward speed
for i = 1:n
   %for j=1:l
CDu(i) = CD0(i)*M(i)^2/(1-M(i)^2);
   %end
end
%Change of thrust with forward speed
CTu = 0;
%Contribution of fuselage and wing to yawing moment due to sideslip (1/rad)
KRl = 0.45*log(Ref)-1.85; %Roskam 7.20
%Effect of Fuselage Reynold's number on CnbetaF
CnbetaF = 57.3*KN*KRl*(Sfs/S)*(lf/b);  % Roskam eq 7.16
%Horizontal tail volume ratio
Vh = lh*Sh/(S*cbar);
%Veritcal tail volume ratio
Vv = lv*Sv/(S*b);
%Lift Coefficient
```

```
CL = W./(Q*S);
for i = 1:n
CLu = CL*M(i)^2/(1-M(i)^2);
end
%Downwash angle
epsilon = 2*CL/(pi*AR);
%Dynamic Pressure at the Horizontal Tail (kg/m^2)
Qh = Q.*cos(epsilon);
%Efficiency factor of the horizontal tail
etah = Qh./Q;
%Efficiency factor of the vertical tail
etav = etah;
%Change in downwash due to change in angle of attack.
depsilon_dalpha = 2*CLalphaw/(pi*AR);
%Airplant Lift Curve Slope
for i = 1:l
   for j=1:n
CLalpha(i) = CLalphaw(i) + CLalphah(i)*etah(i,j)*(Sh/S)*(1-depsilon_dalpha(i));
   end
end
%Variation of Airplane Drag Coefficient with angle of attack
for i = 1:l
for j = 1:n
CDalpha(i,j) = 2*CL(i,j)*CLalpha(i)/(pi*AR*e);
end
end
%Pitching moment coefficient for the tail (Roskam I eq 3.35)
for i = 1:l
for j = 1:n
Cmalphat(i,j) = -etah(i,j)*Vh*CLalphah(i)*(1-depsilon_dalpha(i));
end
end
%Elevator effectiveness (Roskam I p61)
taue = 0.633;
%Change in lift due to change in elevator deflection angle (Ros I 3.36 p79)
for i = 1:l
for j = 1:n
CLdeltae(i,j) = CLalphah(i)*etah(i,j)*(Sh/S)* taue;
end
end
%Elevator control power
for i = 1:l
for j = 1:n
Cmdeltae(i,j) = -CLalphah(i)*etah(i,j)*Vh*taue;
end
end
%Change in sidewash due to change in the sideslip angle (Roskam 7.5)
dsigma_dbeta = 0.724 + (3*Sv)/(S*(1 + cos(LAMBDA)))+ (0.4*Zw/d) -(1./etav);
% kv is the emperical factor defined if fig 7.3 (Roskam)
kv = 1.0;
%Change in Y-force with change in side slip angle
```

```
%Contribution of fuselage to directional stability (Ros 7.1)
ki=1.35; %emberical factor presented in fig 7.1
for i = 1:l
for j = 1:n
Cybetav(i,j) = -kv*etav(i,j)*(Sv/S)*CLalphav(i)*(1 + dsigma_dbeta(i));
end
end
for i = 1:l
for j = 1:n
Cybetaf(i,j) = -2*ki*(S0/S);
end
end
for i = 1:l
for j = 1:n
Cybeta(i,j) = Cybetaf(i,j)+ Cybetav(i,j);
end
end
%Contribution of vertical tail to directional stability
%alpha is the twist angle of the wing.
alpha = -2; %deg
for i = 1:l
for j = 1:n
Cnbetav(i,j) = -(Cybetav(i,j)/b)* (lv*cos(alpha)-Zv*sin(alpha));
end
end
%Rudder effectiveness(Roskam I p61)
taur = 0.55;
%Rudder control power (Ros I p120 eq 3.78)
for i = 1:l
for j = 1:n
Cndeltar(i,j) = -etav(i,j)*Vv*CLalphav(i)*taur;
end
end
%Change in rolling moment coefficient due to aileron deflection.
%Aileron (Rolling) control power
taua = 0.715;
Cldeltaa =2*CLalphaw*taua/(S*b)*Cr*(y2^2/2 - y1^2/2 + ((lambda - 1)/(b/2))*(y2^3/3 -
        y1^3/3));
%Trim angle of attack
for i = 1:n
for j = 1:l
alpha_trim(i,j) = W/(Q(i,j)*S*CLalphaw(i));
end
end
P_Xac=(0.37+(CLalphah(i)/CLalphawf(i))*etah*(Sh/S)*0.29*(1-
        depsilon_dalpha(i)))/(1+(CLalphah(i)/CLalphawf(i))*etah*(Sh/S)*(1-
        depsilon_dalpha(i)));
%Distance from wing leading edge to aerodynamic center (m)
Xac = P_Xac*cbar;
%Contribution of wing to longitudinal stability of the aircraft
for i = 1:n
```

```
for j = 1:l
Cmalphaw(i,j) = CLalphaw(i)*(Xcg/cbar - Xac(i)/cbar);
end
end

%=============================================================
% Equations for Estimating Longitudinal Stability Coefficients
%=============================================================

%==============================
%X-force coefficients
%==============================
%Change in X-force with change in forward speed
Cxu = -(CDu + 2*CD0(i)) + CTu;
%Change in X-force with change in angle of attack
Cxalpha =  -(2*CL0*CLalphaw)/(pi*e*AR);
%Change in X-force with time rate of change of angle of attack
Cxalphadot = 0;
%Change in X-force with change in pitch rate
Cxq = 0;
%Change in X-force with change in elevator deflection angle
Cxdeltae = 0;

%==============================
%Z-force coefficients
%==============================
%Change in Z-force with change in forward speed
Czu = -CLu - 2*CL0;
%Change in Z-force with change in angle of attack
for i = 1:l
for j = 1:n
Czalpha(i,j) = -(CLalphaw(i) + CD0(i));
end
end
%Change in Z-force with time rate of change of angle of attack
for i = 1:l
for j = 1:n
Czalphadot(i,j) = -2*etah(i,j)*CLalphah(i)*Vh*depsilon_dalpha(i);
end
end
%Change in Z-force with change in pitching velocity
for i = 1:l
for j = 1:n
Czq(i,j) = -2*etah(i,j)*CLalphah(i)*Vh;
end
end
%Change in Z-force with change in elevator deflection angle (p 130)
Czdeltae = -CLdeltae;
```

```
%==============================
%Pitching Moment coefficients
%==============================
%Change in pitching moment with change in forward speed
Cmu = CL*0.07;
%Change in pitching moment with change in angle of attack
for i = 1:l
for j = 1:n
Cmalpha(i,j)=Cmalphaw(i,j)+ Cmalphat(i,j);
end
end
%Change in pitching moment with time rate of change of angle of attack Ros
%eq 6.5
for i = 1:l
for j = 1:n
Cmalphadot(i,j) = -2*CLalphah(i)*etah(i,j)*Vh*depsilon_dalpha(i)*lh/cbar;%cmalphadot
        of wing is small
end
end
%Change in pitching moment with change in pitching velocity
for i = 1:l
for j = 1:n
Cmq(i,j) = -2*etah(i,j)*CLalphah(i)*Vh*lh/cbar;
end
end
%Elevator control power
for i = 1:l
for j = 1:n
Cmdeltae(i,j) = -CLalphah(i)*etah(i,j)*Vh*taue;
end
end

%=================================================================
% Equations for Estimating Lateral Stability Coefficients
%=================================================================
%==============================
%Y-Force coefficients
%==============================
%Change in Y-force with change in side slip angle
% kv is the emperical factor defined if fig 7.3 (Roskam)
kv = 1.25;
%Change in Y-force with change in side slip angle
%Contribution of fuselage to directional stability (Ros 7.1)
ki=1.45; %emberical factor presented in fig 7.1
for i = 1:l
for j = 1:n
Cybetav(i,j) = -kv*etav(i,j)*(Sv/S)*CLalphav(i)*(1 + dsigma_dbeta(i));
Cybetaf(i,j) = -2*ki*(S0/S);
Cybeta(i,j) = Cybetaf(i,j)+ Cybetav(i,j);
end
end
```

```
%Change in Y-force with change in roll rate
%Cyp = Cypv Ros eq 8.1
Cyp = 2*Cybetav*(Zv*cos(alpha)-lv*sin(alpha))/b;
%Change in Y-force with change in yaw rate
Cyr = -2*(lv/b)*Cybeta;
%Change in Y-force with change in aileron deflection angle
Cydeltaa = 0;
%Change in Y-force with change in rudder deflection angle
Cydeltar = Sv/S*taur*CLalphav;

%==============================
% Rolling Moment coefficients
%==============================
%Tip shape and aspect ratio effect on Clbeta (1/deg^2) (Etkin p341)and 7.15
%roskam
Clbeta_CL = -0.004*57.3;%1/rad %Etkin fig B9.3
Clbeta_GAMMA = -0.0004*57.3*57.3; %(1/rad^2)
% Compressiblity correction factor to the uniform geometric dihedral effect (Fig 7.16)
KMGAMMA = 1.4;
%Change in rolling moment with change in side slip angle
Clbeta = CL*(Clbeta_CL)+(Clbeta_GAMMA *GAMMA* KMGAMMA) + deltaClbeta;
%Change in rolling moment with change in roll rate
Clp = (-CLalphaw/12)*(1 + 3*lambda)/(1 + lambda);
%Change in rolling moment with change in yaw rate
for i = 1:l
for j = 1:n
Clr(i,j) = (CL(i,j)/11) - 2*(lv/b)*(Zv/b)*Cybeta(i);
end
end
%Change in rolling moment with change in aileron deflection angle
Cldeltaa = 2*CLalphaw*taua/(S*b)*Cr*(1/2*(y2^2-y1^2)+((lambda-1)/(b/2))*1/3*(y2^3-
        y1^3));
%Change in rolling moment with change in rudder deflection angle
Cldeltar = Sv/S*Zv/b*taur*CLalphaw;

%==============================
%Yawing Moment coefficients
%==============================
%Change in yawing moment with change in side slip angle
for i = 1:l
for j = 1:n
Cnbeta = Cnbetav + CnbetaF;
end
end
%Change in yawing moment with change in roll rate
Cnp = CL/8;
%Change in yawing moment with change in yaw rate
for i = 1:l
for j = 1:n
Cnr(i,j) = -2*etav(i,j)*Vv*lv/b*CLalphav(i);
end
```

```
end
%Empirical factor for Cndeltaa estimation (Ros 11.7)
K1 = 0.253;
%Change in yawing moment with change in aileron deflection angle (Ros 11.2)
Cndeltaa = K1*CL0*Cldeltaa;
%Change in yawing moment with change in rudder deflection angle
for i = 1:l
for j = 1:n
Cndeltar(i,j) = -Vv*etav(i,j)*taur*CLalphav(i);
end
end

%=========================================================
% Equations for longitudinal stability derivatives
%=========================================================
%==============================
% X-force Derivatives
%==============================
for i = 1:n
for j = 1:l
Xu(i,j) = -(CDu(i) + 2*CD0(i))*Q(i,j)*S/(m*U(i));
Xalpha(i,j) = -(CDalpha(i,j)-CL0)*Q(i,j)*S/m;
Xdeltae(i,j) = 0;
Xw(i,j) = -(CDalpha(i,j) -CL0)*Q(i,j)*S/(m*U(i));
end
end
Xdeltat(i,j) = 2018.23/m;

%==============================
%Z-force Derivatives
%==============================
for i = 1:n
for j = 1:l
Zu(i,j) = -(CLu(i)+2*CL(i,j))*Q(i,j)*S/(m*U(i));
Zq(i,j) = Czq(i,j)*cbar/(2*U(i))*Q(i,j)*S/m;
Zdeltae(i,j) = Czdeltae(i,j)*Q(i,j)*S/m;
Zw(i,j) = -(CLalpha(i) + CD0(i))*Q(i,j)*S/(m*U(i));
Zalpha(i,j) = -(CLalphaw(i) + CD0(i))*Q(i,j)*S/m;
Zwdot(i,j)= Czalphadot(i,j)*cbar/(2*U(i))*Q(i,j)*S/(U(i)*m);
Zalphadot(i,j) = Czalphadot(i,j)*cbar/(2*U(i))*Q(i,j)*S/m;
end
end
Zdeltat(i,j)=0;

%==============================
%Pitching moment Derivatives
%==============================
for i = 1:n
for j = 1:l
Mu(i,j)= Cmu(i)*Q(i,j)*S*cbar/(U(i)*Iy);
Mw(i,j) = Cmalpha(i,j)*Q(i,j)*S*cbar/(U(i)*Iy);
```

```
Malpha(i,j) = Cmalpha(i,j)*Q(i,j)*S*cbar/Iy;
Mwdot(i,j) = Cmalphadot(i,j)*cbar*cbar*Q(i,j)*S/(2*U(i)*U(i)*Iy);
Malphadot(i,j) = Cmalphadot(i,j)*cbar/(2*U(i))*Q(i,j)*S*cbar/Iy;
Mq(i,j) = Cmq(i,j)*cbar/(2*U(i))*Q(i,j)*S*cbar/Iy;
Mdeltae(i,j) = Cmdeltae(i,j)*Q(i,j)*S*cbar/Iy;
end
end
Mdeltat(i,j)=0;

%=================================================================
% Equations for lateral/directional stability derivatives
%=================================================================
%==============================
%Y-force Derivatives
%==============================
for i = 1:n
for j = 1:l
Ybeta(i,j) = Q(i,j)*S*Cybeta(i,j)/m;
Yp(i,j) = Q(i,j)*S*b*Cyp(i,j)/(2*U(i)*m);
Yr(i,j) = Q(i,j)*S*b*Cyr(i,j)/(2*m*U(i));
Ydeltaa(i,j) = Q(i,j)*S*Cydeltaa/m;
Ydeltar(i,j) = Q(i,j)*S*Cydeltar(i)/m;
end
end

%==============================
%Yawing moment Derivatives
%==============================
for i = 1:n
for j = 1:l
Nbeta(i,j) = Q(i,j)*S*b*Cnbeta(i,j)/Iz;
Np(i,j) = Q(i,j)*S*b^2*Cnp(i,j)/(2*Iz*U(i));
Nr(i,j) = Q(i,j)*S*b^2*Cnr(i,j)/(2*Iz*U(i));
Ndeltaa(i,j) = Q(i,j)*S*b*Cndeltaa(i)/Iz;
Ndeltar(i,j) = Q(i,j)*S*b*Cndeltar(i,j)/Iz;
end
end

%==============================
%Rolling moment Derivatives
%==============================
for i = 1:n
for j = 1:l
Lbeta(i,j) = Q(i,j)*S*b*Clbeta(i,j)/Ix;
Lp(i,j) = Q(i,j)*S*b^2*Clp(i)/(2*Ix*U(i));
Lr(i,j) = Q(i,j)*S*b^2*Clr(i,j)/(2*Ix*U(i));
Ldeltaa(i,j) = Q(i,j)*S*b*Cldeltaa(i)/Ix;
Ldeltar(i,j) = Q(i,j)*S*b*Cldeltar(i)/Ix;
end
end
```

```
%=====================================================================
% A matrices
%=====================================================================
%A matrix for longitudinal dynamics
Along = zeros(4);
for i =1:n
for j=1:l
if i == j | i < j
Along(:,:,i*j) = [Xu(i,j), Xw(i,j), 0, -g; Zu(i,j), Zw(i,j), U(i),0; Mu(i,j) + Mwdot(i,j)*Zu(i,j),
        Mw(i,j) + Mwdot(i,j)*Zw(i,j), Mq(i,j) + Mwdot(i,j)*U(i), 0; 0, 0, 1, 0];
elseif i > j
Along(:,:,2*i+j) = [Xu(i,j), Xw(i,j), 0, -g; Zu(i,j), Zw(i,j), U(i),0; Mu(i,j) +
        Mwdot(i,j)*Zu(i,j), Mw(i,j) + Mwdot(i,j)*Zw(i,j), Mq(i,j) + Mwdot(i,j)*U(i), 0; 0,
        0, 1, 0];
end
end
end

%=====================================
 %A matrix for lateral dynamics
%=====================================
Alat = zeros(4);
for i =1:n
for j=1:l
if i == j | i < j
Alat(:,:,i*j) = [Ybeta(i,j)/U(i), Yp(i,j)/U(i), -(1- (Yr(i,j)/U(i))), g*cos(alpha_trim(i,j))/U(i);
        Lbeta(i,j), Lp(i,j), Lr(i,j), 0; Nbeta(i,j), Np(i,j), Nr(i,j), 0; 0, 1, 0, 0];
elseif i > j
Alat(:,:,2*i+j) = [Ybeta(i,j)/U(i), Yp(i,j)/U(i), -(1- (Yr(i,j)/U(i))),
        g*cos(alpha_trim(i,j))/U(i); Lbeta(i,j), Lp(i,j), Lr(i,j), 0; Nbeta(i,j), Np(i,j), Nr(i,j),
        0; 0, 1, 0, 0];
end
end
end

%=====================================
% B matrices
%=====================================
%B matrix for longitudinal dynamics
Blong = zeros(4,2);
for i = 1:n
   for j = 1:l
      if i == j | i < j
         Blong(:,:,i*j) = [Xdeltae(i,j),Xdeltat(i,j); Zdeltae(i,j),Zdeltat(i,j);
          Mdeltae(i,j),Mdeltat(i,j); 0,0];
      elseif i > j
         Blong(:,:,2*i+j) = [Xdeltae(i,j),Xdeltat(i,j); Zdeltae(i,j),Zdeltat(i,j);
          Mdeltae(i,j),Mdeltat(i,j); 0,0];
      end
   end
end
```

```
%B matrix for lateral dynamics
Blat = zeros(4,2);
for i = 1:n
    for j = 1:l
        if i == j | i < j
   Blat(:,:,i*j) = [0, Ydeltar(i,j)/U(i); Ldeltaa(i,j), Ldeltar(i,j); Ndeltaa(i,j), Ndeltar(i,j); 0, 0];
        elseif i > j
            Blat(:,:,2*i+j) = [0, Ydeltar(i,j)/U(i); Ldeltaa(i,j), Ldeltar(i,j); Ndeltaa(i,j),
             Ndeltar(i,j); 0, 0];
        end
    end
end

%=====================================
%C matrix
%=====================================
Clong = eye(4);
Clat = eye(4);

%=====================================
%D matrices
%=====================================
Dlong = zeros(4,1);
Dlat = zeros(4,2);
%=====================================end
```

FILE NAME: sfun_stspace1.c

C-MEX S-FUNCTION THAT WORKS AS BUILT IN STATE-SPACE BLOCK

```
 /*  File    : sfun_stspace1.c
*  Abstract:
*
*      Example mex file S-function for state-space system.
*
*      Implements a set of state-space equations.
*      You can turn this into a new block by using the
*      S-function block and Mask facility.
*
*      This example MEX-file performs the same function
*      as the built-in State-space block. This is an
*      example of a MEX-file where the number of inputs,
*      outputs, and states is dependent on the parameters
*      passed in from the workspace.
*
*      Syntax  [sys, x0] = stspace(t,x,u,flag,A,B,C,D,X0)
*
*      For more details about S-functions, see simulink/src/sfuntmpl_doc.c
*
*  Copyright 1990-2000 The MathWorks, Inc.
*  $Revision: 1.8 $
*/
#define S_FUNCTION_NAME sfun_stspace1
#define S_FUNCTION_LEVEL 2
#include "simstruc.h"
#include "math.h"
#include "intpl.c"
#define U(element) (*uPtrs[element])  /* Pointer to Input Port0 */
static real_T C[8][8]={ { 1.0,0.0,0.0,0.0,0.0,0.0,0.0,0.0},
                        { 0.0,1.0,0.0,0.0,0.0,0.0,0.0,0.0},
                        { 0.0,0.0,1.0,0.0,0.0,0.0,0.0,0.0},
                        { 0.0,0.0,0.0,1.0,0.0,0.0,0.0,0.0},
                        { 0.0,0.0,0.0,0.0,1.0,0.0,0.0,0.0},
                        { 0.0,0.0,0.0,0.0,0.0,1.0,0.0,0.0},
                        { 0.0,0.0,0.0,0.0,0.0,0.0,1.0,0.0},
                        { 0.0,0.0,0.0,0.0,0.0,0.0,0.0,1.0}
                      };
real_T A[8][8]={0.0};
real_T B[8][4]={0.0};

#define Xu_IDX 0
#define Xu_PARAM(S) ssGetSFcnParam(S, Xu_IDX)

#define Xw_IDX 1
#define Xw_PARAM(S) ssGetSFcnParam(S, Xw_IDX)

#define Zu_IDX 2
#define Zu_PARAM(S) ssGetSFcnParam(S, Zu_IDX)
```

```
#define Zw_IDX 3
#define Zw_PARAM(S) ssGetSFcnParam(S, Zw_IDX)

#define Mu_IDX 4
#define Mu_PARAM(S) ssGetSFcnParam(S, Mu_IDX)

#define Mw_IDX 5
#define Mw_PARAM(S) ssGetSFcnParam(S, Mw_IDX)

#define Mwdot_IDX 6
#define Mwdot_PARAM(S) ssGetSFcnParam(S, Mwdot_IDX)

#define Mq_IDX 7
#define Mq_PARAM(S) ssGetSFcnParam(S, Mq_IDX)

#define Xdeltat_IDX 8
#define Xdeltat_PARAM(S) ssGetSFcnParam(S, Xdeltat_IDX)

#define Xdeltae_IDX 9
#define Xdeltae_PARAM(S) ssGetSFcnParam(S, Xdeltae_IDX)

#define Zdeltae_IDX 10
#define Zdeltae_PARAM(S) ssGetSFcnParam(S, Zdeltae_IDX)

#define Mdeltae_IDX 11
#define Mdeltae_PARAM(S) ssGetSFcnParam(S, Mdeltae_IDX)

#define Ybeta_IDX 12
#define Ybeta_PARAM(S) ssGetSFcnParam(S, Ybeta_IDX)

#define Yp_IDX 13
#define Yp_PARAM(S) ssGetSFcnParam(S, Yp_IDX)

#define Nbeta_IDX 14
#define Nbeta_PARAM(S) ssGetSFcnParam(S, Nbeta_IDX)

#define Np_IDX 15
#define Np_PARAM(S) ssGetSFcnParam(S, Np_IDX)

#define Nr_IDX 16
#define Nr_PARAM(S) ssGetSFcnParam(S, Nr_IDX)
#define Lbeta_IDX 17
#define Lbeta_PARAM(S) ssGetSFcnParam(S, Lbeta_IDX)

#define Lp_IDX 18
#define Lp_PARAM(S) ssGetSFcnParam(S, Lp_IDX)

#define Lr_IDX 19
#define Lr_PARAM(S) ssGetSFcnParam(S, Lr_IDX)

#define Ydeltar_IDX 20
```

```
#define Ydeltar_PARAM(S) ssGetSFcnParam(S, Ydeltar_IDX)

#define Ndeltaa_IDX 21
#define Ndeltaa_PARAM(S) ssGetSFcnParam(S, Ndeltaa_IDX)

#define Ndeltar_IDX 22
#define Ndeltar_PARAM(S) ssGetSFcnParam(S, Ndeltar_IDX)

#define Ldeltaa_IDX 23
#define Ldeltaa_PARAM(S) ssGetSFcnParam(S, Ldeltaa_IDX)

#define Ldeltar_IDX 24
#define Ldeltar_PARAM(S) ssGetSFcnParam(S, Ldeltar_IDX)

#define G_IDX 25
#define G_PARAM(S) ssGetSFcnParam(S, G_IDX)

#define H1_IDX 26
#define H1_PARAM(S) ssGetSFcnParam(S, H1_IDX)

#define V1_IDX 27
#define V1_PARAM(S) ssGetSFcnParam(S, V1_IDX)

#define H_IDX 28
#define H_PARAM(S) ssGetSFcnParam(S, H_IDX)

#define V_IDX 29
#define V_PARAM(S) ssGetSFcnParam(S, V_IDX)

#define ALPHATRIM_IDX 30
#define ALPHATRIM_PARAM(S) ssGetSFcnParam(S, ALPHATRIM_IDX)

#define Malpha_IDX 31
#define Malpha_PARAM(S) ssGetSFcnParam(S, Malpha_IDX)

#define NPARAMS 32

real_T Xu[] = {0.0};
real_T Xdeltae[] = {0.0};
real_T Xdeltat[] = {0.0};
real_T Xw[] = {0.0};
real_T Zu[] = {0.0};
real_T Zdeltae[] = {0.0};
real_T Zw[] = {0.0};
real_T Mu[] = {0.0};
real_T Mw[] = {0.0};
real_T Mwdot[] = {0.0};
real_T Mq[] = {0.0};
real_T Mdeltae[] = {0.0};
real_T Malpha[] = {0.0};
real_T Ybeta[] = {0.0};
```

```
real_T Yp[] = {0.0};
real_T Yr[] = {0.0};
real_T Ydeltaa[] = {0.0};
real_T Ydeltar[] = {0.0};
real_T Nbeta[] = {0.0};
real_T Np[] = {0.0};
real_T Nr[] = {0.0};
real_T Ndeltaa[] = {0.0};
real_T Ndeltar[] = {0.0};
real_T Lbeta[] = {0.0};
real_T Lp[] = {0.0};
real_T Lr[] = {0.0};
real_T Ldeltaa[] = {0.0};
real_T Ldeltar[] = {0.0};
real_T alpha_trim[] = {0.0};

FILE *fp1;
FILE *fp2;
FILE *fp3;
FILE *fp4;

/*====================*
* S-function methods *
*====================*/
#define MDL_CHECK_PARAMETERS
#if defined(MDL_CHECK_PARAMETERS) && defined(MATLAB_MEX_FILE)
  /* Function: mdlCheckParameters
=============================================
   * Abstract:
   *    Validate our parameters to verify they are okay.
   */
  static void mdlCheckParameters(SimStruct *S)
  {
  }
#endif /* MDL_CHECK_PARAMETERS */

/* Function: mdlInitializeSizes
=============================================
* Abstract:
*    The sizes information is used by Simulink to determine the S-function
*    block's characteristics (number of inputs, outputs, states, etc.).
*/
static void mdlInitializeSizes(SimStruct *S)
{
       ssSetNumSFcnParams(S, NPARAMS);  /* Number of expected parameters */
#if defined(MATLAB_MEX_FILE)
    if (ssGetNumSFcnParams(S) == ssGetSFcnParamsCount(S)) {
       mdlCheckParameters(S);
       if (ssGetErrorStatus(S) != NULL) {
          return;
       }
```

```
    } else {
        return; /* Parameter mismatch will be reported by Simulink */
    }
#endif

    ssSetNumContStates(S, 8);
    ssSetNumDiscStates(S, 0);

    if (!ssSetNumInputPorts(S, 1)) return;
    ssSetInputPortWidth(S, 0, 6);
    ssSetInputPortDirectFeedThrough(S, 0, 0);

    if (!ssSetNumOutputPorts(S, 1)) return;
    ssSetOutputPortWidth(S, 0, 8);

    ssSetNumSampleTimes(S, 1);
    ssSetNumRWork(S, 0);
    ssSetNumIWork(S, 0);
    ssSetNumPWork(S, 0);
    ssSetNumModes(S, 0);
    ssSetNumNonsampledZCs(S, 0);

    /* Take care when specifying exception free code - see sfuntmpl_doc.c */
    ssSetOptions(S, SS_OPTION_EXCEPTION_FREE_CODE);
}

/* Function: mdlInitializeSampleTimes
=========================================
* Abstract:
*    S-function is comprised of only continuous sample time elements
*/
static void mdlInitializeSampleTimes(SimStruct *S)
{
    ssSetSampleTime(S, 0, CONTINUOUS_SAMPLE_TIME);
    ssSetOffsetTime(S, 0, 0.0);
}

#define MDL_INITIALIZE_CONDITIONS
/* Function: mdlInitializeConditions
=========================================
* Abstract:
*    If the initial condition parameter (X0) is not an empty matrix,
*    then use it to set up the initial conditions, otherwise,
*    set the intial conditions to all 0.0
*/
static void mdlInitializeConditions(SimStruct *S)
{
    real_T *x0 = ssGetContStates(S);
    int_T  i;
        for (i = 0; i < 8; i++) {
            *x0++ = 0.0;
```

```
      }
}
#define MDL_START  /* Change to #undef to remove function */
#if defined(MDL_START)
  /* Function: mdlStart
=============================================================
   * Abstract:
   *    This function is called once at start of model execution. If you
   *    have states that should be initialized once, this is the place
   *    to do it.
   */
static void mdlStart(SimStruct *S)
{
    fp1 = fopen("A_B_Matrix.txt", "w");
    fp2 = fopen("Init_Speed.mat", "w");
    fp3 = fopen("A_B_Matrix.mat", "w");
    fp4 = fopen("validate_result.mat","w");

    fprintf(fp1,"h           " "v         " "A[0][0] " "A[0][1]   "
"A[0][3]  " "A[1][1]    " "A[1][2]  " "A[2][0]   " "A[2][1]   "
"A[2][2]   "
"A[3][2]   " "A[4][1]  "  "A[4][3]    " "A[5][5]   " "A[5][6]   "
"A[5][7]  "
"A[5][8]  " "A[6][5]  " "A[6][6]  " "A[6][7]  " "A[7][5]  " "A[7][6]"
"A[7][7]  " "A[8][6]  " "B[0][0]  " "B[1][0]  " "B[2][0]   " "B[5][3] "
"B[6][2]   " "B[6][3]   " "B[7][2]   " "B[7][3]""\n");
}
#endif /*  MDL_START */

/* Function: mdlOutputs
=============================================================
* Abstract:
*      y = Cx + Du
*/
static void mdlOutputs(SimStruct *S, int_T tid)
{
   real_T            *y      = ssGetOutputPortRealSignal(S,0);
   real_T            *x      = ssGetContStates(S);
   InputRealPtrsType uPtrs    = ssGetInputPortRealSignalPtrs(S,0);
   int_T i;

  UNUSED_ARG(tid); /* not used in single tasking mode */

   for(i=0;i<8;i++)
   {

y[i]=C[i][0]*x[0]+C[i][1]*x[1]+C[i][2]*x[2]+C[i][3]*x[3]+C[i][4]*x[4]+C[i][5]*x[5]+C[i][
          6]*x[6]+C[i][7]*x[7];
   }
}
#define MDL_DERIVATIVES
```

```
/* Function: mdlDerivatives
=============================================
* Abstract:
*      xdot = Ax + Bu
*/
static void mdlDerivatives(SimStruct *S)
{
   real_T            *dx     = ssGetdX(S);
   real_T            *x      = ssGetContStates(S);
   InputRealPtrsType uPtrs   = ssGetInputPortRealSignalPtrs(S,0);

   /* Matrix Multiply: dx = Ax + Bu */
   real_T      *h    = mxGetPr(H_PARAM(S));
   real_T      *U0    = mxGetPr(V_PARAM(S));
   real_T      *h1    = mxGetPr(H1_PARAM(S));
   real_T      *U1    = mxGetPr(V1_PARAM(S));
   real_T *Xu1 = mxGetPr(Xu_PARAM(S));
   real_T *Xw1 = mxGetPr(Xw_PARAM(S));
   real_T *Zu1 = mxGetPr(Zu_PARAM(S));
   real_T *Zw1 = mxGetPr(Zw_PARAM(S));
   real_T *Mu1 = mxGetPr(Mu_PARAM(S));
   real_T *Mw1 = mxGetPr(Mw_PARAM(S));
   real_T *Mwdot1 = mxGetPr(Mwdot_PARAM(S));
   real_T *Mq1 = mxGetPr(Mq_PARAM(S));
   real_T *Xdeltae1 = mxGetPr(Xdeltae_PARAM(S));
   real_T *Xdeltat1 = mxGetPr(Xdeltat_PARAM(S));
   real_T *Zdeltae1 = mxGetPr(Zdeltae_PARAM(S));
   real_T *Mdeltae1 = mxGetPr(Mdeltae_PARAM(S));
   real_T *Malpha1 = mxGetPr(Malpha_PARAM(S));

   real_T *Ybeta1 = mxGetPr(Ybeta_PARAM(S));
   real_T *Yp1 = mxGetPr(Yp_PARAM(S));
   real_T *Nbeta1 = mxGetPr(Nbeta_PARAM(S));
   real_T *Np1 = mxGetPr(Np_PARAM(S));
   real_T *Nr1 = mxGetPr(Nr_PARAM(S));
   real_T *Lbeta1 = mxGetPr(Lbeta_PARAM(S));
   real_T *Lp1 = mxGetPr(Lp_PARAM(S));
   real_T *Lr1 = mxGetPr(Lr_PARAM(S));
   real_T *Ydeltar1 = mxGetPr(Ydeltar_PARAM(S));
   real_T *Ndeltaa1 = mxGetPr(Ndeltaa_PARAM(S));
   real_T *Ndeltar1 = mxGetPr(Ndeltar_PARAM(S));
   real_T *Ldeltaa1 = mxGetPr(Ldeltaa_PARAM(S));
   real_T *Ldeltar1 = mxGetPr(Ldeltar_PARAM(S));

   real_T *alpha_trim1 = mxGetPr(ALPHATRIM_PARAM(S));
   real_T *g = mxGetPr(G_PARAM(S));

   #define NUMEL(m)    mxGetM(m)*mxGetN(m)
   int_T m = NUMEL(V1_PARAM(S));
   int_T n = NUMEL(H1_PARAM(S));
   #undef NUMEL
```

```
int_T i;

intpl(U1,h1,Xu1,U0,h,Xu,m,n);
intpl(U1,h1,Xw1,U0,h,Xw,m,n);
intpl(U1,h1,Zu1,U0,h,Zu,m,n);
intpl(U1,h1,Zw1,U0,h,Zw,m,n);
intpl(U1,h1,Mu1,U0,h,Mu,m,n);
intpl(U1,h1,Mw1,U0,h,Mw,m,n);
intpl(U1,h1,Mwdot1,U0,h,Mwdot,m,n);
intpl(U1,h1,Mq1,U0,h,Mq,m,n);
intpl(U1,h1,Xdeltae1,U0,h,Xdeltae,m,n);
intpl(U1,h1,Xdeltat1,U0,h,Xdeltat,m,n);
intpl(U1,h1,Zdeltae1,U0,h,Zdeltae,m,n);
intpl(U1,h1,Mdeltae1,U0,h,Mdeltae,m,n);
intpl(U1,h1,Malpha1,U0,h,Malpha,m,n);

intpl(U1,h1,Ybeta1,U0,h,Ybeta,m,n);
intpl(U1,h1,Yp1,U0,h,Yp,m,n);
intpl(U1,h1,Nbeta1,U0,h,Nbeta,m,n);
intpl(U1,h1,Np1,U0,h,Np,m,n);
intpl(U1,h1,Nr1,U0,h,Nr,m,n);
intpl(U1,h1,Lbeta1,U0,h,Lbeta,m,n);
intpl(U1,h1,Lp1,U0,h,Lp,m,n);
intpl(U1,h1,Lr1,U0,h,Lr,m,n);
intpl(U1,h1,Ydeltar1,U0,h,Ydeltar,m,n);
intpl(U1,h1,Ndeltaa1,U0,h,Ndeltaa,m,n);
intpl(U1,h1,Ndeltar1,U0,h,Ndeltar,m,n);
intpl(U1,h1,Ldeltaa1,U0,h,Ldeltaa,m,n);
intpl(U1,h1,Ldeltar1,U0,h,Ldeltar,m,n);
intpl(U1,h1,alpha_trim1,U0,h,alpha_trim,m,n);
A[0][0] = *Xu;
A[0][1] = *Xw;
A[0][3] = -(*g);
A[1][0] = *Zu;
A[1][1] = *Zw;
A[1][2] = *U0;
A[2][0] = (*Mu) + (*Mwdot)*(*Zu);
A[2][1] = (*Mw) + (*Mwdot)*(*Zw);
A[2][2] = (*Mq) + *Mwdot*(*U0);
A[3][2] = 1.0;
A[4][4]= (*Ybeta)/(*U0);
A[4][5]= (*Yp)/(*U0);
A[4][6]= -(1-(*Yr)/(*U0));
A[4][7] = (*g)*cos(*alpha_trim)/(*U0);
A[5][4] = *Lbeta;
A[5][5] = *Lp;
A[5][6] = *Lr;
A[6][4] = *Nbeta;
A[6][5] = *Np;
A[6][6] = *Nr;
A[7][5] = 1.0;
```

```
    B[0][0] = *Xdeltae;
    B[0][1] = *Xdeltat;
    B[1][0] = *Zdeltae;
    B[2][0] = (*Mdeltae) + (*Mwdot)*(*Zdeltae);
    B[4][3] = (*Ydeltar)/(*U0);
    B[5][2] = *Ldeltaa;
    B[5][3] = *Ldeltar;
    B[6][2] = *Ndeltaa;
    B[6][3] = *Ndeltar;

    for(i=0;i<8;i++)
    {
dx[i]=A[i][0]*x[0]+A[i][1]*x[1]+A[i][2]*x[2]+A[i][3]*x[3]+A[i][4]*x[4]+A[i][5]*x[5]+A[
        i][6]*x[6]+A[i][7]*x[7]+B[i][0]*U(0)+B[i][1]*U(1)+B[i][2]*U(2)+B[i][3]*U(3);
    }
    fprintf(fp1,"%f %f %f %f %f %f %f %f %f %f %f %f %f %f %f %f %f %f %f %f %f %f %f
        %f\n",*h,*U0,A[0][0],A[0][1],A[1][0],A[1][1],A[2][1],A[2][2],A[4][4],A[4][5],A[
        4][6],A[4][7],A[5][4],A[5][5],A[5][6],A[6][4],A[6][5],A[6][6],B[0][0],B[1][0],B[2]
        [0],B[4][3],B[5][2],B[5][3],B[6][2],B[6][3]);
    fprintf(fp2,"%f",*U0);
    fprintf(fp3,"%f %f %f %f %f %f %f %f %f %f %f %f %f %f %f %f %f %f %f %f %f %f %f
        %f\n",*h,*U0,*Malpha,A[0][0],A[0][1],A[1][0],A[1][1],A[2][1],A[2][2],A[4][4],A
        [4][5],A[4][6],A[4][7],A[5][4],A[5][5],A[5][6],A[6][4],A[6][5],A[6][6],B[0][0],B[1
        ][0],B[2][0],B[4][3],B[5][2],B[5][3],B[6][2],B[6][3]);
    fprintf(fp4,"%f %f %f\n", *Mw,*h,*U0);
}
/* Function: mdlTerminate
=============================================================
* Abstract:
*    No termination needed, but we are required to have this routine.
*/
static void mdlTerminate(SimStruct *S)
{
UNUSED_ARG(S); /* unused input argument */
}
#ifdef  MATLAB_MEX_FILE    /* Is this file being compiled as a MEX-file? */
#include "simulink.c"      /* MEX-file interface mechanism */
#else
#include "cg_sfun.h"       /* Code generation registration function */
#endif
```